

論文 / 著書情報
Article / Book Information

題目(和文)	
Title(English)	PHOTOCATALYTIC MEMBRANE INTEGRATING Zr-BASED METAL ORGANIC FRAMEWORK AND GRAPHENE OXIDE FOR WATER TREATMENT
著者(和文)	HEURina
Author(English)	Rina Heu
出典(和文)	学位:博士(工学), 学位授与機関:東京工業大学, 報告番号:甲第11627号, 授与年月日:2020年9月25日, 学位の種別:課程博士, 審査員:吉村 千洋,藤井 学,鼎 信次郎,中村 隆志,ANDREWS EDEN MARIQU,山村 寛
Citation(English)	Degree:Doctor (Engineering), Conferring organization: Tokyo Institute of Technology, Report number:甲第11627号, Conferred date:2020/9/25, Degree Type:Course doctor, Examiner:,,,,,
学位種別(和文)	博士論文
Type(English)	Doctoral Thesis

**PHOTOCATALYTIC MEMBRANE INTEGRATING Zr-
BASED METAL ORGANIC FRAMEWORK AND
GRAPHENE OXIDE FOR WATER TREATMENT**

By HEU Rina

July 2020

**A Dissertation Submitted in Partial Fulfillment of the Requirements
for the Degree of Doctor of Engineering
Department of Civil and Environmental Engineering
School of Environment and Society
Tokyo Institute of Technology
Academic Year 2017-2020**

ACKNOWLEDGEMENTS

This doctoral thesis would have not been completed without the help and support from kind and beloved people around me. I'd like to express my sincere thanks to everyone who helped and supported me throughout this crucial and hard time.

I cannot express enough thanks to my respectful and supportive supervisor, Assoc. Prof. YOSHIMURA Chihiro for his continuous support, guideline and encouragement throughout the research. For these three years, I've learnt many things from him, not only scientific knowledge but also communication and management skills which will be benefic for my future career as a lecturer or researcher. To my thesis committees, Assoc. Prof. FUJII Manabu, Prof. KANAE Shinjiro, Assoc. Prof. YAMAMURA Hiroshi, Dr. Eden Mariquit-Andrews and Assoc. Prof. NAKAMURA Takashi, I am deeply indebted for their assistance, fruitful discussion and constructive suggestions.

I'd like to express my profound gratitude to Water Environment laboratory, Department of Civils and Environment Engineering, Tokyo Institute of Technology, for offering me the opportunity to conduct my research. I'd like to thank Ms. MIYAMOTO Manami and TAKAHASHI Kaori, laboratory technicians and Ms. NAMBA Yumi and Ms. ANDO Kimiko, laboratory secretaries for their support. My sincere gratefulness goes to my seniors, Dr. ATEIA Mohamed and Dr. SIEV Sokly, colleagues, and friends for their support and contribution in my research work and daily life.

I'd like to acknowledge the financial support from the ASEAN University Network/Southeast Asia Engineering Education Development Network (AUN/SEED-Net) program of the Japan International Cooperation Agency (JICA). I'm highly indebted to Mr. NABESHIMA Mitsuhiro, a JICA coordinator, and Dr. HUL Seingheng, a AUN/SEED-Net coordinator for their assistance and support throughout the program.

I'd like to dedicate this achievement to the soul of my father. Even though, he's not physically in this world anymore and I cannot remember much about him, but I believe his soul is here with me. By looking to the sky, I believe he is looking over me

and always guide me to the bright path. I'd like to extend the special gratitude to my beloved and respectful mother for her unconditional love and belief in me. As a widow mother who's raised her four children alone for almost 30 years, she's never tired to support us and always make sure that all her children can pursue high education at least Master's degree. I'd like to express my profound thank to my great brothers, sister in-laws, aunts, uncles, nieces and nephews who always make efforts to provide me financial support and motivation to complete my degree in this doctoral program.

ABSTRACT

Nanocomposite of Zr-based organic framework and graphene oxide (UiO-66_GO) was synthesized by one-step hydrothermal method, and then a 0.5% GO loading in the nanocomposite was layered on nanofiltration (NF) membrane by pressure-assisted self-assembly (PASA) to fabricate a novel photocatalytic NF membrane (UiO-66_GO/NF) using for water and wastewater treatment. As a result from characterization, graphene oxide enhanced photocatalytic activity of UiO-66 about 2.8 and 1.7 times higher than those over pristine GO and UiO-66 by increasing surface area and porosity and narrowing the band gap. Consequently, the composite membrane with a 10% UiO-66_GO loading (UiO-66_GO/NF-10%) showed a higher water flux (up to 63 kg/m² h bar), flux recovery (80%), and total fouling resistance (33%) than did the pristine NF membrane. Physical and chemical characterization revealed that this performance was attributed to improvements in hydrophilicity, porosity, surface smoothness, and charge repulsion. The UiO-66_GO/NF-10% composite membrane exhibited better physical stability with a relatively low mass loss (8.64%) after five washes than the membranes with mass loadings of 5 and 15 wt %. Furthermore, the UiO-66_GO/NF-10% composite membrane exhibited considerable photocatalytic activity under UV irradiation (bandgap: 3.45 eV), which reduced irreversible fouling from 20.7% to 2.4% and increased flux recovery to 98%. This study demonstrated that surface modification with the UiO-66_GO nanocomposite produced a high-flux and anti-fouling photocatalytic NF membrane, which is promising for water purification.

Keyword: Graphene Oxide; Metal-Organic Framework; Organic Micro-pollutant; Nanofiltration Membrane; Photocatalysis; UiO-66.

TABLE OF CONTENTS

ACKNOWLEDGEMENTS	i
ABSTRACT	iii
TABLE OF CONTENTS	iv
CHAPTER I	1
Introduction.....	1
1.1 Background.....	1
1.2 Knowledge Gap and Technical Limitations	7
1.3 Objectives	7
1.4 Structure of the Thesis.....	8
CHAPTER II.....	11
A Review on Recent Development of Photocatalytic Membrane for Water Treatment Application	11
2.1 Organic Micropollutants.....	11
2.1.1 Organic Micropollutants and Their Environmental Risks.....	11
2.1.2 Standard Regulation	12
2.1.3 OMP removal methods.....	12
2.2 Membrane filtration technology	13
2.2.1 Applications in Water Treatment	13
2.2.2 Nanofiltration	15
2.2.3 Photocatalytic Membrane Filtration.....	21
2.3 Metal Organic Framework.....	22
2.3.1 Photocatalytic Property of MOFs	24
2.3.2 MOF Based Membrane.....	25
2.3.3 Composites of MOF Carbonaceous Materials.....	26
2.4 Conclusion, Limitation and Research Needs.....	28
CHAPTER III.....	31
Materials and Characterization	31
3.1 Materials	31
3.2 Synthesis Methods	31

3.2.1	GO Synthesis.....	31
3.2.2	UiO-66 Synthesis.....	32
3.2.3	UiO-66_GO Synthesis.....	34
3.2.4	Preparation of UiO-66_GO NF Membrane.....	35
3.3	Characterization of UiO-66_GO composite.....	36
3.4	Characterization of UiO-66_GO/NF Membrane	37
3.4.2	Surface Functional Groups.....	38
3.4.3	SEM Morphology	39
3.4.4	TEM Morphology and Element Composition	40
3.4.5	Specific surface areas, principal pore sizes, and pore volumes	41
3.4.6	UV-Vis Light Absorption	45
3.4.7	Composite Membrane	47
3.4.8	Morphology of Composite Membrane	48
3.4.9	Hydrophilicity of Membrane.....	51
3.4.10	Porosity and Pore Size of Membrane	51
3.5	Conclusion	52
CHAPTER IV		54
Photocatalytic Activity of Zr-based Metal Organic framework Enhanced by Graphene Oxide		54
4.1	Introduction.....	54
4.2	Experimental Method.....	55
4.3	Results and Discussion.....	56
4.3.1	Effect of Photocatalyst Compositions	56
4.3.2	Effect of Photocatalyst Dose	59
4.3.3	Effect of Initial CBZ Concentration	61
4.3.4	Effect of pH.....	62
4.3.5	Photodegradation Mechanism and Identification of Reactive Species	64
4.3.6	Recyclability of the Composites	67
4.4.	Conclusions.....	70
CHAPTER V		71
UiO66_GO NF Membrane and Its Filtration Performance		71

5.1	Introduction.....	71
5.2	Experimental Method.....	72
5.3	Results and Discussion.....	74
5.3.1	Water Flux.....	74
5.3.2	Membrane Stability.....	75
5.3.3	Anti-Fouling Properties.....	77
5.3.4	Photocatalytic Activity of UiO-66_GO/NF for Flux Recovery.....	79
5.3.5	Separation Performance.....	81
5.4	Conclusion.....	83
CHAPTER VI.....		84
Conclusion and Recommendations.....		84
6.1	Conclusion.....	84
6.2	Recommendations and Further Research.....	86
REFERENCES.....		90
APPENDICES.....		108

CHAPTER I

Introduction

1.1 Background

To date, more than 700 compounds of emerging organic contaminants (OCs) have been found in drinking water sources and classified into more than 20 groups based on their origins (Geissen et al., 2015). Among them, organic micropollutants (OMPs) which are the synthetic chemicals found in environment in the range of microgram/liter or lower such as pesticides, pharmaceuticals, personal care products, plasticizer and endocrine disruptors have been attracted a great concern because of their low degradability and high biological effect (Petrović et al., 2003; Snyder et al., 2003). The widespread presence and distribution of those OMPs emerge the particular concerns in several environmental toxicity and cause many problems in soil, air and particularly in water resources including surface water, ground water and other water sources (Glassmeyer et al., 2017; Padhye et al., 2014; Upadhyayula et al., 2009). For example, pharmaceuticals and personal care products (PPCPs), which are used in human and veterinary medicine, have been detected in surface waters, groundwater, or even drinking water in 71 countries (**Fig. 1.1**) and increasing environmental concern over past decades because it toxic to aquatic organisms such as fish, algae, and bacteria and threats to human health due to the unpredicted ecotoxicological effect (Ding et al., 2017; Ferrari et al., 2003). Furthermore, pesticides were reported as hazard substances which caused potential health risks even at very low concentration such as cancer, endocrine disruption, immune system damages, potential carcinogens, neuro developmental disorders and other diseases in humans, (Skinner et al., 1997; Sanborn et al., 2004; Mckinlay et al., 2008, Mrema et al., 2013; WHO, 2016). Since the surface water and ground water are the main water sources of drinking water production around the world, the presence of those OMP groups in natural water shows the potential risk

in quality of drinking water supply (Geissen et al., 2015; Knepper et al., 1999) and need to be removed.

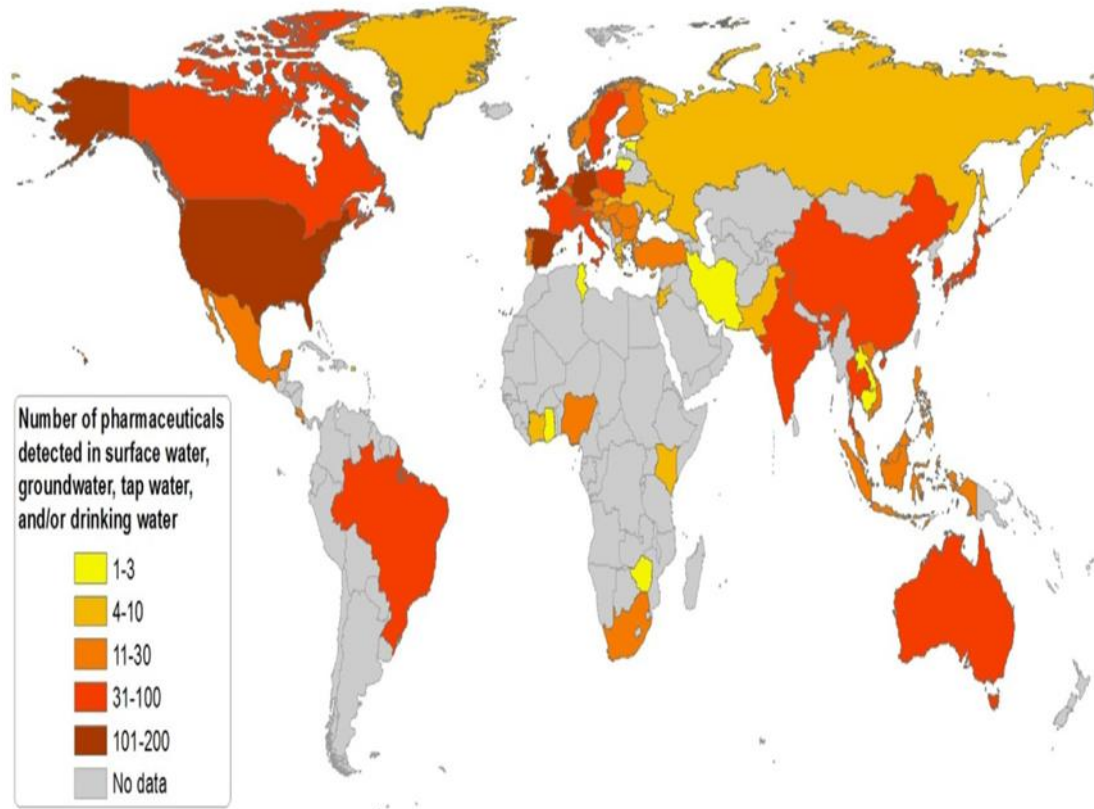


Fig. 1.1 The number of pharmaceutical substances detected in surface waters, groundwater, or tap/drinking water (Beek et al., 2015).

Various methods to remove OMPs from surface water, ground water, and wastewater have been studied and developed. Conventional treatment processes including coagulation, flocculation, and sand filtration are found to be ineffective to remove OMPs (Kim et al., 2007; H. Jiang & Adams, 2006; Petrović et al., 2003). Membrane filtration give a good removal efficiency of various OMPs, fouling is one of the main challenges in any membrane separation technology (B. Van der Bruggen et al., 2008; Mo et al., 2008). Chlorination and ozonation showed highly effective in removing some types of OMPs e.g. glyphosate and aminomethyl phosphonic acid (AMPA) (Jönsson et al., 2013). However, these processes produce disinfection by-products (DBPs), some of which are seriously harmful to human health (Richardson, 2003;

Cantor et al., 1999). Advanced oxidation processes (AOPs) produce no sludge and show a efficient degradation but their mineralization is low (by-product) and separation of catalyst from water is hard (Bolton and Cotton, 2011). Activated carbon adsorption is a popular technique for elimination of OMPs because of its economic benefits and simple application (Tobergte & Curtis, 2013; Ali & Gupta, 2006), but the significant problems are mainly related to its saturation, toxic solid waste, and difficulties in removing small polar compounds (Plakas & Karabelas, 2012a; Ormad et al., 2008). Biological treatment including activated sludge is simple and cheap method but its kinetic rate is slow, requires large space, and limited degradation for OMPs (Chon et al., 2012). Advantages and disadvantages of various water and wastewater treatment methods were summarized in **Table 1.1**.

Table 1.1 Advantages and disadvantages of various water and wastewater treatment methods

Treatment methods	Advantages	Disadvantages
Coagulation/flocculation	Process simplicity; low cost	High sludge, ineffective for OMP removals
Biological methods	Simple and economical attraction	Slow process; limited biodegradation to OMPs
Chlorination/ozonation	Simple, rapid and efficient process	High dose of chemical requirement, toxic by-products
Adsorption	Simple equipment; highly effective process with fast kinetic	Rapid saturation and expensive regeneration
Photocatalysis	No sludge production; rapid and efficient degradation	Formation of by-products; hard to separate the fine catalyst
Membrane filtration	Small space requirement; simple, rapid and efficient process	Limited flow rates; rapid membrane fouling

In recent decades, membrane technology has become attractive in the fields of wastewater treatment, surface and ground water treatment, water desalination, oil-water and protein effluent separation, ultrapure water production, product recycling and pharmacy industrial and food processing (Mimoso et al., 2015; Madsen & Sogaard, 2014; Singh et al., 2013; Tian et al., 2010; Bruggen et al., 2003). This membrane system is growing much attention as one of the most promising separation methods for water purification because of their effective potential, no chemical treatment require and low environmental footprint (Peter-Varbanets et al., 2009) resulting in increasing the worldwide popularity of improving water quality and meeting the standard regulation for drinking water (WHO, 2011). Pressure-driven membranes pressure exerted on the feed side of membrane to separate feed solute into permeate and a retentate. Pressure-driven membranes are clarified into microfiltration (MF), ultrafiltration (UF), nanofiltration (NF) and reverse osmosis (RO) based on characteristics of membrane pore size, charge of retained particle or molecule and pressure applied on membranes (**Fig. 1.2**) (Bruggen et al., 2003). Membrane filtrations have been reported successfully installation in water treatment plant for drinking water production which provide high capacity in some countries such as USA (152,000 m³/d), France (140,000 m³/d), Holland (57,000 m³/d), Spain (30,000 m³/d) and England (30,000 m³/d) (Plakas & Karabelas, 2012a). The one of the best documented example of membrane filtration treatment plant is the Mery Sur Oise plant in the northern part of Paris which use NF technology since 1999 to remove pesticide and other organic pollutants from Oise River

for drinking water production. Its performance is very satisfactory and successful to eliminate pesticides and other organic pollutants (Cyna et al., 2002).

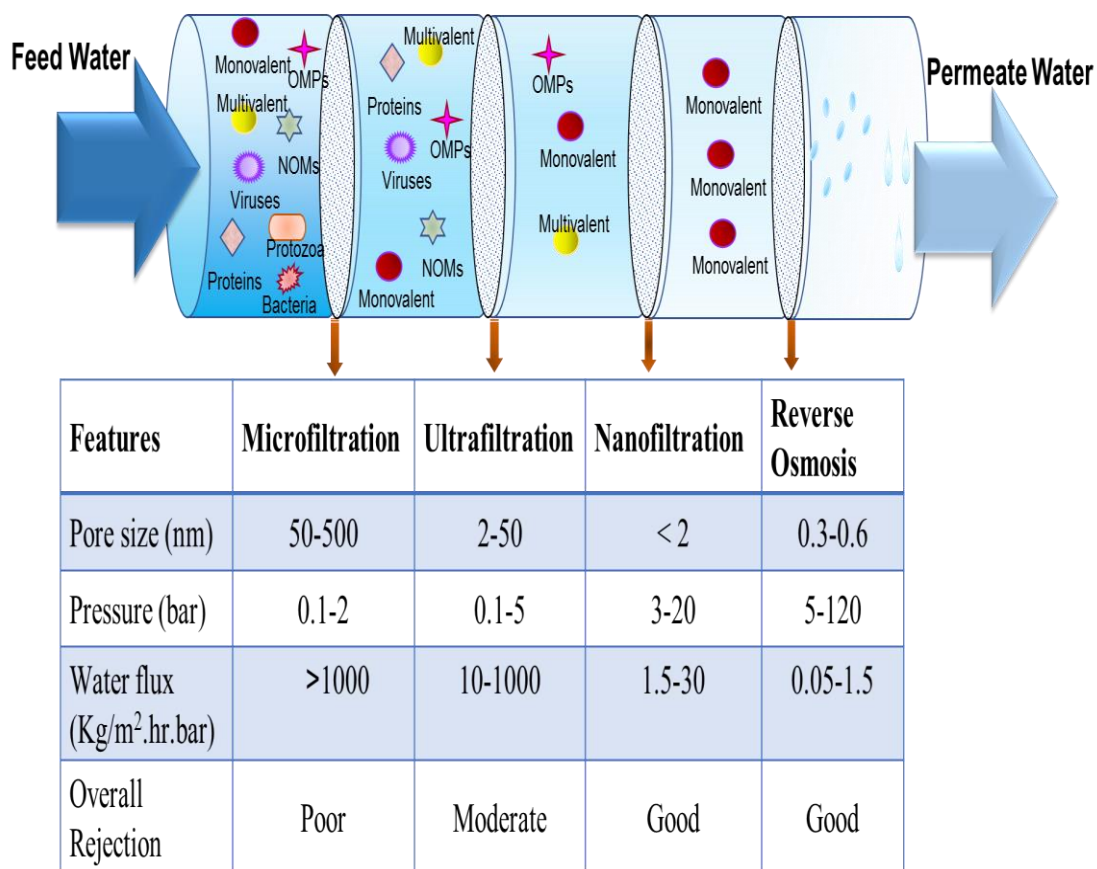


Fig. 1.2 Typical properties of pressure driven membranes

After the introduction in the late 1980s for water softening and organic removal (Eriksson, 1988), the application range of NF has extended in drinking water production such as removal of pesticides (Plakas and Karabelas, 2012), endocrine disruptors and pharmaceuticals (Yoon et al., 2007), arsenic (Waypa et al., 1997) and chemicals (bisphenol A) (Zhang et al., 2006), and desalination (Semiati, 2000). NF can be employed as a final process in treatment train which can offer the higher quality of drinking water production than UF, and lower pressure (1.5-30 bars) and energy consumption than RO (5-120 bars) (Mohammad et al., 2015). Since molecular weight cut off (MWCO) (lowest molecular weight (MW) of solute that greater than 90% of solute is retained by membrane) of NF membranes are often the same range as MW of OMPs (200-400 Da), NF are considered as promising method for OMPs removals

(Konstantinos V Plakas et al., 2006; Kiso et al., 2000). Polymeric membranes overcome the membrane market and are mostly applied in NF membrane technology because of their easy and cheap fabrication (Alpatova et al., 2013; Fane et al., 2011). However, the hydrophobic surface and malleable characteristic of polymeric membranes are the major drawbacks of using them in membrane applications (B. Van der Bruggen et al., 2008; Lin, 2017; Wu et al., 2008). Modification of polymeric membrane surface with hydrophilic materials can be potential solutions to overcome current NF membrane issues.

Regarding selection of hydrophilic material to modify polymeric membrane, UiO-66, a new class of highly porous materials of metal organic framework (MOFs), has a hydrophilic nature, which improve water flux in membrane application (Ma et al., 2017). UiO66 membrane also shows a good membrane stability, high resilience to mechanical stress and be easily handled (Denny and Cohen, 2015) because the organic linker of UiO66 could provide a platform for chemical modifications of the surface, which offer a better adhesion to polymeric membrane compared to other inorganic materials (J. R. Li et al., 2012). Nonetheless, agglomeration and aggregation of UiO-66 particles on membrane surface decrease the smoothness of membrane surface and block the membrane pores, which reduce water flux (Ahmed and Jung, 2014).

The combination of UiO66 with appropriate materials could greatly improve its physio-chemical structure in membrane application. Graphene oxide (GO), a product after oxidation of exfoliated graphite, GO has high hydrophilicity and dispersibility due to the oxygen containing functional groups including carboxyl, epoxy, hydroxyl groups on its panel and edge (Compton and Nguyen, 2010). Those various oxygen functional group of GO has ability to improve UiO66 formation by suppressing UiO66 aggregation, increasing dispersion force within the UiO66, and controlling their physical-chemical properties including morphology, size and structure (Ma et al., 2017). This UiO-66_GO composite is expected to improve NF surface hydrophilicity and smoothness, resulting in water flux enhancement. Thus, UiO-66/GO NF membrane can

produce a higher water capacity from the feed water-containing OMPs comparing to commercial NF membrane.

1.2 Knowledge Gap and Technical Limitations

UiO66_GO membrane give higher flux and anti-fouling compared to pristine PES membrane because of its hydrophilicity and membrane smoothness (Ma et al., 2017; Ying et al., 2017). However, they only applied UiO66_GO composite on ultrafiltration membrane to reject macromolecule compounds such as humic acid and protein. To date, there has been no report on application of UiO66_GO composites on NF membrane: membrane synthesis method, water flux and OMP rejection are remained unknown.

Moreover, humic acid which is the main composition in natural feed water will be adsorbed in membrane pores and then generate the cake layer on membrane surface, causing the serious membrane fouling and flux decline (Lee et al., 2001). A total control of fouling is compulsory to reduce the operational and maintaining costs of membrane and increase membrane stability and lifetime for sustainable applications. Currently, backwashing is the most popular membrane cleaning by running a reversed flow pushed from the permeate side to the feed side of a membrane. But this cleaning method may loosen or wash out of UiO66_GO composites that were deposited on the NF membrane surface and decrease composite membrane stability. UiO-66 also has a photocatalytic activity with the band gap about 3.76 eV (Musho et al., 2014), might be able to degrade humic acid fouling membrane but the photocatalytic activity of UiO66_GO composite is unknown and need to be investigated. Thus, the effective method to clean and recovery the fouled UiO66_GO NF membrane by photocatalysis not yet confirmed and need to be studied.

1.3 Objectives

The main objective of this study was to develop a novel photocatalytic NF membrane using Zr-based organic framework enhanced by graphene oxide for water and wastewater treatment. The specific objectives are listed as following:

1. To present a facile hydrothermal method for preparing UiO-66_GO nanocomposites with different GO loading and characterize their physio-chemical properties (chapter 3).
2. To investigate the enhancing effect of GO on the photocatalytic activity of UiO-66 and report for the first time on the photodegradation of a persistent OMP (CBZ) (chapter 4).
3. To test the photodegradation of CBZ with different GO contents in the composites, catalyst doses and solution pH and the optimum conditions were underlined (chapter 4).
4. To introduce the pressure-assisted self-assembly (PASA) method to fabricate UiO-66_GO/NF membranes and confirm the membrane stability with different loadings of UiO-66_GO nanocomposite (chapter 3).
5. To evaluate the effect of UiO66_GO nanocomposite on water flux improvement of NF membranes, check stability of the composite membranes after five-time washes and point out the optimum loading of UiO66_GO composite on NF membrane (chapter 5).
6. To investigate the effect of UiO66_GO nanocomposite on the flux recovery and anti-fouling properties of NF membranes (chapter 5).
7. To determine the rejection of various OMP groups with different physio-chemical properties by UiO66_GO/ NF membranes (chapter 5).
8. To examine the effects of photocatalysis on regeneration of UiO66_GO/NF membranes in order to degrade irreversible foulant and improve flux recovery (chapter 5).

1.4 Structure of the Thesis

This study has been divided into seven chapter as shown in **Fig. 1.3** and briefly summarize as following:

- **Chapter 1:** to provide the overall background information and the current problem statements and figure out the importance and objective of this study.

- **Chapter 2:** critical review on recent development of photocatalytic membranes for water treatment application.
- **Chapter 3:** to describe the synthesis and characterization methods of material and membrane.
- **Chapter 4:** to confirm the photocatalytic activity of Zr-based metal organic framework enhanced by graphene oxide.
- **Chapter 5:** to evaluate the filtration performance of UiO66_GO NF membrane including synthesis method, its stability, water flux, OMP rejection.
- **Chapter 6:** to recovery the fouled UiO66_GO NF membrane by photocatalysis.
- **Chapter 7:** to summarize the main findings and suggest the recommendations for further research.

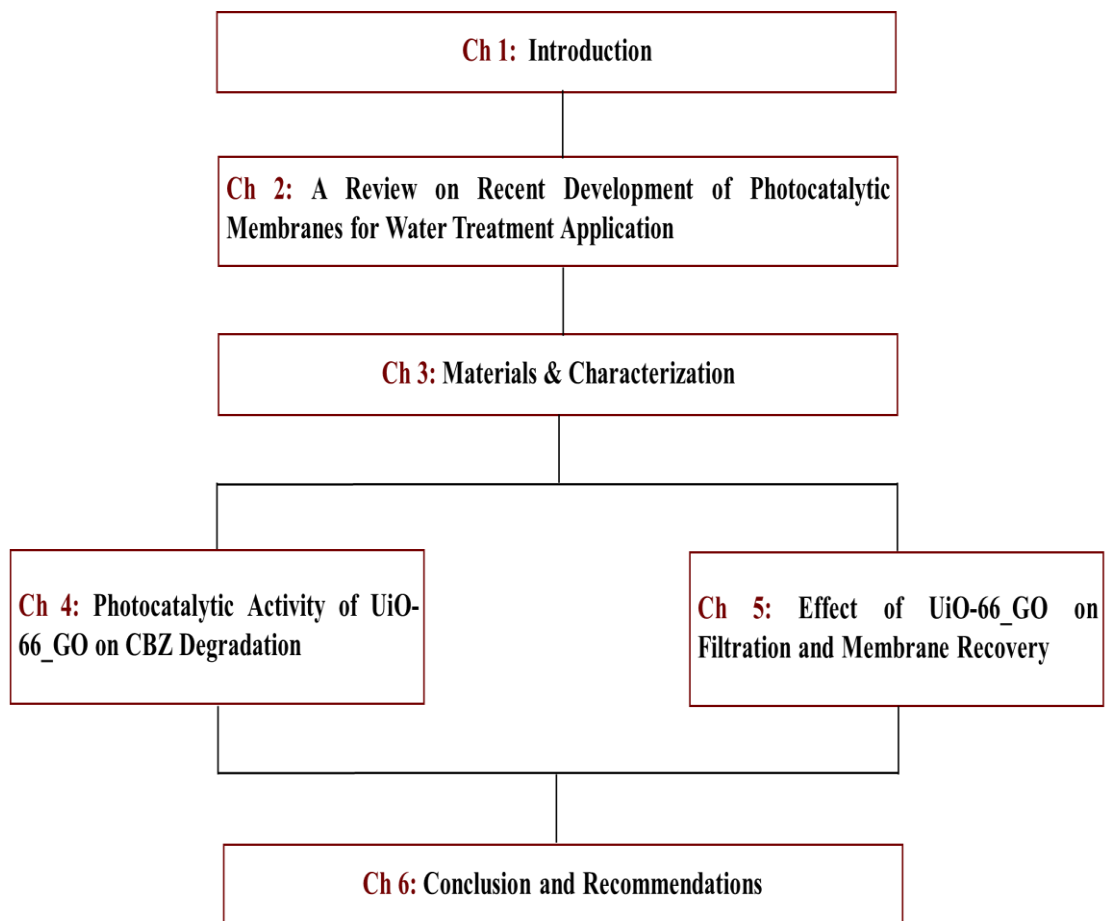


Fig. 1.3 The structure of the thesis

CHAPTER II

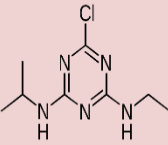
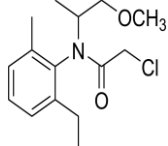
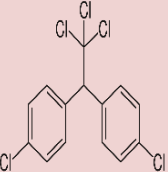
A Review on Recent Development of Photocatalytic Membrane for Water Treatment Application

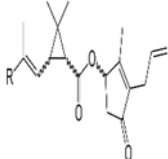
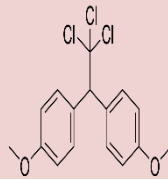
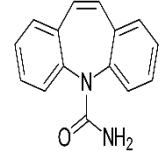
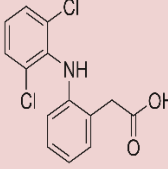
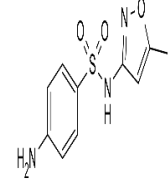
2.1 Organic Micropollutants

2.1.1 Organic Micropollutants and Their Environmental Risks

In recent decades, occurrence of organic micropollutants (OMPs) including pesticides, pharmaceuticals, personal care products, plasticizer, endocrine disruptors and other emerging compounds in aquatic environment has become increasing environmental concerns due to their toxicity and long persistence in environment. Because of directly discharge and ineffective removal of OMPs by conventional wastewater treatment, wastewater effluent, surface water, ground water and drinking water show from ng/l to µg/l (Luo et al., 2014). Amongst other OMs, pesticides and pharmaceuticals deserve a particular concern because it has a high solubility, poor degradation, and high toxicity (Table 2.1).

Table 2.1 The physical and chemical properties of commonly used pesticides

Category	Compound	Chemical structure	MW g/mol	Toxicity mg/kg/d	Solubility mg/l (20°C)	Degradation n DT ₅₀ (d)
Pesticides	Atrazine: C ₈ H ₁₄ ClN ₅		215.7	0.035	35	60
	Metolachlor: r:C ₁₅ H ₂₂ Cl NO ₂		283.8	0.15	530	90
	DDT: C ₁₄ H ₉ Cl ₅		354.4	0.0005	0.001	Up to 15 years

	Allethrin: $C_{19}H_{26}O_3$		302.4		4.6	1-2 years
	Methoxychlor: $C_{16}H_{15}Cl_3O_2$		345.6	0.005	0.1	120
Pharmaceuticals	Carbamazepine: $C_{15}H_{12}N_2O$		236.2	0.013	17.7	40
	Diclofenac: $C_{14}H_{11}Cl_2NO_2$		296.1	N/A	2.37	20
	Sulfamethoxazole: $C_{10}H_{11}N_3O_3S$		253.2	N/A	1000	17.1

Note: N/A: Not Available information

2.1.2 Standard Regulation

To ensure a safe drinking water for public consumer, drinking water standard regulations has been established with the main target of restricting the level of pesticides in the water. According to the European Council Directive 98/83 (1998), the residue limits and guideline levels of total pesticides were assigned in maximum concentration of 0.5 $\mu\text{g}/\text{l}$ and 0.1 $\mu\text{g}/\text{l}$ for individual pesticides and their relevant decay, metabolites, and reaction products.

2.1.3 OMP removal methods

Because of risk and hazard of OMs to human, animal, and environment, the various OM removal methods have been studied and developed.

Some conventional treatment processes including coagulation, flocculation, and sand filtration are ineffective to remove OMs (William et al., 1996; Ternes et al., 2002; Verstraeten et al., 2002). Chlorination and ozonation showed highly effective in removing the concentration of some types of pesticides e.g. glyphosate and aminomethylphosphonic acid (AMPA) (Hopman et al., 1995; Lang & Post., 2000; Brosillon et al., 2006). However, one of the weak points of water chlorination and ozonation process is the production of disinfection by-products (DBPs) which harmful to human health (Krasner et al., 2006; Richardson, 2003; Mills et al., 1998). UV irradiation alone at dose used in water treatment isn't effective to OMPs in water (Bolton and Cotton., 2008; US EPA, 2006; Lund-Hoie and Friestad., 1986). Activated carbon adsorption is popular technique for elimination of organic micro-pollutants because of its economic benefits and simply application (El-Temseh et al., 2016; Gupta and Ali., 2008; Paknikar et al., 2005). By the way, this method also has the significant problems mainly related to its saturation, toxic chemical by-products, and difficulties in small polar compound removal is still challenging (Plakas and Karabelas, 2012; Ormad et al., 2008; Jiang and Adams, 2006). Because of characteristics of OMPs with high solubility in water and low Henry's law constant suggested that it's not expected to be able to remove by air stripping (Jonsson et al., 2013; SRC 2012).

2.2 Membrane filtration technology

2.2.1 Applications in Water Treatment

Over past 30 years, membrane filtration showed effectively deal with the weakness in the conventional treatment process by removing aquatic substances (natural organic matters, pathogen, viruses, etc.) and micro-pollutants (arsenic, pharmaceutical, pesticides, etc.) in the water (Chew et al., 2011; Jacangelo et al., 1997). This membrane system is growing much attention as one of the most promising separation methods for water purification because of their effective potential, no chemical treatment require and low environmental footprint (Peter-varbanets et al., 2009) resulting in increasing the worldwide popularity of improving water quality and meeting the standard regulation for drinking water (WHO, 2011). Various membrane

filtration techniques have been applied in water treatment, particularly, pressure driven membranes.

Pressure-driven membranes are pressure exerted systems on the feed side of membrane to separate feed solute into permeate and a retentate such microfiltration (MF), ultrafiltration (UF), nanofiltration (NF) and reverse osmosis (RO). Different pressures are applied on feed and permeate side serves as driving force to transport the feed solute through the membrane. Permeate is considered as a clean water and retentate is concentrated solution which need to be disposed of or treated by other methods. To select the proper process membrane filtration, it is very important, which not only focus on quality of water but also the treatment cost. The comparative features of four pressure driven membranes were summarized in **Table 2.2**.

Table 2.2 Comparative features of pressure driven membrane (Bart Van der Bruggen et al., 2003).

Features	RO	NF	UF	MF
Pore Size (nm)	0.3-0.6	<2	2-50	>50-500
Water permeability (kg/m².hr.bar)	0.05-1.5	1.5-30	10-1,000	>1,000
Operational pressure (bar)	5-120	3-20	0.1-5	0.1-2
Rejection:				
▪ Particles	Yes	Yes	Yes	Yes
▪ Macromolecules	Yes	Yes	Yes	No
▪ Small organic compounds	Yes	Yes/No	No	No
▪ Multivalent ions	Yes	Yes	Yes/No	No

▪ Monovalent ions	Yes	No	No	No
Overall rejection ability	Good	Good	Moderate	Poor
Separation mechanism	Solution-diffusion	Sieving, Charge-effects	Sieving	Sieving
Membrane fouling	yes	yes	yes	yes
Applications	Desalination; Ultrapure water	Removal of hardness, metal ions, micropollutants	Removal of viruses, colloid, macromolecules	Clarification; Pretreatment

2.2.2 Nanofiltration

Nanofiltration (NF), a pressure driven membrane, is growing much attention as one of the most promising separation methods for water treatment application because of its high separation efficiency, facile operation, compact design and low energy consumption (Vatanpour et al., 2014). Introduction in late 1980s in purpose of water softening and organic removal (Eriksson, 1988), the application range of NF has extended in drinking water production such as removal of pesticides (Plakas and Karabelas, 2012), pharmaceuticals (Yoon et al., 2007), arsenic (Waypa and Elimelech, 1997) and chemicals (Zhang et al., 2006), and desalination (Semiat, 2000).

2.2.2.1 Separation Mechanism

Separation mechanism of NF is a complex process which involve with the membrane surface characteristics and membrane pore size. The combination of size exclusion (steric effects), charge repulsion (Donnan effects), adsorption and dipole interaction are highly affected on the rejection of NF (Mohammad et al., 2015).

Size exclusion or sieving mechanism basically depend on molecules size and membrane pore size. MW is the simplest parameter to indicate the retention of molecule by NF membrane. The larger MW gives the higher rejection efficiency. NF membrane showed positive results to retain the solute with molecular weight cut-off (MWCO) from 300 to 500 Da (Mohammad et al., 2015). MWCO is defined as lowest molecular weight (MW) of solute that greater than 90% of solute is retained by membrane. However, MW is only a helpful indicator for correlative retention and cannot recommend for modeling work because the geometry of molecule such as molecular length and width are also good parameters to estimate the molecule rejection by NF membrane (Chen et al., 2004).

Since NF membrane have ionic groups such carboxylic and sulfonic acid groups, resulting in surface charge, when the feed solution is presented. The interaction of charged molecules and charged membrane retains the ionic compound (Donnan exclusion). This separation mechanism (charge effects) allows the ion retention on membrane surface, even though the ions size is below the membrane pore size. The divalent ions (sulphate and hardness) are reported more effectively removed than monovalent ions (Bruggen et al., 2003).

Polar effect is one of the most important physicochemical effects in NF separation when the polar organic compounds are the target compound to be retained (Matsuura and Sourirajan, 1973). It was concluded that retention of polar solutes is negatively influenced by interaction of solutes and membrane surface and the greater polarity moment gave the higher retention (Van Der Bruggen et al., 1998). The possible explanation of this conclusion is correlated to electrostatic interaction. Once the opposite charge of dipole is attached to membrane, molecule is directed straight-through membrane pore and permeate more easily into the pore structure. As the results, polarity effect of solute is necessary for membrane which pore size bigger than compound size (Van Der Bruggen et al., 1999; B. Van Der Bruggen et al., 2001; Košutić & Kunst, 2002).

Many studies claimed that there is significance of adsorption phenomenon on rejection during filtration process due to hydrophobic interaction and hydrogen bonding. Membrane hydrophobicity was measured by membrane contact angle and solute hydrophilicity/hydrophobicity was measured by its octanol water partition coefficient ($\log K_{ow}$ or $\log P$) whereas $\log K_{ow}$ value is higher than 2 is considered as hydrophobic compound. Based on Kiso et al. who investigated the relationship between $\log K_{ow}$ and adsorption by using hollow fiber NF membrane, reported that there was significant correlation between adsorption and $\log K_{ow}$ value (Kiso et al., 2000; Kiso et al., 2001).

2.2.2.2 Types of NF Membrane and Its Characteristics

Solute rejection by membrane process is greatly correlated to the type of membrane chosen. To select appropriate membrane, there are some parameters to be considered such as MWCO, membrane porosity, membrane surface charge, membrane material and stabilized salt rejection (degree of ions rejection). Some commercial NF membranes with their manufacturing specifications were listed in **Table 2.3**.

Table 2.3 Types of NF membrane with their specifications (Mohammad et al., 2015)

Manufacturer	Type	Pore size/MWCO	Polymer	Feed	pH	Flux (GFD/psi)	Rejection
Dow Filmtec™	NF270	~200-400 Da	Polyamide-TFC	Surface/Groundwater	2-11	72-98/130	99.2% MgSO ₄
	NF90	~200-400 Da	Polyamide-TFC	Industrial/Commercial Water	2-11	46-60/130	99.0% MgSO ₄
	NF	~200-400 Da	Polyamide-TFC	Foods/Beverages	2-11	26.5-39.5/130	99.0% MgSO ₄
GE Osmonics™	Duracid	~150-200 Da	Polyamide-TFC	Surface/Groundwater	0-9	10-19/225	98.0% MgSO ₄
	DL	~150-300 Da	Polyamide-TFC	Foods/Industrial Water	2-10	28/220	98.0% MgSO ₄
	HL	~150-300 Da	Polyamide-TFC	Industrial/Commercial Water	3-9	39/100	98.0% MgSO ₄
	DK	~150-300 Da	Polyamide-TFC	Foods/Industrial Water	2-10	22/100	96.0% MgSO ₄
	CK	~2,000 Da	Cellulose Acetate	Industrial/Commercial Water	2-8	28/200	94.0% MgSO ₄
Synder™	NFX	~150-300 Da	Polyamide-TFC	Foods/Industrial/Wastewater	3-10.5	20-25/110	99.0% MgSO ₄ (40% NaCl)
	NFW	~300-500 Da	Polyamide-TFC	Foods/Industrial/Wastewater	4-10	45-50/110	97.0% MgSO ₄ (20% NaCl)
	NFG	~600-800 Da	Polyamide-TFC	Foods/Industrial/Wastewater	4-10	55-60/110	50.0% MgSO ₄ (10% NaCl)
	NDX	~800-1,000 Da	Polyamide-TFC	Foods/Industrial/Wastewater	3-10.5	45-55/110	90.0% MgSO ₄ (30% NaCl)
TriSep™	TS80	~150 Da	Polyamide-TFC	Foods/Industrial/Wastewater	2-11	20/110	99.0% MgSO ₄ (80-90% NaCl)
	SB90	~150 Da	Cellulose Acetate Blend	Liquid Foods	NA	30/225	97.0% MgSO ₄ (85% NaCl)
	SBNF	~2,000 Da	Cellulose Acetate	Surface Waters	2-11	NA	40-60% NaCl
	TS40	~200 Da	Polypiperazine-amide-TFC	Foods/Industrial/Wastewater	2-11	20/110	90.0% MgSO ₄ (40-60% NaCl)
	XN45	~500 Da	Polypiperazine-amide-TFC	Foods/Industrial/Wastewater	2-11	35/110	95.0% MgSO ₄ (10-30% NaCl)
Microdyn Nadir™	NP010	~1,000 Da	PES	Foods/Industrial/Wastewater	0-14	>200 l/h/40 bar	35-75%(Na ₂ SO ₄)
	NP030	~500 Da	PES	Foods/Industrial/Wastewater	0-14	>40 l/h/40 bar	35-75%(Na ₂ SO ₄)

2.2.2.3 Examples of Water Treatment Plants Using NF Membranes

NF have reported successfully installation in water treatment plant for drinking water production in some countries as listed in **Table 2.4**. The best documented example of NF treatment plant is the Mery Sur Oise plant in the northern part of Paris which use NF technology since 1999 to remove pesticide and other organic pollutants from Oise River for drinking water production. Its performance is very satisfactory and successful to eliminate pesticides and organic matters (Cyna et al., 2002).

Table 2.4. Some case study of water treatment plant using NF technology (Plakas & Karabelas, 2012a).

Location	Capacity (m ³ /d)	Application
Boca Raton, Florida, USA	152, 000	Groundwater softening
Mery-sur-Oise, Paris, France	140,000	Pesticide removal for drinking water supply
Heemskerk, Holland	57,000	Surface water treatment for drinking water supply
Bajo Almanzora, Andalusia, Spain	30,000	Groundwater softening
Debden Road, Saffron Walden, England	30,000	Pesticide removal for drinking water supply

The conventional NF treatment plant simply consists of pre-treatment (acid addition, antiscalant, sand filtration), membrane filtration (NF), and post-treatment (aeration, disinfection) as shown in **Fig. 2.1**.

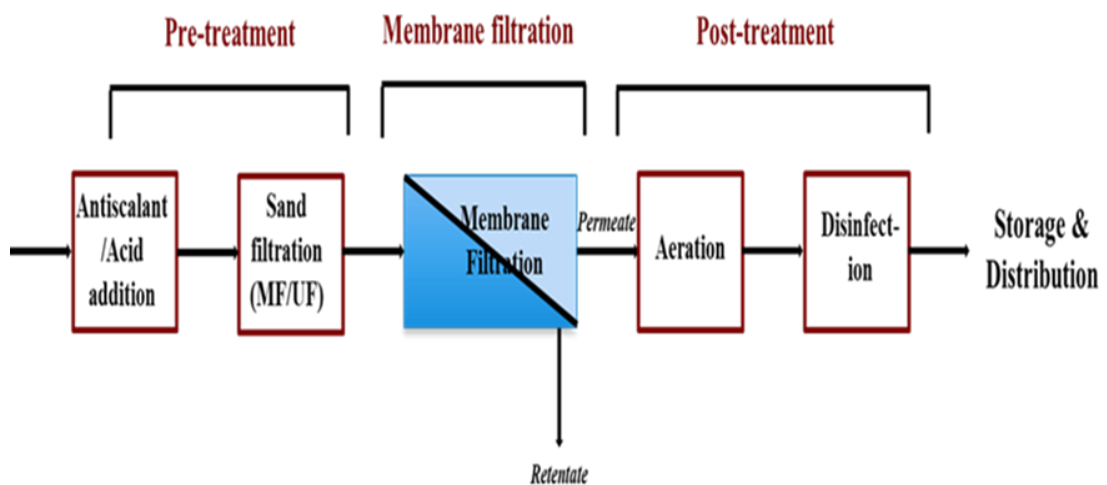


Fig. 2.1 Conventional water treatment system using NF membrane

2.2.2.4 Problems in NF Technology

Drinking water production, which is the largest application of NF, recently faces some challenges such as insufficient separation, membrane fouling, and further treatment of concentrate.

▪ Insufficient Separation

Rejection of uncharged solute by NF membranes can be roughly estimated by sigmoidal rejection curve (rejection is the function of MW) (**Fig. 2.2**), resulting in an insufficient rejection between compounds based on their various MW (Van der Bruggen and Vandecasteele, 2002). Rejection is also related to other physicochemical of the membrane including charge interaction, hydrophobicity, and polarity. Consequently, the permeate from the process may contain molecules with variable MW, both below or above the pore size of the membrane and the actual rejection needs to be investigated. For ion rejection by NF, it was reported that rejection of multi-valent ions is higher than monovalent ions. The rejection of divalent ions which are the same charge of NF membrane can be achieved greater than 95% while monovalent ion rejection is between 20 and 80% (Schaep et al., 2001).

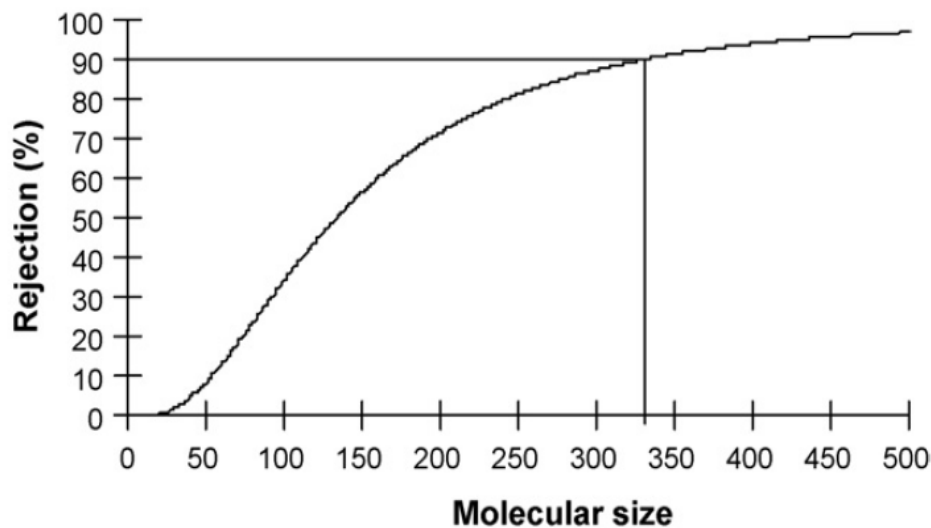


Fig. 2.2 Rejection curve for rejection of uncharged solutes with NF membrane (Schaep et al., 2001).

- **Membrane Fouling**

Fouling is one of the main challenges in any membrane separation technology, particularly for NF where fouling take place in the nanoscale. The undesirable adsorption and deposited of organic solutes, inorganic solutes, biological solids and colloids on membrane surface play a major role in NF membrane fouling (B. Van der Bruggen et al., 2008). The characteristics of membrane surface such as hydrophilicity and roughness are the main factor in fouling phenomenon (Mo & Ng, 2008). Membrane fouling causes variety of problems including pretreatment requirement, flux decline, membrane cleaning, feed water loss, limited recoveries, decrease membrane stability and short lifetime of membrane (Van der Bruggen, 2008). A total control of fouling is compulsory to reduce the operational and maintaining costs of membrane and increase membrane stability and lifetime for sustainable applications.

- **Treatment Concentrates**

The generation of concentrate after separation process is the common problem for membrane filtration system, including NF. Concentrate or retentate is unwanted by-product during water purification process. The concentrate compositions are similar to the compositions of the feed water but with increased concentration. Since the typical function of NF membrane is separation, neither destruction nor transformation, those unwanted concentrates have to be disposed or further treated. Incineration, reuse, discharge directly or indirectly to surface and ground water, direct or indirect landfill disposal, and further treatment by removal of contaminants are the possible methods to deal with concentrate. However, the release of micropollutants to concentrate stream was considered as a risk (Nghiem and Schäfer, 2006) and integration of appropriate treatment method with membrane system is the most attractive option that needs a further study.

2.2.3 Photocatalytic Membrane Filtration

NF is growing much attention as one of the most promising separation methods for water treatment application because of its high separation efficiency, facile operation, compact design and low energy consumption (Vatanpour et al ., 2014).

Introduction in late 1980s in purpose of water softening and organic removal (Eriksson, 1988), the application range of NF has extended in drinking water production such as removal of pesticides, pharmaceuticals and other OM_s (Plakas & Karabelas, 2012; Yoon et al., 2007; Zhang et al., 2006) because molecular weight (MW) of OM_s are often in the same as molecular weight cut-off (MWCO) of NF membrane from 200 to 500 Da (Mohammad et al., 2015). Besides its advantages, membrane fouling is biggest challenge of NF (Van der Bruggen and Vandecasteele, 2002) and further developments of this system to deal with these issues are required.

Photocatalytic membrane is an integration of photocatalysis with membrane filtration system. Basically, during photocatalytic process, the refractory organics, a membrane foulants, are transformed to biodegradable compounds, convert them to carbon dioxide and water (Nan et al., 2010) and remove from membrane surface. This hybrid system is not only combining advantages of their treatment techniques but also extinguish challenges of one another. On one hand, photocatalysis could permanently eliminate the membrane fouling and minimize the concentrated effluent by degradation of pollutants which were retained on membrane surface. Membrane filtration, on the other hand, could separate the fine catalysts from the system for recovery and recycle and retained the toxic by-products which might be generated during photocatalytic process. However, selection of appropriate catalysts to apply in this integrated system is crucial to consider since those catalytic materials should have benefits for both photocatalysis and membrane filtration.

2.3 Metal Organic Framework

Metal organic frameworks (MOFs) are inorganic-organic hybrid porous materials with crystalline structure and large surface area. These materials are constructed through inorganic metal ions as connecting centers and organic moieties as linkers (**Fig. 2.3**, Li et al., 2012) which significantly offer chemical diversity since they can be modified by various functional groups (Wen et al., 2017). Currently, there are about 20,000 different kinds of MOFs have been synthesized by using different methods such

as solvothermal, electrochemical and microwave-assisted heating (Sharma and Feng, 2017).



Fig. 2.3 Schematic diagram of classification porous solids and construction procedures of MOFs

Because of their crystalline nature, structures of MOFs is easy to be characterized by single-crystal X-ray diffraction or powder X-ray diffraction (PXRD) (J. Li et al., 2012). Thermogravimetric analyses (TGA) and nuclear magnetic resonance (NMR) also can be used to characterize their structures (J. Li et al., 2012). MOFs have emerged for about 20 years ago, quickly developed and have attracted a lot attention because of their various potential applications such as adsorption (Khan et al., 2013), gas capture and storage (Kitagawa et al., 2004), molecule separation (Jian-rong Li et al., 2012), catalysis (Kuila et al., 2017), smart sensor (Kreno et al., 2011) and membrane separation (Eddaoudi, 2015). Adsorption, advanced oxidation processes (AOPs) and membrane separation have been sought for applications of MOFs in water treatment.

Among MOF family, UiO-66 which UiO stands for University of Oslo and chemical formula $Zr_6O_4(OH)_4(BDC)_6$ have been reported of having very high stabilities. The UiO-66 showed a high thermal stability above 500 °C and quite resistant to various

solvents such as water, dimethylformamide (DMF), benzene and acetone (Cavka et al., 2008). The structure of UiO-66 remain crystalline even after exposing to high external pressure up to 10,000 kg/cm² (Cavka et al., 2008). With their excellent stabilities and huge surface areas (1187 m²/g) (Cavka et al., 2008), UiO-66 can be a potential candidate among MOFs in water treatment field.

2.3.1 Photocatalytic Property of MOFs

Currently, metal oxides, particularly TiO₂, have been widely used as catalyst because of their high catalytic activity, availability and low cost but low adsorption capacity and poor degradation under visible light are the major challenges of those metal oxides and further researches of new photocatalytic materials have been encouraged to exploit (Dong et al., 2015).

MOF family has unique characteristics in using the photo energy like metal oxide photocatalysts (Hoskins and Robson, 1990) and can be applied as photocatalysts, co-catalysts, and host for photocatalysis (Wang and Wang, 2015). Under light irradiation, the organic linker of MOFs play role as antenna to capture the light to generate electron holes. The electrons get excited from highest occupied molecular orbital (HOMO) to lowest occupied molecular orbital (LOMO) of organic linker and then those photo-excited electrons move to inorganic cluster of MOFs (metal nodes) through a linker to cluster charge transfer mechanism (LCCT) to activate metal node of MOFs, subsequently induce a heterogenous photoredox reaction such water splitting, CO₂ production, and organic pollutant degradation (Wen et al., 2017). Various groups of MOFs have been used as photocatalysts including MOF-5, MIL-53, IRMOF-1, UiO66 and UiO67 under UV irradiation with high photodegradation (Wang et al., 2011; Mahata et al., 2006). Later on, more effort has been made to develop MOF photocatalysts to work under visible light. The study of Long et al. which used an amine-functional UiO66 (UiO66-NH₂) under visible light showed a good result with high efficiency and selectivity such as alcohols, cyclic alkanes, and olefins because its high specific surface area (1207.5 m²/g), low band gap 2.71 eV and various functional

groups (Chavan et al., 2014; Musho et al., 2014a; Long et al., 2012). The photocatalytic mechanism of UiO66-NH₂ photocatalysts was illustrated in Fig. 2.4.

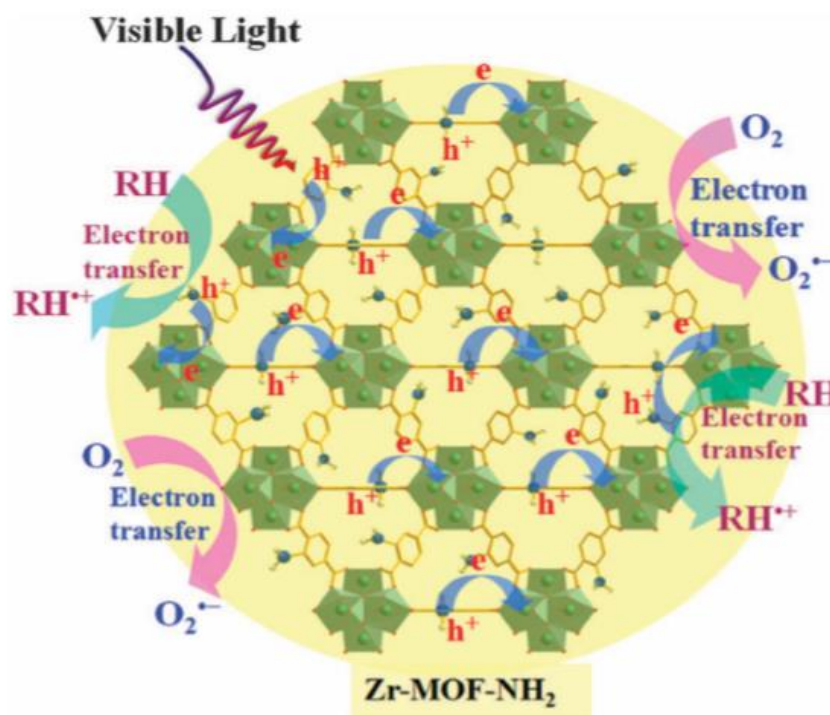


Fig.2.4. Schematic diagram of mechanism of UiO66-NH₂ photocatalyst (Long et al., 2012)

2.3.2 MOF Based Membrane

Inorganic and polymeric membranes are mostly applied in membrane technology (Fane et al., 2011). Despite their advantages including stable pore structure, chemical inertness and temperature resistance, inorganic membranes have been suffering with several problems such as complicated fabrication process, nonselective cracks and prohibitive cost (Safarpour et al., 2014). Polymeric membranes, on the other hand, overcome the membrane market because of their easy and cheap fabrication (Alpatova et al., 2013). However, the hydrophobic surface and malleable characteristic of polymeric membranes are the major drawbacks of using them in membrane applications (Wu et al., 2008). Integrate the composite material with polymeric substrates could be potential options. Pore size and shape, high surface area and variety of chemical modification are the attractive features of MOFs.

Composites MOF particles on polymeric membrane could strengthen the membrane softness and improve their hydrophilic nature. Also, the organic linker of MOFs could provide a helpful platform for chemical modifications of the surface, which offer a better adhesion to polymeric membrane comparing to other inorganic materials (J. R. Li et al., 2012). As the result, some groups of MOFs such as UiO-66, HKUST-1 and MIL53(Fe) in mixed-matrix membrane (MMM) are resilient to mechanical stress and be easily handled (**Fig. 2.5**). From the same report (Denny & Cohen, 2015) demonstrated that crystalline structure of MOF on membrane remained the same as those in MOF particles.

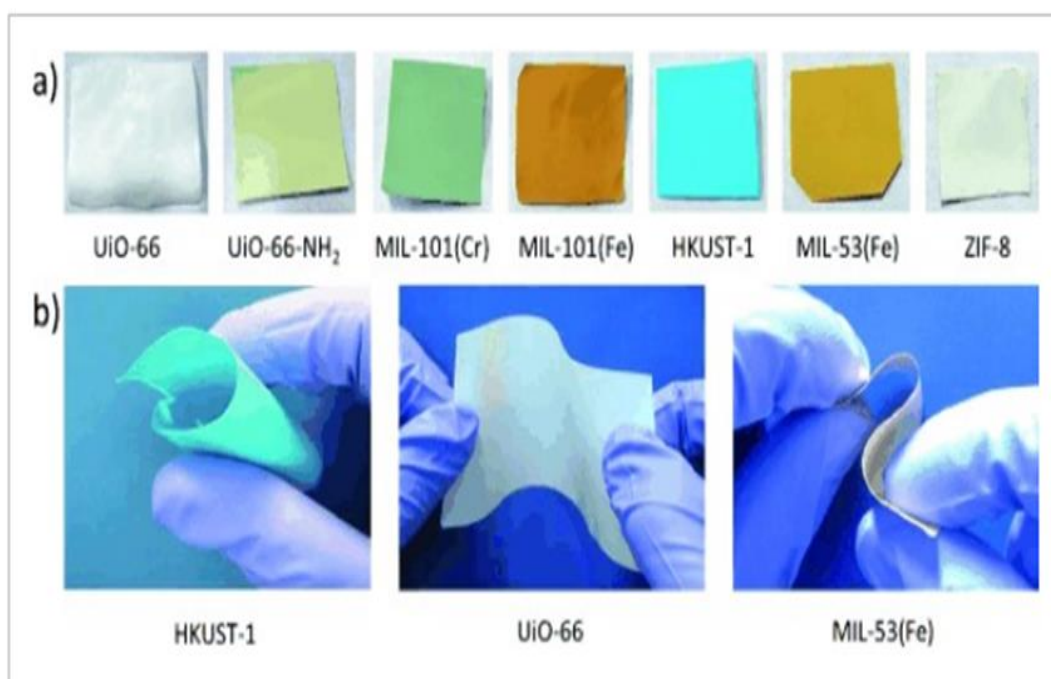


Fig. 2.5. Several of MOFs based mixed-matrix membrane and their strong resilience to mechanical stress (Denny and Cohen, 2015)

2.3.3 Composites of MOF Carbonaceous Materials

Incorporation of MOFs and carbonaceous materials such as activated carbon (Dawoud et al., 2007), carbon nanotube (Anbia & Sheykhi, 2013; Prasanth et al., 2011), and graphene oxide (GO) (Cao et al., 2015; Zhao et al., 2013) as composite materials

could improve MOF properties and expand their applications in water wastewater treatment (**Fig. 2.6**).

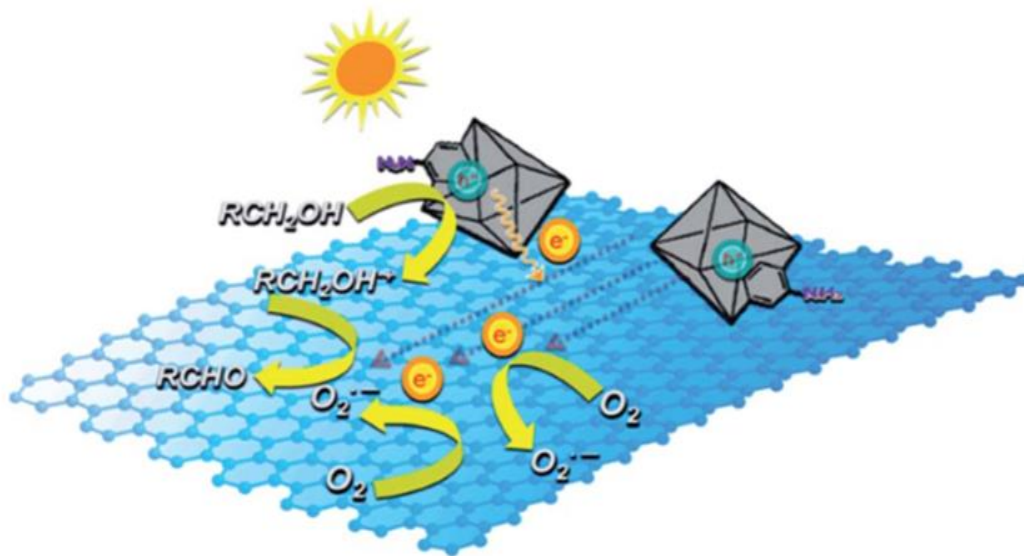


Fig. 2.6 Photocatalytic mechanism of composite UiO66-NH2@GO (Xu et al., 2015)

Recent studies have reported that the synthesis of MOF and GO composites could create new pores between MOF units and GO sheets and their adsorption capacity consequently became higher than parent MOFs (Petit and Bando, 2009). MOFs could anchor to GO layers due to incorporation of metal ions of MOFs and carboxyl groups of GO, then widen the interlayer space and form the porous structure on GO layers (Ma et al., 2017). Also, GO has high hydrophilicity and dispersibility due to the oxygen containing functional groups including carboxyl, epoxy, hydroxyl groups on its panel and edge (Compton and Nguyen, 2010). As the result, GO also has ability to improve MOF formation by suppressing MOF aggregation, increasing dispersion force within the MOFs, and controlling their physical-chemical properties including morphology, size and structure (Ma et al., 2017). The studies of Ma et al and Ying et al reported that UiO-66@GO membrane gave higher flux and anti-fouling compared to pristine polyethersulfone (PES) membrane because of its hydrophilicity and membrane smoothness (Ma et al., 2017; Ying et al., 2017).

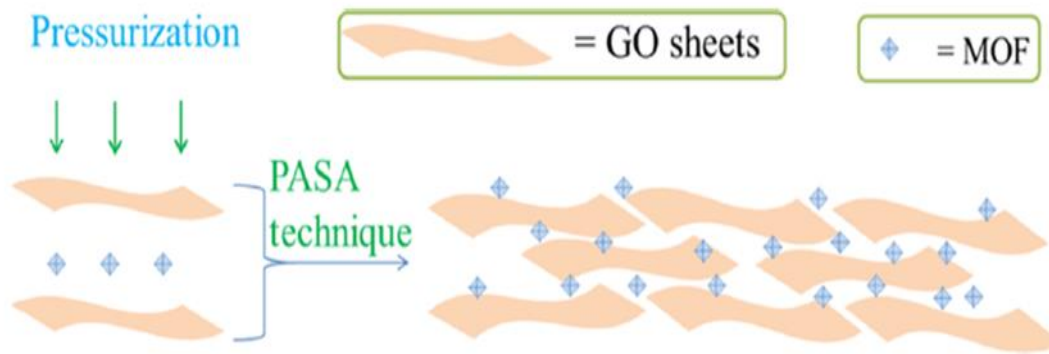


Fig. 2.7 Structure of MOF@GO was synthesized by using a pressure-assisted self-assembly (PASA) method (Ma et al., 2017)

2.4 Conclusion, Limitation and Research Needs

The occurrence of organic micropollutants (OMPs) in aquatic environment has become increasing environmental concerns due to their toxicity and long persistence in environment. The concentration of those OMPs from ng/l to $\mu\text{g/l}$ was found in wastewater effluent, surface water, ground water and even drinking water and need to be eliminated.

Nanofiltration (NF) membrane is growing much attention as one of the most promising separation methods for water treatment application because of its high separation efficiency, facile operation, compact design and low energy consumption. With MWCO often in the same range as MW of OMPs (200-500 Da), NF membrane show a high potential to remove OMPs from water. However, membrane fouling is one of the major challenges in membrane technology, particularly in NF where the fouling take place in nanoscale. Modification of membrane surface and integration with another technique can be potential solutions to deal with currently NF issue.

Photocatalytic membrane is an integration of photocatalysis during membrane filtration process. This hybrid system is not only combine advantages of their treatment techniques but also extinguish challenges of one another. On one hand, photocatalysis could permanently eliminate the membrane fouling and minimize the concentrated effluent by degradation of pollutants which were retained on membrane surface. Membrane filtration, on the other hand, could separate the fine catalysts from the

system for recovery and recycle and retained the toxic by-products which might be generated during photocatalytic process. However, selection of appropriate catalysts to apply in this hybrid system is crucial to consider since those catalytic materials should have advantages for both photocatalysis and membrane filtration.

Metal organic frameworks (MOFs) are inorganic-organic hybrid porous materials which are constructed through inorganic metal ions as connecting centers and organic moieties as linkers. Applications of MOFs in membrane filtration have been increasing due to attractive features of MOFs such as their physico-chemical properties. Composites MOF particles on polymeric membrane could strengthen the membrane softness and improve their hydrophilic nature. Also, the organic linker of MOFs could provide a helpful platform for chemical modifications of the surface which offer a better adhesion to polymeric membrane comparing to other inorganic materials. In photocatalysis, MOFs have a perfect crystalline structure, high BET surface area, various functional groups and show a photocatalytic property with band gap about 3 eV which could overcome inorganic photocatalysts.

GO has high hydrophilicity and dispersibility due to the oxygen containing functional groups including carboxyl, epoxy, hydroxyl groups on its panel and edge. The combination of MOFs and GO are considered as a novel catalyst in photocatalytic membrane. The high conductivity and mobility of charge carriers of GO can enhance the catalytic activity in the system. GO also has ability to improve MOF formation by suppressing MOF aggregation, increasing dispersion force within the MOFs, and controlling their physical-chemical properties including morphology, size and structure. The previous studies claimed that MOFs@GO membrane gave higher flux and anti-fouling comparing to pristine PES membrane because of its hydrophilicity and membrane smoothness.

Up to date, there's no application of photocatalysis during UiO66@GO NF membrane process are reported yet. Since UiO66@GO composites are expected to have a hydrophilicity and give a catalytic property, integrate UiO66@GO membrane with

photocatalytic process will be a novel sustainable method to improve water flux, membrane regeneration, minimize the waste after filtration.

CHAPTER III

Materials and Characterization

3.1 Materials

Atrazine ($\leq 100\%$), carbamazepine ($>98\%$), diclofenac sodium salt ($\leq 100\%$), hydrochloric acid (35–37%), hydrogen peroxide (30–35.5%), methanol (99.9%), p-benzoquinone ($\geq 98\%$), potassium permanganate ($>99.0\%$), sulfamethoxazole ($\leq 100\%$), sulfuric acid ($\geq 95\%$), terephthalic acid ($\geq 98\%$), and zirconium(IV) chloride ($>99.5\%$) were purchased from Sigma-Aldrich (Tokyo, Japan). N,N'-Dimethylformamide (DMF; 99.5%) and potassium peroxodisulfate ($\geq 98\%$) were purchased from Kanto Chemical (Tokyo, Japan). Graphite flakes (325 mesh, 99.8%), isopropanol ($\leq 100\%$), and sodium oxalate ($\geq 99.5\%$) were obtained from Wako Chemical (Tokyo, Japan). Suwannee River humic acid was purchased from the International Humic Substances Society (IHSS, USA). All chemical reagents were of analytical grade and were used immediately after purchase without further purification. Milli-Q water was used as a solvent for all experiments. GLK8MQ UVC lamp (254 nm) was purchased from Sankyo Denki Co., Ltd. (Kanagawa, Japan). Synder polyamide (PA) nanofiltration membrane sheet (NFX) with molecular weight cut off 150-300 Da was supplied by Sterlitech Corporation (Washington, USA) and a Millipore stirred cell (Amicon UFSC40001, Merck-Millipore, Burlington, MA, USA) was used for the filtration experiment.

3.2 Synthesis Methods

3.2.1 GO Synthesis

GO was synthesized by the method of Abdolhosseinzadeh et al with a little modification (**Fig. 3.1**) (Abdolhosseinzadeh et al., 2015). First, 1 g of graphite flakes was added to 50 mL concentrated sulfuric acid (H_2SO_4) while stirring in an ice-water bath. Then, 3 g of potassium permanganate (KMnO_4) was slowly added in the mixture to maintain the temperature under 10 °C. Then, the suspension was stirred for 25 mins and sonicated for 5 mins by ultrasonic bath at room temperature. After repeating the

stirring-sonication process for 12 times, the suspension was diluted by 200 mL distilled water, followed by extra 2h sonication. After sonication, 20 mL of hydrogen peroxide (H_2O_2) was added to the exfoliated graphite oxide suspension and stirred until gas evolution ceased to reduce residual permanganate. Then the mixed solute was washed by 1M hydrochloric acid (HCl) and distill water several times and centrifuged each time for 30 mins at 4500 rpm. Finally, graphene oxide precipitates was freeze-dried at room temperature and kept dried until use.

3.2.2 UiO-66 Synthesis

The synthesis of UiO66 followed the method as described in Ma, et al (Ma et al., 2017) with a little modification (**Fig. 3.2**). First, 1.16 g (5mmol) of zirconium (IV) chloride (ZrCl_4) and 0.83 g (5mmol) of terephthalic acid (H_2BDC) were dissolved in 150 mL of N,N'- dimethylformamide (DMF). Then, the mixture was placed into a 200 mL Teflon liner within a stainless-steel autoclave and kept reaction in a drying oven at 120 °C for 24 h. After the reaction, the product was cooled down in the room temperature, centrifuged and washed with DMF and methanol repeatedly. Afterward, the washed sample was re-dispersed in methanol for 2 days, centrifuged, and dried in a freeze dryer overnight. Finally, the crystalline UiO-66 kept dried until further use.

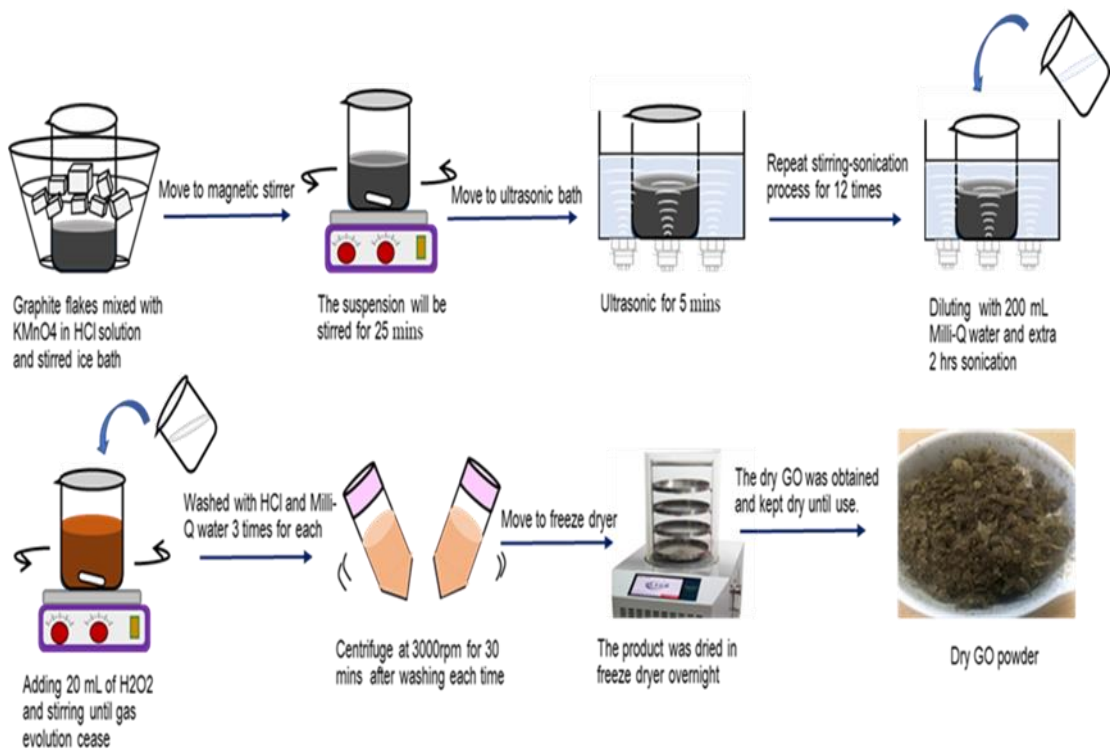


Fig. 3.1 The summary of GO synthesis

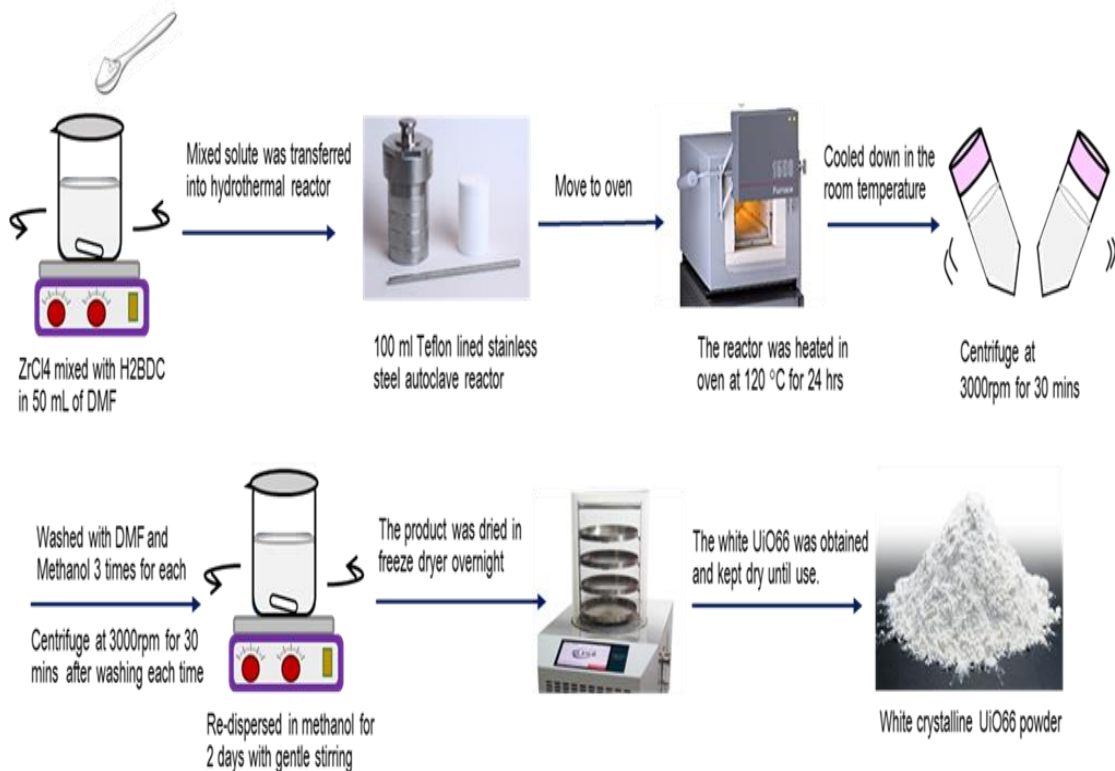


Fig. 3.2 The summary of UiO-66 synthesis

3.2.3 UiO-66_GO Synthesis

To prepare composites of UiO-66 and GO (**Fig. 3.3**), different amounts of GO (0.1, 0.5, 1, and 5 wt.% with respect to the total amount of ZrCl₄ and H₂BDC) were dispersed in DMF (150 mL) with the aid of sonication for 8 h. Each GO solution was then mixed with ZrCl₄ (1.16 g) and stirred overnight. H₂BDC (0.83 g) was then added, and the mixture was stirred until complete dissolution and transferred to the reaction vessel. After solvothermal reaction for 24 h at 120 °C, the obtained composite material was cooled down to room temperature, centrifuged (4,500 rpm for 15 min), and repeatedly washed with DMF and methanol. Finally, the product was dried in a freeze-dryer overnight and kept dry until use. The obtained composites with different GO contents ((0.1, 0.5, 1, and 5 wt.%) are designated as UiO66_GO-0.1, UiO66_GO-0.5, UiO66_GO-1, and UiO66_GO-5, respectively.

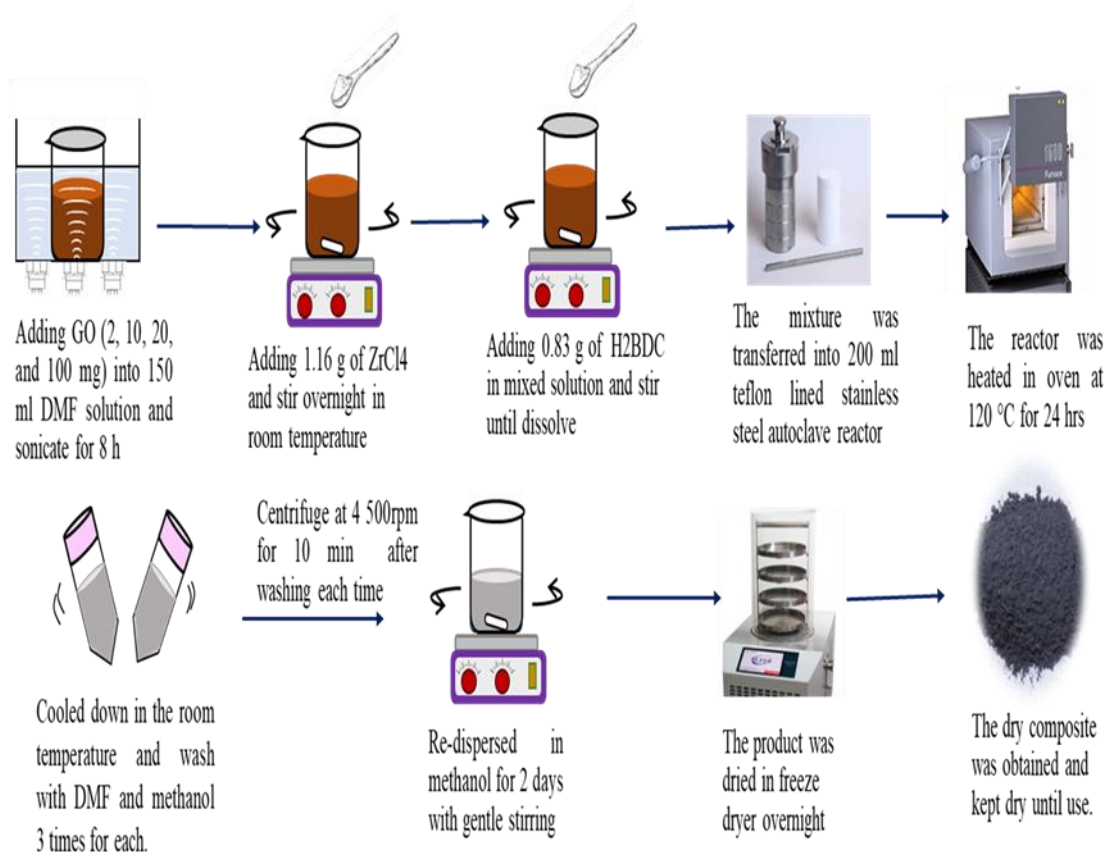


Fig. 3.3 The summary of UiO-66 _GO synthesis

3.2.4 Preparation of UiO-66 _GO NF Membrane

Nanocomposite NF membranes were prepared by pressure-assisted self-assembly (PASA) system. I used a 0.5% GO loading in the composite material because it showed the highest photodegradation rate for carbamazepine as shown in Chapter 4. First, difference contents of UiO-66_GO (5, 10, 15, 20, 30 wt% of pristine NF membrane) were dispersed in MilliQ water with concentration of 0.5 g/l and sonicated for 15 mins. Then the solutions were filtrated through 76 mm in diameter of NFX membrane by stirred cell apparatus at 5 bars. After filtration, the composite membranes was dried in air at room temperature overnight and moved to freeze dryer overnight.

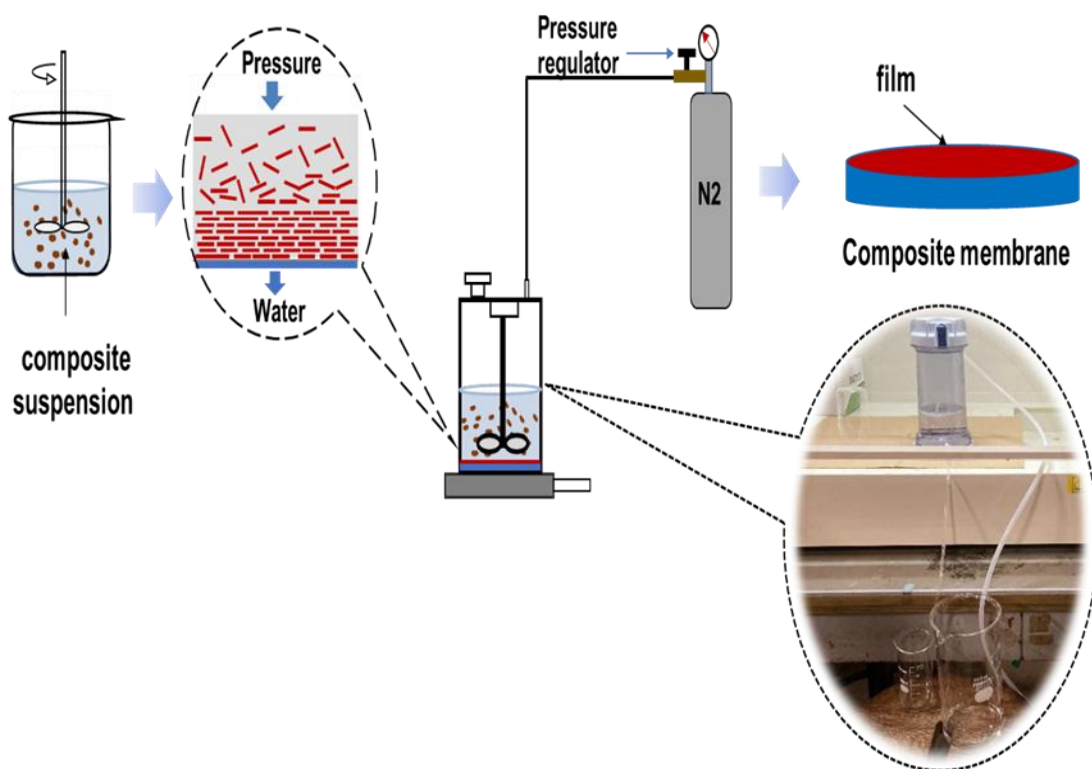


Fig. 3.4 The summary of UiO-66_GO NF membrane preparation

3.3 Characterization of UiO-66_GO composite

The crystalline structures of UiO-66, GO, and UiO-66_GO composites were confirmed by X-ray diffraction (XRD) analysis (Miniflex 600, Rigaku, Japan) in the 2θ range $5\text{--}50^\circ$ employing $\text{Cu-K}\alpha$ radiation ($\lambda=0.15406\text{ nm}$). The surface morphologies, microstructures, and elemental compositions of the prepared catalysts were examined by means of both a scanning electron microscope (SEM; SU9000, Hitachi, Japan) and a transmission electron microscope equipped with an energy-dispersive X-ray spectroscopy attachment (TEM-EDS; JEM-2010 F, JEOL, Japan). Fourier-transform infrared (FTIR) spectra were recorded from samples in KBr pellets in the range $\nu=400\text{--}4,000\text{ cm}^{-1}$ to identify the functional groups present (FTIR 4600, JASCO, Japan). Specific surface areas, principal pore sizes, and pore volumes were determined by recording N_2 adsorption–desorption isotherms on an Autosorb-iQ analyzer (Quantachrome, USA) at 77 K. UV/Vis absorption spectra were measured with a UV-2600 spectrophotometer (Shimadzu, Japan). For further investigation of the optical

properties of the materials, their indirect band gaps were calculated by the Trauc plot method as described in Wang et al. (2016).

3.4 Characterization of UiO-66_GO/NF Membrane

The static water contact angle of the membrane surface was determined with a contact angle meter (Simage AUTO 100, Excimer Inc., Yokohama, Japan) to confirm their hydrophilicity. Three measures of surface roughness were measured by AFM (Asylum CypherS, Oxford Instruments, Abingdon, UK) with a scan area of $3 \times 3 \mu\text{m}$. The measures were average roughness (S_a) and root mean square roughness (S_q), which are the average deviation and standard deviation of peaks and valleys, respectively, and the mean height difference between the highest peaks and lowest valleys (S_y). In addition, the membrane thickness (l) was manually measured by using a scale ruler.

Overall porosity (ε) and mean pore radius (r_m) of the membranes were calculated by the gravimetric method (**Eq. 1**) and the Guerout-Elford-Ferry model (**Eq. 2**), respectively (Safarpour et al., 2014b).

$$\varepsilon = \frac{m_1 - m_2}{lAd_w} \quad (1)$$

$$r_m = \sqrt{\frac{(2.9 - 1.75\varepsilon) 8\eta l Q}{A\varepsilon P}} \quad (2)$$

Here, m_1 and m_2 are the masses of the wet and dry membranes (kg), respectively, l is the membrane thickness (m), A is the membrane surface area (m^2), d_w is water density (10^3 kg/m^3), η is water viscosity ($8.9 \times 10^{-9} \text{ bar s}$), Q is the volume flow rate (m^3/s), and P is the operational pressure (bar).

3.4 Result and Discussion

3.4.1 Crystalline Structure

The pristine graphite used showed a peak at $2\theta \approx 26.52^\circ$ corresponding to an interlayer spacing of 0.34 nm, whereas the most intense peak of GO appeared at $2\theta \approx 10.08^\circ$, corresponding to an interlayer spacing of 0.88 nm (**Fig. 3.5**). The increase in interlayer spacing after oxidation was due to the presence of oxygen functional groups on each carbon layer, as could be confirmed by FTIR (seen **section 3.4.2**), indicating that graphite was oxidized to GO. The XRD pattern of UiO-66 was in good agreement with that reported in the literature (Cavka et al., 2008; Kalidindi et al., 2015).

Similar peaks to those of UiO-66 were observed in the diffraction patterns of the UiO-66_GO composites, but the crystalline peak of GO was not observed due to its low loadings in the composites (0.1, 0.5, 1, and 5 wt.%) and its good dispersion in DMF (Cai and Song, 2007; Cao et al., 2015). The observations suggest that GO did not interfere with the crystalline structure of UiO-66 in the composites.

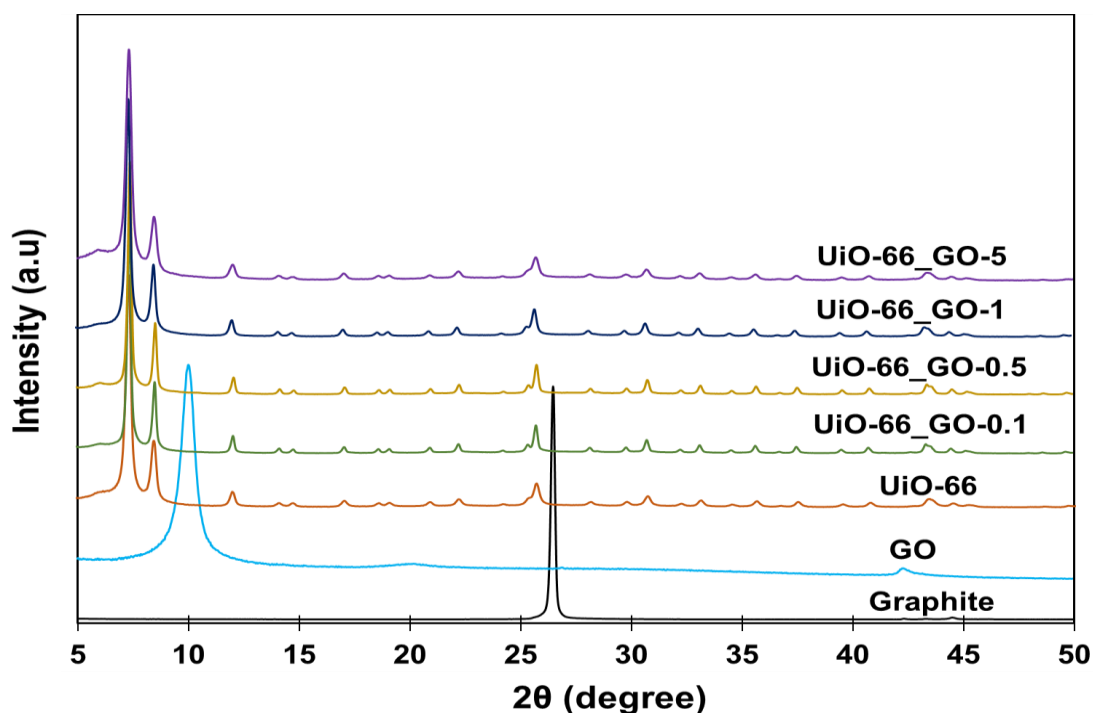


Fig. 3.5 XRD patterns of graphite, GO, UiO-66, and UiO-66_GO composites

3.4.2 Surface Functional Groups

The FTIR spectrum of GO (Fig. 3.6) featured absorption peaks at $\nu=1,734\text{ cm}^{-1}$ due to the C=O bonds of carboxyl and carbonyl groups, $3,365$, $1,625$, and $1,409\text{ cm}^{-1}$ due to the O–H bonds of hydroxyl groups, and $1,050\text{ cm}^{-1}$ due to the C–O bonds of epoxy and alkoxy groups (Guo et al., 2009; C. Yang et al., 2017), confirming the presence of oxygen functional groups. The absorption peaks of UiO-66 showed the fingerprint groups, including the C=O bond of carboxylate groups in the 1,4-benzenedicarboxylic acid (BDC) ligand (1670 cm^{-1}), the O–C–O unit of BDC (1585 and 1395 cm^{-1}), C=C of the benzene ring (1506 cm^{-1}), the O–H bonds of hydroxyl groups (3365 and 746 cm^{-1}), a Zr–O mode (659 cm^{-1}), and Zr–O–C symmetric

stretching (Jin and Yang, 2017; Ma et al., 2017). However, no significant absorption bands of GO were observed in the spectra of the UiO-66_GO composites, which suggests that the oxygen atoms of carboxyl groups (-COO-) on the GO layer are bonded with the coordinatively unsaturated metal complex (Zr-OH/OH₂⁺) of UiO-66 (Petit and Bandoz, 2009; Qiu et al., 2015), similarly to the bonding between the H₂BDC linker and the metal complex in pristine UiO-66. However, the occupation of sites on the coordinatively unsaturated metal complex (Zr-OH/OH₂⁺) of UiO-66 by GO might interfere with the adsorption capacity of CBZ, which would be expected to bind at the same site.

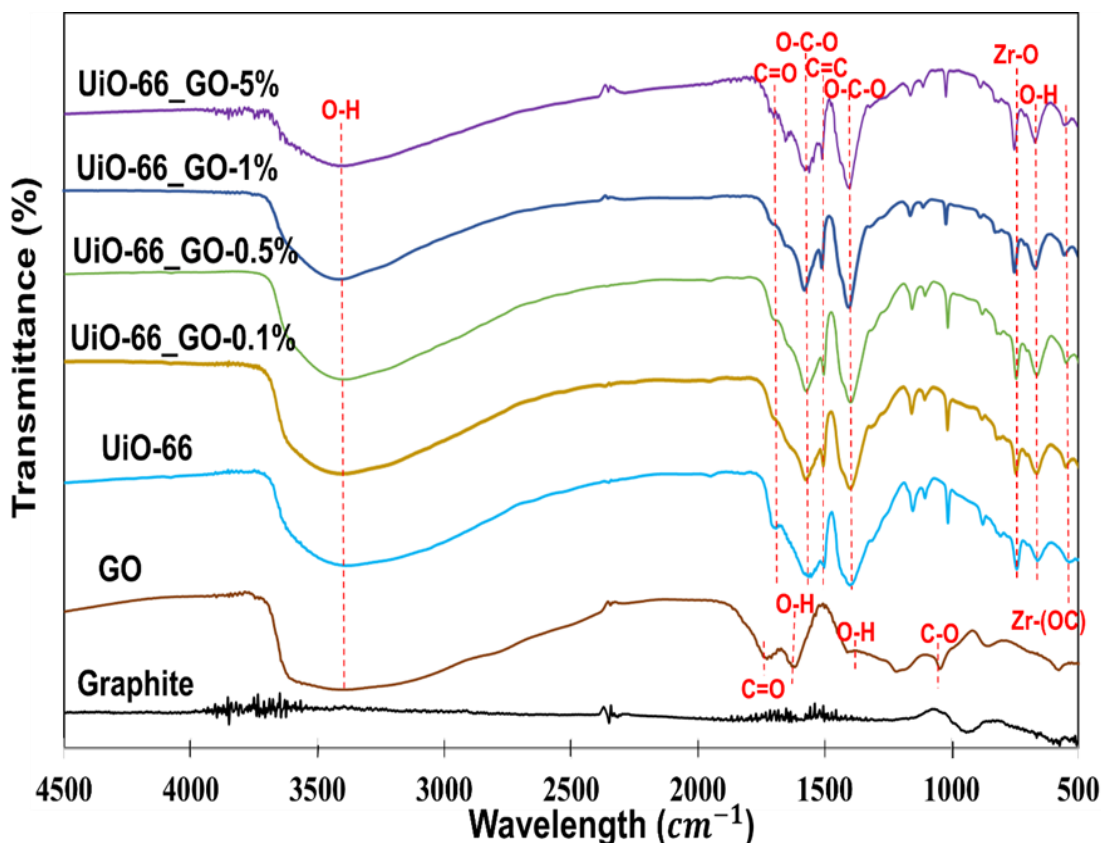


Fig. 3.6. FTIR spectra of graphite, GO, UiO-66, and UiO-66_GO composites

3.4.3 SEM Morphology

SEM images revealed dense layered sheets of GO (**Fig. 3.7A**) and cubic crystalline particles of UiO-66 (**Fig. 3.7B**), the size of the latter (70 nm) being smaller than that reported in the literature (>100 nm) (Cao et al., 2018; Ma et al., 2017). The

smaller particle size is probably due to the different ratio of $ZrCl_4$, H_2BDC , and DMF used in the synthetic process. Moreover, the UiO-66 particle size in the composites decreased with increasing GO content, as shown in **Fig. 3.7**, which may be related to the limited growth space on the GO layers (Ma et al., 2017). Thus, this may be regarded as further evidence for different loadings of GO in composite materials.

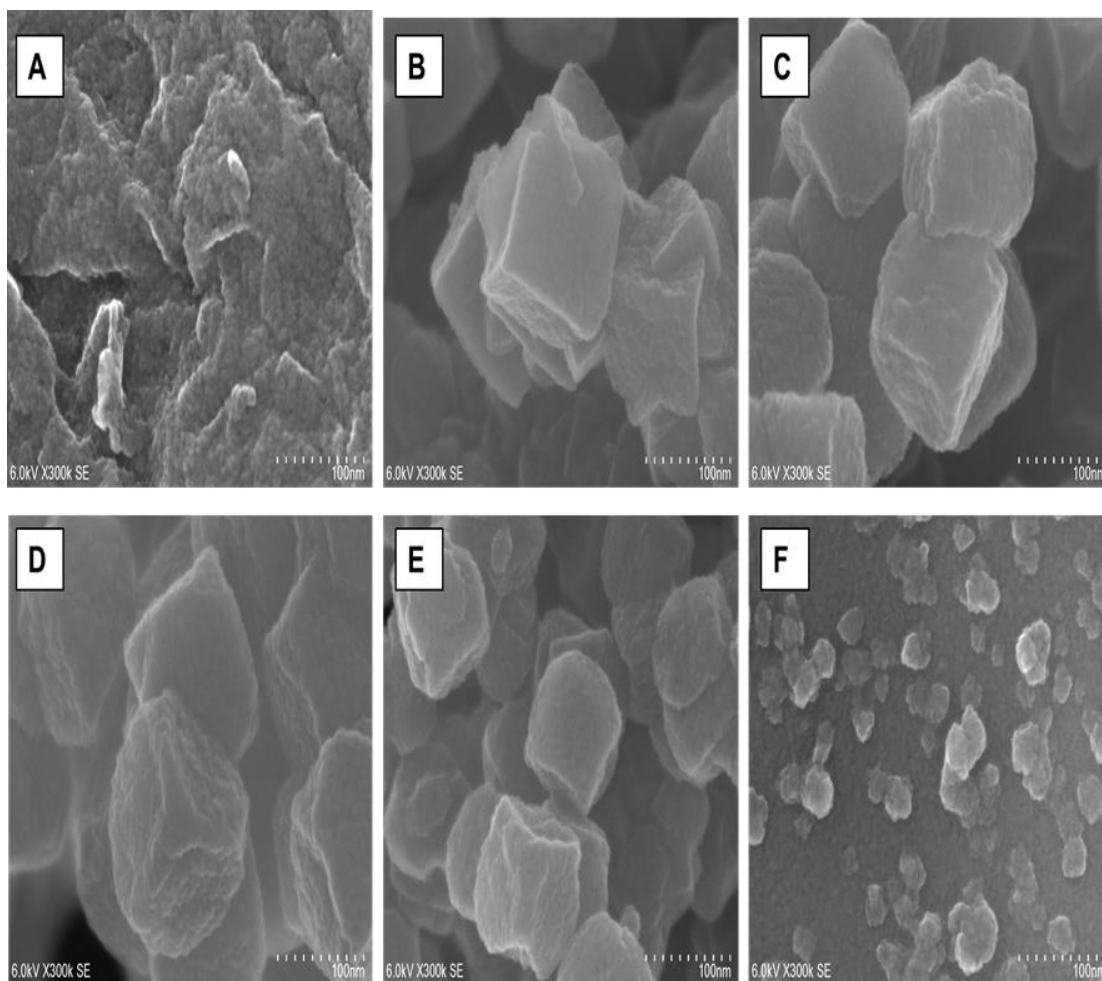


Fig. 3.7 SEM images of [A] GO, [B] UiO-66, [C] UiO-66_GO-0.1%, [D] UiO-66_GO-0.5%, [E] UiO-66_GO-1% and [E] UiO-66_GO-5%

3.4.4 TEM Morphology and Element Composition

Differences in microstructure and elemental composition among the composites could be discerned from their TEM images and EDS patterns, respectively (**Fig. 3.8**). A uniform distribution of UiO-66 particles on a large GO sheet could clearly be observed (Fig. 2C). It can be envisaged that the Zr^{4+} metal nodes in UiO-66 are

coordinated by oxygen functional groups on the GO layer, thus preventing the aggregation of UiO-66 and improving its dispersion, as suggested previously (Petit and Bandosz, 2009). Additionally, the EDS pattern from a TEM image of GO (Fig. 3.8D) showed C and O as the main elements, whereas UiO-66 and the composites showed C, O, and Zr (Figs. 3.8E and 3.8F).

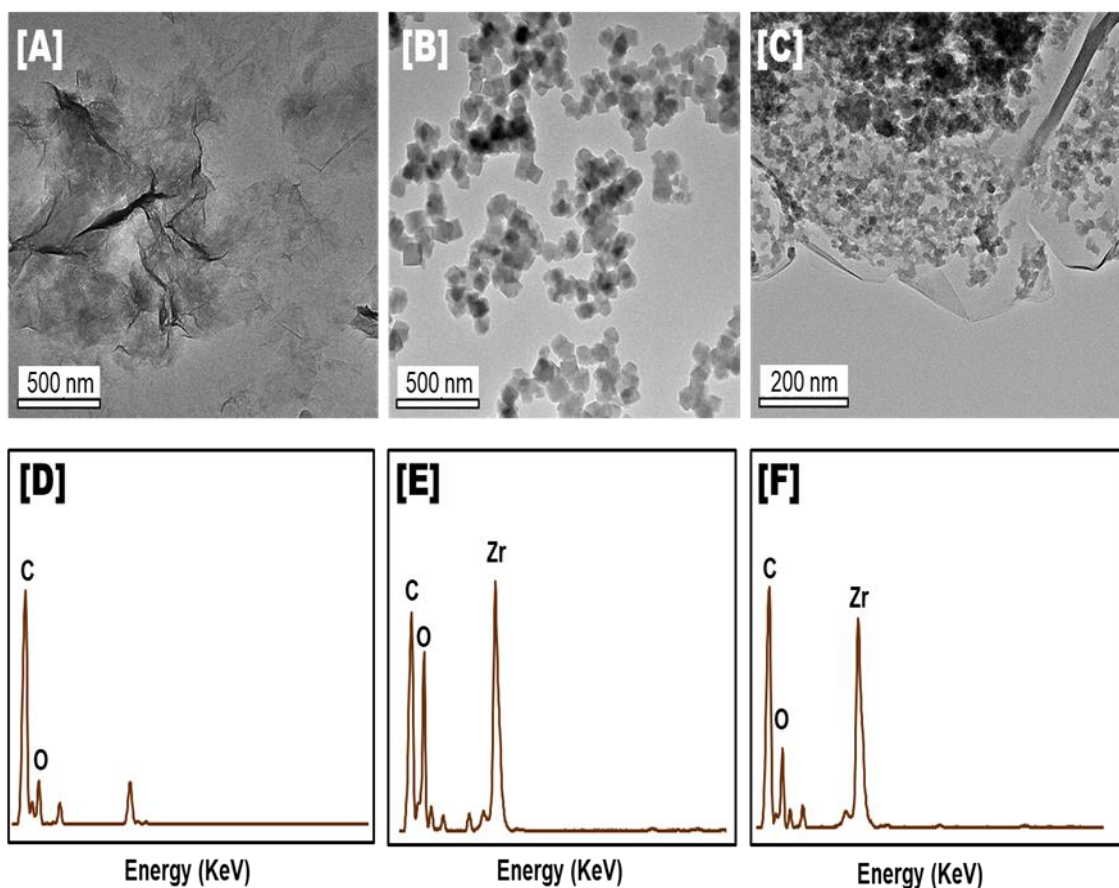


Fig. 3.8. TEM images of [A] GO, [B] UiO-66, and [C] composite (UiO-66_GO-5) and EDS spectra of [D] GO, [E] UiO-66, and [F] composite (UiO-66_GO-5)

3.4.5 Specific surface areas, principal pore sizes, and pore volumes

The surface area of UiO-66 was determined as 420 m²/g, which falls within a similar range (400–600 m²/g) as reported in some previous studies (C. Chen et al., 2017; Ding et al., 2017; Shafiei-alavijeh et al., 2018), but lower than that in other reports (800–1200 m²/g) (Lin et al., 2014; Smith et al., 2015; Wang et al., 2016). The different

surface areas may be associated with different preparation methods of the material (Ding et al., 2017). The micropores of UiO-66 were predominantly in the size range of 0.4–1 nm, although some pores in the range of 1–2.45 nm were also discerned. The surface area and pore volume of GO were evaluated as 56 m²/g and 0.23 cm³/g, respectively. The former is higher than those reported in previous studies (7–30 m²/g) (Bradder et al., 2011; Liu et al., 2016; Lonkar and Dubois, 2015). This might be attributed to different degrees of exfoliation of GO during preparation of the material (Pignatello, 2005; Zhou et al., 2015).

Although the surface area of GO is low, its presence in the respective composites significantly increases their surface areas, total pore volumes, and micropore volumes compared to those of the pristine UiO-66. The increase in the porosity of UiO-66_GO is apparent at both the micro- and macropore levels (**as shown in Table 3.1**). The enhancement of the macroporosity of the composite surface can be attributed to a new porous structure produced at the interface between the GO layer and the UiO-66 “block,” as seen in the pore size distribution (PSD) plot (**Fig. 3.9**). Meanwhile, the microporosity might be improved by the enhancement of crystalline structure dispersion along with the GO layer inducing smaller particle size. At high GO contents, as in UiO-66_GO-1 and UiO-66_GO-5, the surface area and total pore volume were significantly decreased as a result of GO sheet stacking and cubic UiO-66 particles being enveloped by the GO sheets. These observations imply that the introduction of GO markedly affects the pore structure of the composites, but that a continuous increase in GO content (>0.5 wt%) does not have a beneficial effect. Nonetheless, the large surface area and pore volume of UiO-66_GO composites likely provide more active sites for adsorption and photocatalytic performance. Conversely, the accessibility of CBZ into the micropore structure of UiO-66 might be impaired by the presence of GO layers and the rigid 3D structure of the composite, which will be less accessible than an MOF with a 1D flexible structure.

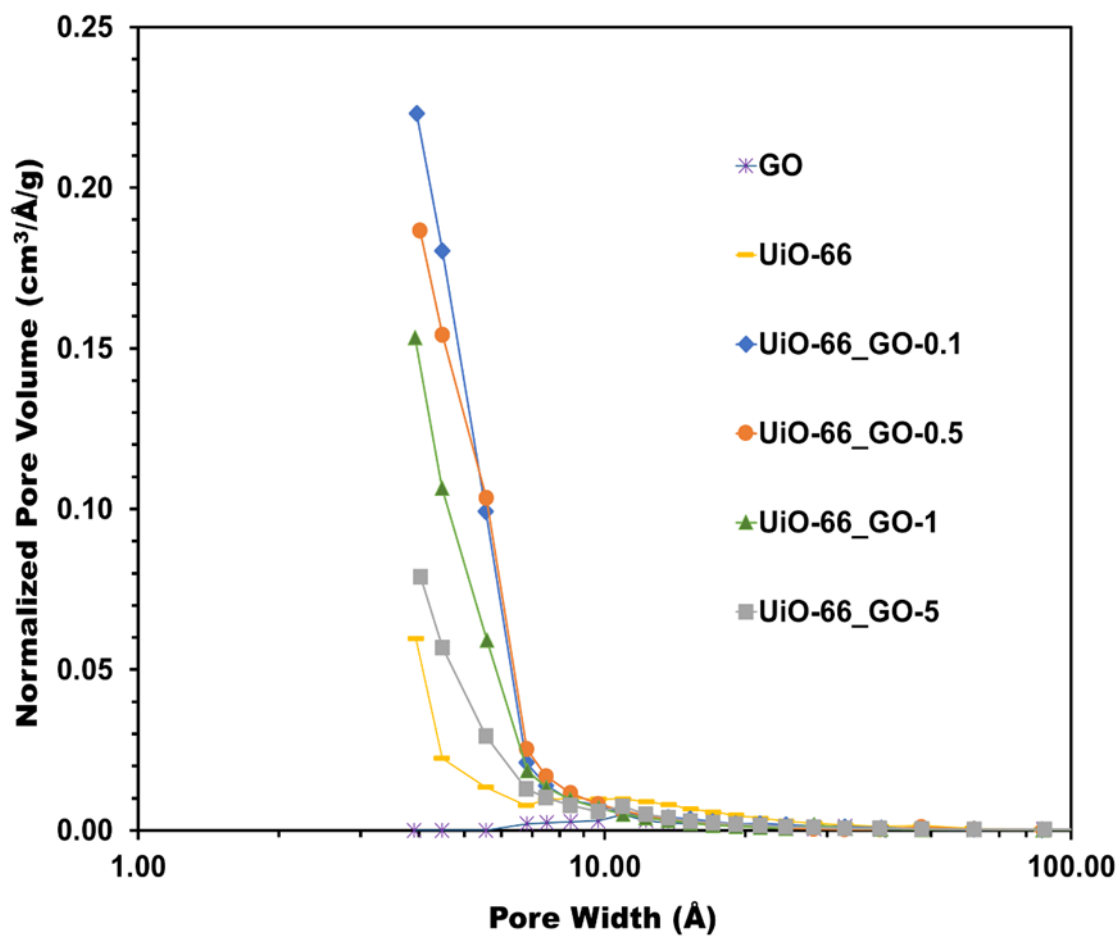


Fig. 3.9 Pore size and pore volume distribution for GO, UiO-66 and composites

Table 3.1 Surface areas, pore sizes, pore volumes, and indirect band gaps of GO, UiO-66, and composites.

Catalyst	SSA_{BET}^a m ² /g	Main pore size ^b nm	PV_{total}^c cm ³ /g	BJH pore volume distribution ^d			Indirect band gap ^e eV
				$PV_{micro}(<2\text{ nm})$ cm ³ /g, [%]	$PV_{meso}(2-50\text{ nm})$ cm ³ /g, [%]	$PV_{macro>(>50\text{ nm})}$ cm ³ /g, [%]	
GO	56.4	10.94	0.588	0.027 [4.63]	0.004 [0.68]	0.557 [94.69]	N/A
UiO-66	419.9	3.94	0.448	0.177 [39.41]	0.013 [2.99]	0.258 [57.60]	3.55
UiO-66_GO-0.1	1004.6	3.95	0.879	0.577 [65.65]	0.007 [0.83]	0.295 [33.52]	3.55
UiO-66_GO-0.5	913.4	4.02	1.052	0.526 [50.04]	0.004 [0.36]	0.522 [49.6]	3.45
UiO-66_GO-1	778	3.92	0.811	0.385 [47.45]	0.005 [0.56]	0.522 [51.99]	3.30
UiO-66_GO-5	552.4	4.03	0.398	0.226 [56.79]	0.005 [1.33]	0.167 [41.87]	3.20

^a Specific surface area calculated from N₂ adsorption data using the Brunauer–Emmett–Teller (BET) method.

^b Pore diameter calculated from N₂ adsorption data using the Barrett–Joyner–Halenda (BJH) method.

^c Total pore volume calculated from N₂ adsorption data using the BJH method at P/P₀ = 0.99.

^d Pore volume distribution classified according to the IUPAC definition and calculated by the BJH method.

^e Indirect bandgap calculated from UV/Vis absorption data by the Trauc plot method.

N/A: not available.

3.4.6 UV-Vis Light Absorption

The pristine GO showed light absorption in the wavelength range of 200–800 nm (**Fig. 3.10a**), in agreement with previous reports by Peng et al. (Peng et al., 2012) and Yang et al. (Z. Yang et al., 2017). The absorption spectrum of UiO-66 featured a peak due to the Zr-O clusters at 255 nm and a ligand-based absorption at 290 nm (**Fig. 3.10a**) (Sun et al., 2015; Wang et al., 2016). After adding GO, all of the UiO-66_GO composites showed higher light absorption in the UV region (200–400 nm) and extended absorption in the visible region (400–700 nm) compared to the pristine UiO-66 (**Fig. 3.10a**). Increased GO content evidently decreased the band gap of UiO-66, as previously observed for MOF_GO, TiO₂_GO, and other GO-based semiconductor composites (Fan et al., 2011; Xu et al., 2015; Yu et al., 2014). The band gap of UiO-66 was measured as 3.55 eV, corresponding to a wavelength of 350 nm, whereas that of the composite UiO-66_GO-5 was only 3.2 eV, corresponding to a wavelength of 390 nm (**Fig. 3.10b**). This indicates that GO plays the role of an electron acceptor and enhances carrier separation of photogenerated electron and holes in the MOF (Z. Yang et al., 2017). This modified light absorption and band gap serves to enhance the photocatalytic activity of UiO-66_GO composites.

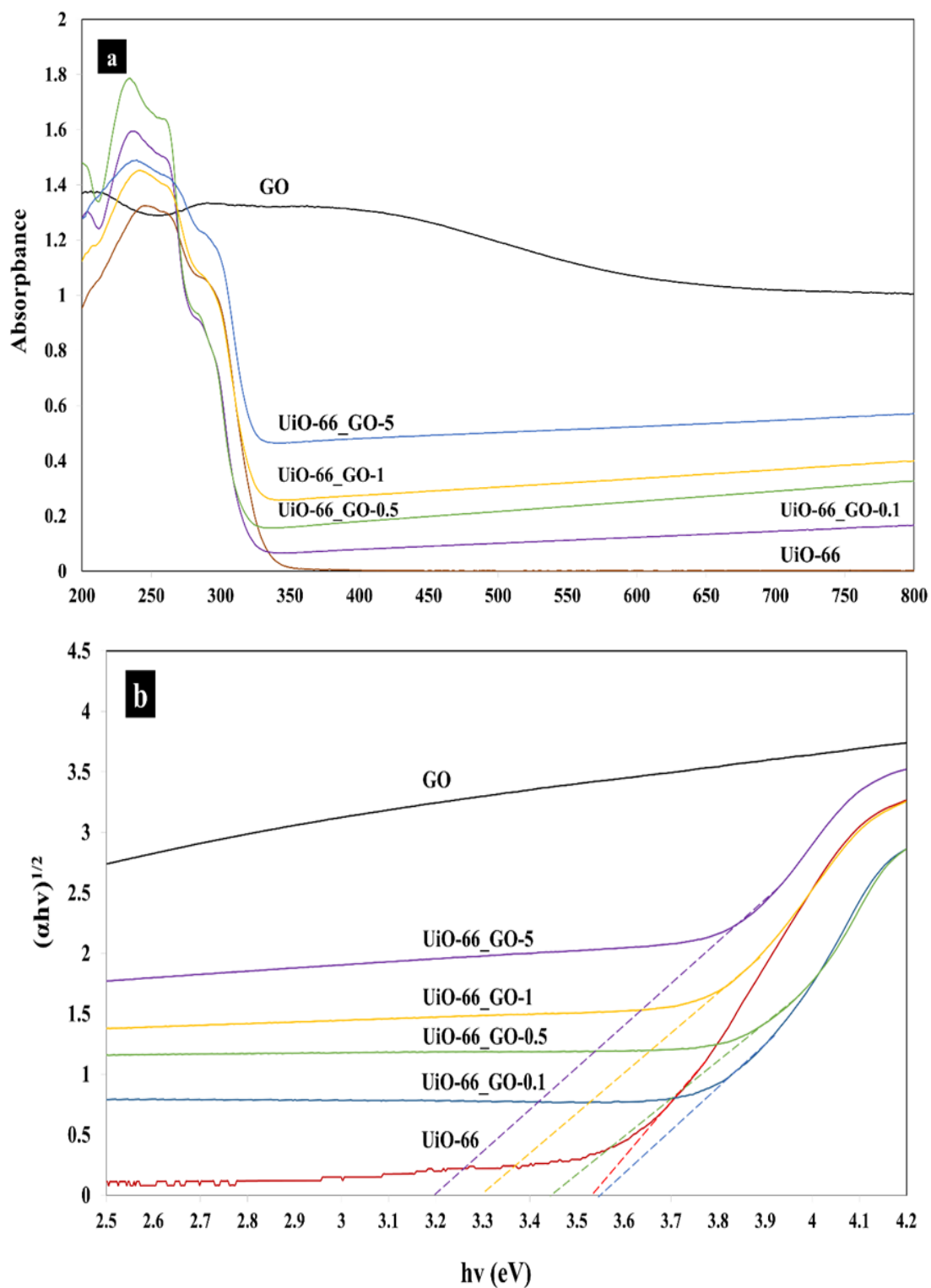


Fig. 3.10 UV-vis absorption spectra (a) and (b) optical bandgap of GO, UiO-66 and composite

3.4.7 Composite Membrane

The images of composite membranes with different UiO-66_GO composite loadings (5, 10, 15, 20, 30 wt%) on NF membrane after synthesis were observed in **Fig. 3.11**. The 5, 10, 15 wt% of UiO-66_GO composite showed a better adhesion on membrane surface with the mass loss < 10 wt% after shaking and bending whereas in 20 and 30 wt% membranes, UiO-66_GO nanocomposite was detached from membrane surface with the mass loss ≥ 10 wt%. Therefore, 5, 10, 15 wt% of UiO-66_GO loadings have good stability and resilience to mechanical stress and were selected for further study in the next section.

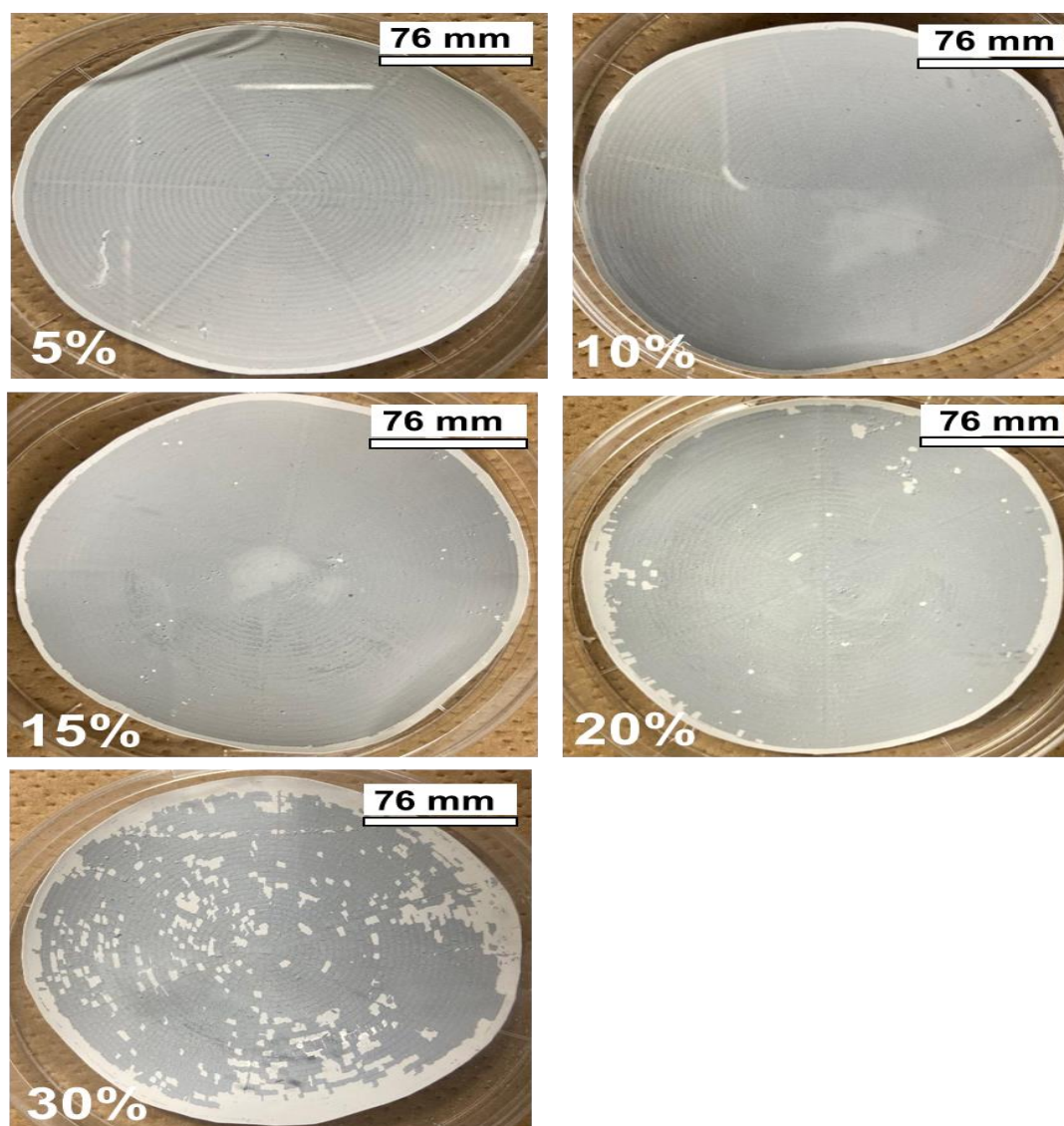


Fig. 3.11 Composite NF membranes with different UiO-66_GO loadings

3.4.8 Morphology of Composite Membrane

SEM revealed the rough surface of the pristine NF membrane, which contained many nodules and globules on its surface (**Fig. 3.12A**), similar to previously reported polyamide membranes (Safarpour et al., 2015; Shen et al., 2013). The deposition of the UiO-66_GO nanocomposite on the NF membrane created the smooth surface (**Fig. 3.12 B, C, and D**), possibly because the nodules were covered by UiO-66_GO sheets. In addition, the SEM images showed that the surface morphology depended on the UiO-66_GO content. Some areas of the UiO-66_GO/NF-5% membrane were not completely covered by UiO-66_GO (red circle in **Fig. 3.12B**), whereas the UiO-66_GO/NF-10% membrane showed a homogenous surface without uncovered areas or cracks (**Fig. 3.12C**). The UiO-66_GO/NF-15% membrane showed some cracks (**Fig. 3.12D**), indicating that a UiO-66_GO content higher than 10% decreased the stability of the composite membrane.

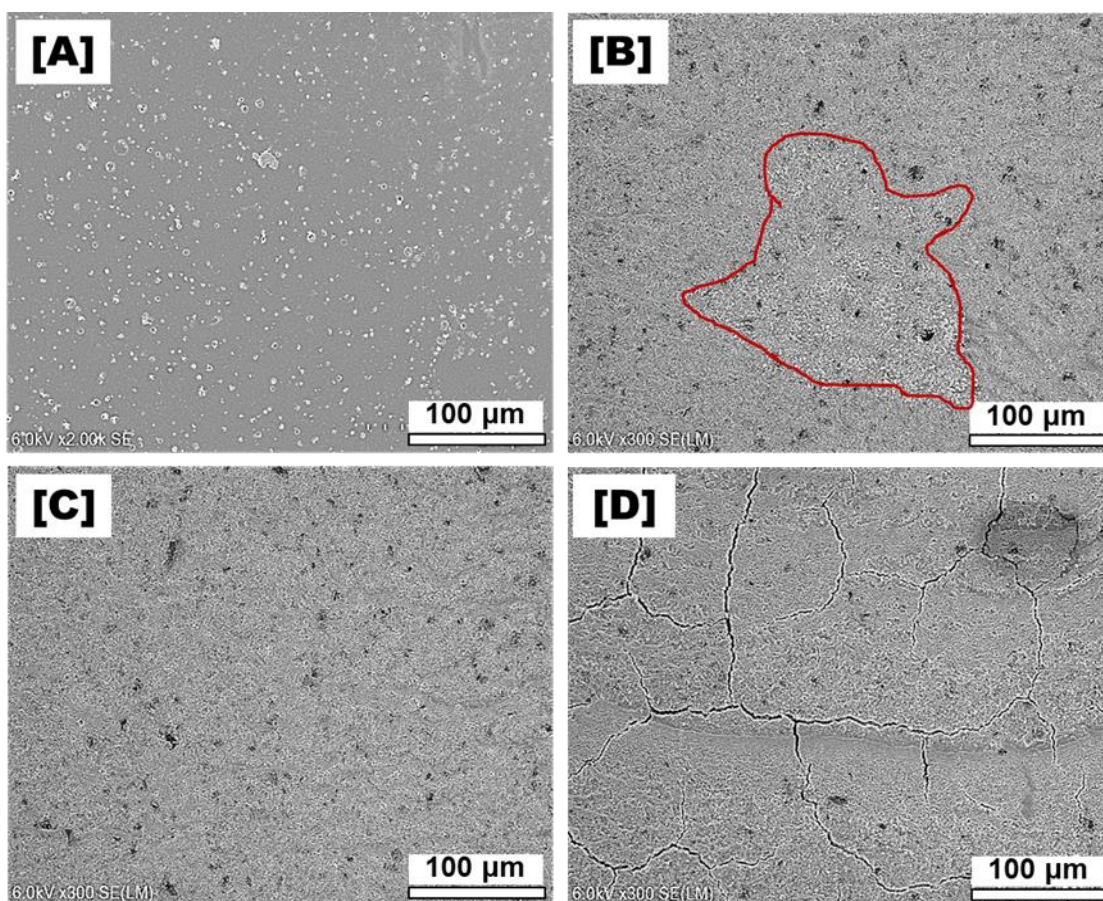


Fig. 3.12 SEM images of the [A] pristine NF membrane, and the composite membranes with UiO-66_GO loadings of [B] 5%, [C] 10%, and [D] 15%.

The roughness parameters showed that the roughness of all the composite membranes was lower than that of the pristine NF membrane due to the presence of the UiO-66_GO sheets (**Fig. 3.13, Table 3.2**). The UiO-66_GO sheets covered the rough membrane surface, possibly by hydrogen bonding between the functional groups of the UiO-66_GO nanocomposite and the surface layer of the polyamide membrane (Ma et al., 2017; Ying et al., 2017). Consequently, unlike other inorganic nanoparticles, which typically show aggregation (Vatanpour et al., 2012; Wu et al., 2013), the UiO-66_GO nanocomposite was uniformly distributed on the membrane surface, increasing the surface smoothness. A similar modification has been reported by other studies in which hydrophilic materials were loaded on polyamide membranes (Fathizadeh et al., 2011; Safarpour et al., 2015; Ying et al., 2017). In addition, pressure-assisted self-assembly (PASA) at a constant pressure of 5 bar may produce tighter, denser, and smoother membranes than physical mixing of UiO-66 and GO. Increasing the UiO-66_GO nanocomposite loading to 15% gave higher roughness parameters (average roughness [S_a] and root mean square roughness [S_q]) than loadings of 5% and 10% because of the aggregation and agglomeration of UiO-66_GO particles on the membrane surface.

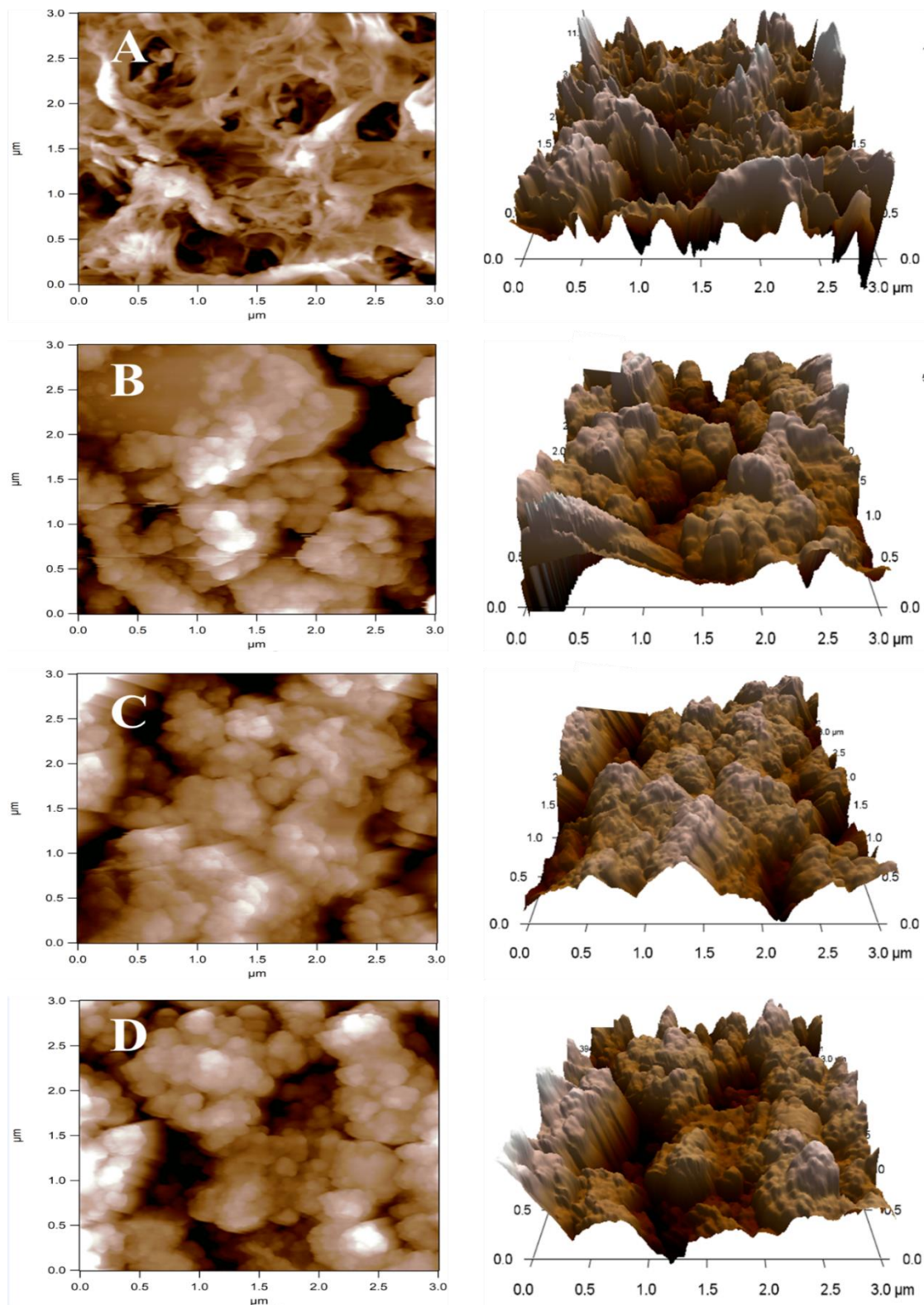


Fig. 3.13 Two- and three-dimensional AFM images of [A] the pristine NF membrane, and the composite membranes with UiO-66_GO loadings of [B] 5%, [C] 10%, and [D] 15%.

3.4.9 Hydrophilicity of Membrane

The pristine NF membrane showed a water contact angle of 39.5° (**Fig. 3.14, Table 3.2**). Addition of 5%, 10%, and 15% UiO-66_GO nanocomposite to the NF membrane surface decreased the water contact angles to 22.7°, 14.2°, and 5.63°, respectively (**Fig. 3.14, Table 3.2**). This means that the presence of hydrophilic functional groups (O–C–O, C=O, and O–H) on the UiO-66_GO surface resulted in the higher hydrophilicity and wettability of the membrane, which improve filtration and anti-fouling performance.

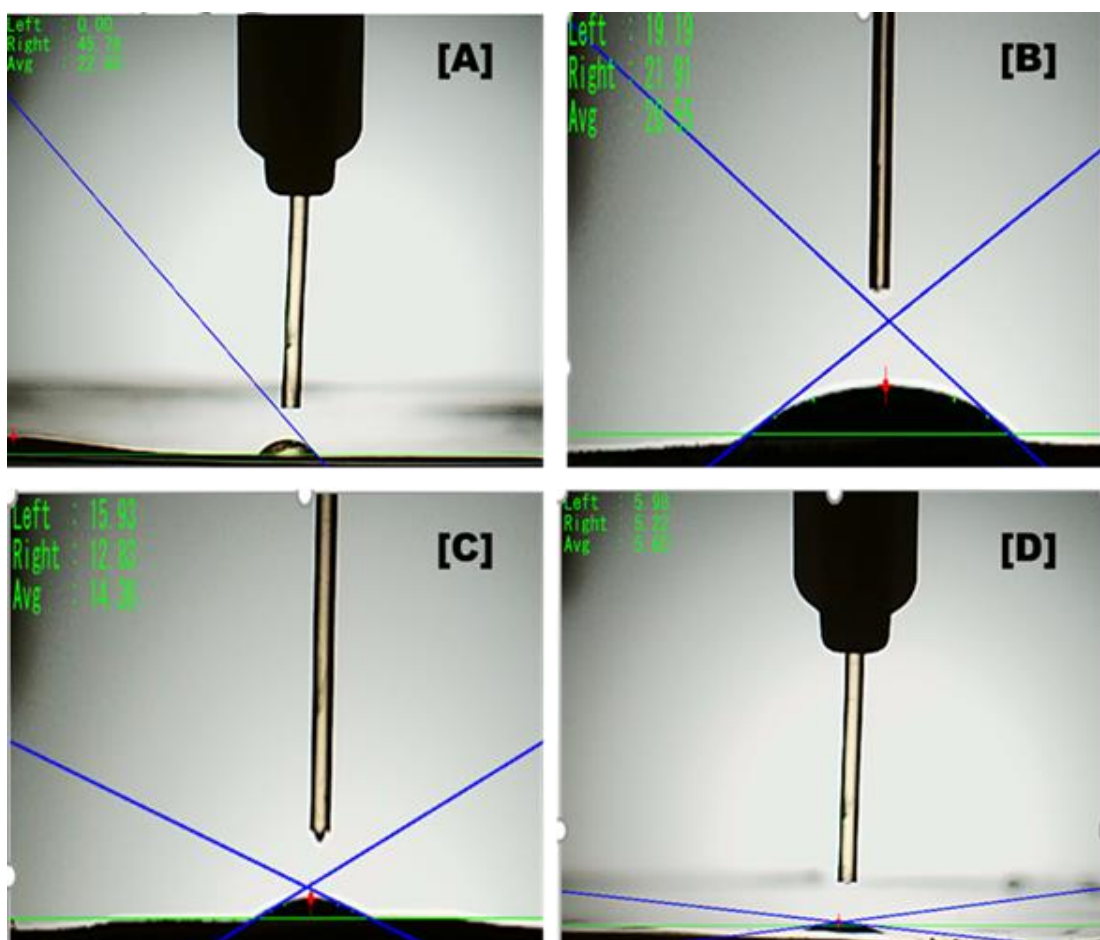


Fig. 3.14 Water contact angle measurement of [A] pristine NF, and [B] 5%, [C] 10%, and 15% of UiO-66_GO loading in composite membranes

3.4.10 Porosity and Pore Size of Membrane

The overall porosity and the mean pore radius of the pristine NF were 64.8% and 2.78 nm, respectively (**Table 3.2**). The addition of 5%, 10%, and 15% UiO-66_GO to the NF membrane increased the overall porosities to 72.1%, 76.4%, and 78.3%, respectively (**Table 3.2**). The composite membranes also showed higher mean pore

radii (2.98, 3.26, and 3.51 nm, respectively) compared with the pristine NF membrane (2.78 nm). The higher porosity and larger pore radius of the composite membrane explained why UiO-66_GO on the membrane did not block the membrane pores and water pathway. These properties were achieved by the in situ one-step hydrothermal method, and thus the composites possessed high porosity at the micro- and macropore levels, as confirmed previously (Heu et al., 2020).

Table 3.2 Characterization of the pristine and composite membranes.

Membrane	Thickness mm	Porosity %	pore size nm	Roughness parameters			Contact angle deg
				S_a	S_q	S_y	
				nm	nm	nm	
Pristine NF	0.252	64.8	2.78	217	283	1986	39.5
UiO-66_GO/NF- 5%	0.267	72.1	2.98	161	211	1723	22.7
UiO-66_GO/NF- 10%	0.275	76.4	3.26	122	161	1564	14.2
UiO-66_GO/NF- 15%	0.310	78.3	3.51	136	176	1442	5.63

S_a : average roughness; S_q : root mean square roughness; S_y : mean height difference between the highest peaks and lowest valleys.

3.5 Conclusion

Nanocomposite of UiO-66_GO with different GO loadings (0.1, 0.5, 1, and 5 wt%) was synthesized by one-step hydrothermal method and their physio-chemical properties were well characterized by crystalline structure, surface functional groups, morphology, element compositions, specific surface area, porosity and light absorption. Furthermore, a 0.5% GO loading in the composite material was used to prepare the composite membrane because it showed the highest photodegradation rate for carbamazepine as shown in Chapter 4. The composite UiO-66_GO/NF membranes with different UiO-66_GO loadings (5, 10, 15, 20, 30 wt%) were synthesized by pressure-assisted self-assembly (PASA) and their physio-chemical properties were well characterized by surface morphology and roughness, hydrophilicity, porosity, thickness,

and pore size . However, only 5, 10 and 15 wt% of UiO-66_GO loadings showed a good adhesion on NF membrane surface and were selected for further study.

CHAPTER IV

Photocatalytic Activity of Zr-based Metal Organic framework Enhanced by Graphene Oxide

4.1 Introduction

Heterogeneous photocatalysis is one of the so-called advanced oxidation processes (AOPs) and has attracted a great deal of attention over the past few decades for water purification and disinfection due to its advantages of being non-selective, chemical-free, cost-effective, and simple to operate (Dong et al., 2015; Kuila et al., 2017; Nan et al., 2010; Uyguner-Demirel et al., 2017). New semiconductor photocatalysts have been developed with the aim of achieving improved photocatalytic performance (Kisch, 2013; Wen et al., 2017). In this regard, metal–organic frameworks (MOFs), as crystalline porous materials, have attracted extensive interest as emerging metal complex photocatalysts and semiconductor photocatalysts in recent years (Sharma and Feng, 2017; Wang and Wang, 2015).

MOFs are composed of inorganic metal ions as connecting centers and organic moieties as linkers and offer two significant advantages in photocatalysis. First, their high surface areas (up to 3000 m²/g), high porosity (up to 1 cm³/g), and abundance of functional groups increase the number of active sorption sites, while also providing additional pathways for photo-induced electron migration, facilitating charge carrier separation (Jin and Yang, 2017; Wang et al., 2016). Second, the organic linkers and metal nodes of MOFs can be integrated with, or replaced by, other linkers and metal ions, making MOFs chemically and structurally diverse materials (Denny and Cohen, 2015; Deria et al., 2014; Kim et al., 2012). UiO-66, a zirconium-based MOF, has been proposed as a potential photocatalyst due to its thermal and chemical stability, modifiability, high surface area, and photoactivity (Cavka et al., 2008; Kalidindi et al., 2015; Musho et al., 2014a). However, photodegradation rates over UiO-66 are limited by its low adsorption capacity and wide band gap (3.7 eV) (Akpınar and Yazaydin, 2018; Musho et al., 2014a). A few studies have demonstrated that graphene oxide (GO)

enhances the photocatalytic activity of UiO-66 by increasing its adsorption capacity, reducing charge recombination, and acting as a light sensitizer (Lin et al., 2014; Xu et al., 2015; Z. Yang et al., 2017).

In this study, we present a facile hydrothermal method for preparing UiO-66_GO nanocomposites, and report for the first time on the photodegradation of an organic micropollutant (OMP). Carbamazepine (CBZ) was selected as a model OMP due to its high potential risk to the environment (Atkinson et al., 2007; Galus et al., 2013; Painter et al., 2009) and resistance to biological degradation under UV irradiation (Ali et al., 2018; H. Chen et al., 2017; Hai et al., 2018). The specific objectives of this study were: 1) to investigate the enhancing effect of GO on the photocatalytic activity of UiO-66, 2) to test the photodegradation of CBZ with different GO contents in the composites, and on varying the catalyst doses and solution pH, 3) to elucidate the photocatalytic mechanism of UiO-66_GO composites under UV irradiation, and 4) to test the recyclability and stability of the photocatalyst after five consecutive cycles.

4.2 Experimental Method

The photocatalytic activities of the prepared photocatalysts with particle size 200 μm mesh were evaluated by the photodegradation of CBZ under irradiation with UVC light of wavelength 254 nm and intensity 0.16 W/cm². The prepared photocatalysts were mixed in a 100 mL glass beaker containing CBZ solution (50 mL) at an initial concentration of 5 mg/L. The mixture was stirred in the dark at room temperature (25 °C) for 1 h until the CBZ adsorption–desorption reached equilibrium. The experiment of blank CBZ solution without catalysts was conducted to check the effect of hydrolysis and photolysis. The adsorption capacity of CBZ was then calculated according to (Eq. 4.1):

$$q_t = \left(\frac{C_0 - C_t}{M} \right) \times V \quad (\text{Eq. 4.1})$$

where q_t is the adsorption capacity at equilibrium (mg/g), C_0 is the initial concentration of CBZ (mg/L), C_t is the concentration of CBZ at time t (mg/L), M is the mass of adsorbent (g), and V is the total volume of solution (L).

After adsorption–desorption equilibrium had been attained, the UVC light was turned on and samples were collected at different time intervals: 20, 40, 60, 90, 120, and 180 min. After the irradiation, the solution was passed through a syringe filter (0.22 μm PES filter, Membrane Solution, Japan) to remove the photocatalyst, and then 100 μL of the filtrate was used for CBZ analysis. The analysis was carried out by injecting the sample into a high-performance liquid chromatography (HPLC) system (Prominence UFLC, Shimadzu, Japan) equipped with a UV/Vis absorbance detector (SPD-20 UFLC, Shimadzu, Japan). A C18 column of dimensions 4.6 mm \times 250 mm \times 5 μm (Kinetex Phenomenex, USA) was used. The UV/Vis detector was operated at 285 nm and the oven temperature was set at 40 $^{\circ}\text{C}$. The mobile phase consisted of methanol (60%) and water (40%) at a flow rate of 0.6 mL/min. The degradation rate was determined according to a pseudo-first-order kinetic model (**Eq. 4.2**)

$$\ln \frac{C_t}{C_{eq}} = -kt \quad (\text{Eq. 4.2})$$

where k is degradation rate (mn^{-1}), C_{eq} is the concentration of CBZ at equilibrium adsorption (mg/L), C_t is the concentration of CBZ at time t (mg/L), and t is photodegradation time (min). Coefficient of determination ranged from 0.95 to 0.99 in this study (**Fig. S5**).

The pH of the solutions was adjusted using 0.1 m HCl or 0.1 m NaOH solutions. A recycling experiment involving five runs was conducted to investigate the stability and recyclability of the catalyst. After each run, the catalyst was collected, sonicated, and freeze-dried prior to reuse under identical conditions.

4.3 Results and Discussion

4.3.1 Effect of Photocatalyst Compositions

The result of blank CBZ experiment showed that hydrolysis and photolysis had no significant effect on CBZ concentration, and in the adsorption phase all photocatalysts reached equilibrium within 1 h (**Fig. 4.1**). At equilibrium (**Fig. 4.1B**), each of the UiO-66_GO composites showed an adsorption capacity up to 2.5 times higher than that of pristine UiO-66, attributable to the larger surface areas and pore volumes indicated by BET analysis. The adsorption of CBZ on UiO-66 is principally

through Van der Waals interactions with metal clusters (C. Chen et al., 2017), whereas its adsorption on GO is mainly through π - π electron donor–acceptor interactions (Cai and Larese-casanova, 2014; Wang et al., 2013). Among the composite materials, UiO-66_GO-0.1 showed the highest adsorption capacity of approximately 2.96 mg/g, which corresponds to its highest surface area and porosity. Higher GO content resulted in lower adsorption capacity because of its lower surface area and porosity. These results further imply that excessive GO wrapped around the UiO-66 reduces the number of adsorption sites, consistent with the results from BET analysis and SEM observation.

Under UVC irradiation, the presence of GO increased the photodegradation rate of CBZ over UiO-66 (**Fig. 4.1B**), except in the case of UiO-66_GO-5. The improvement at the lower loadings can be attributed to the increased photocatalyst surface area and the narrower band gap, as indicated by the BET analysis and UV/Vis absorption spectra, respectively. The maximum degradation rate ($k = 0.0135 \text{ min}^{-1}$) was obtained over UiO-66_GO-0.5. However, the CBZ degradation rate was lower at GO contents of less than 0.5 wt% (as seen for UiO-66_GO-0.1), probably because the GO content was too low to narrow the band gap of UiO-66. When the GO content exceeded 0.5 wt% (UiO-66_GO-1 and UiO-66_GO-5), the degradation rate sharply decreased. This was because the excessive GO reduced the number of catalyst active sites, as shown by the BET analysis, and shielded the UiO-66 by absorbing light, which resulted in far fewer photogenerated charges (Xu et al., 2015; Yu et al., 2014).

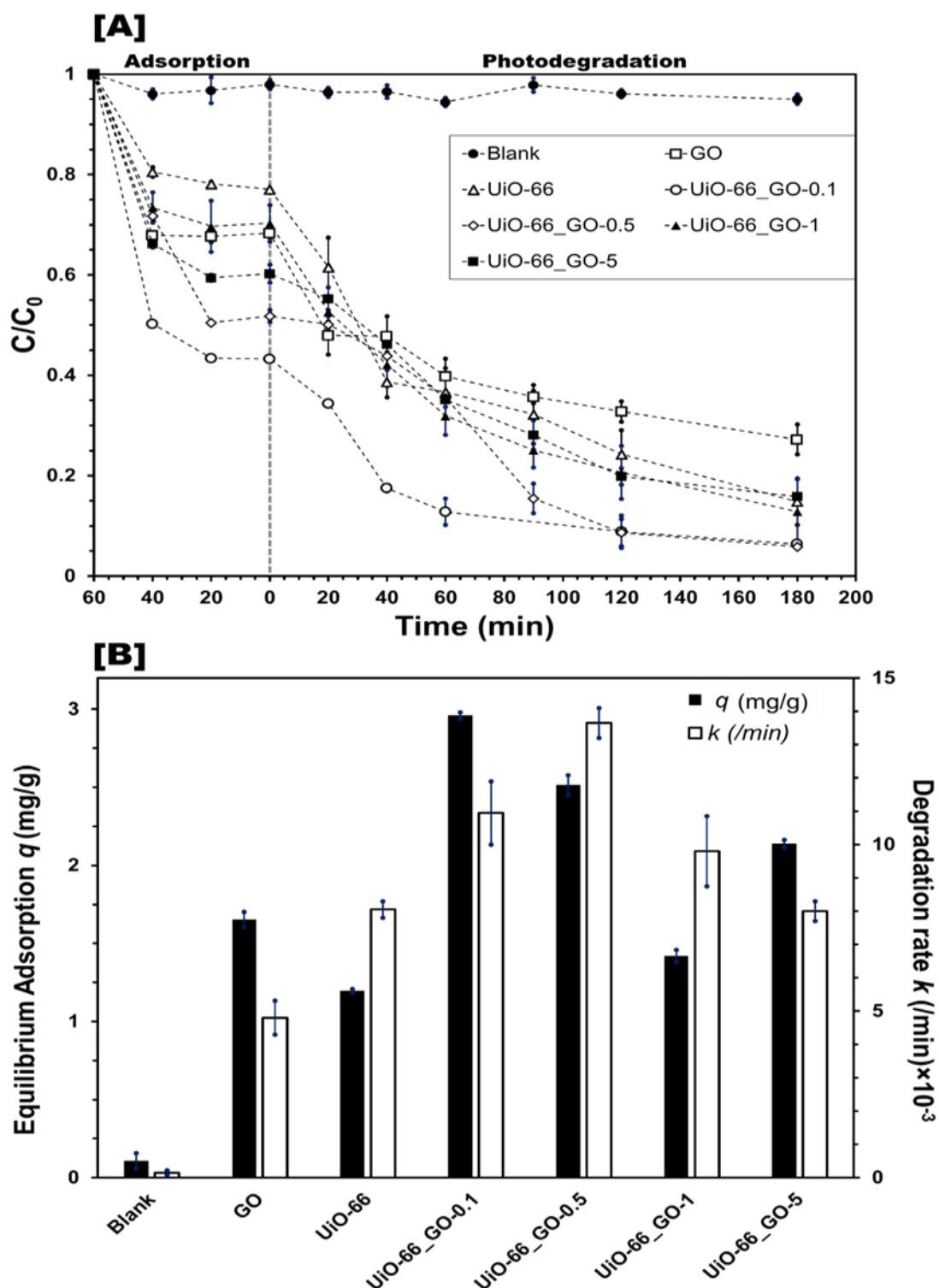


Fig. 4.1. [A] Adsorption and photodegradation of CBZ, [B] adsorption capacity and photocatalytic rate k with no photocatalyst, GO, UiO66, 0.5 wt%, 1 wt%, and 5 wt% GO-loaded UiO-66 composites (experimental conditions: initial CBZ concentration = 5 mg/L; pH 7 ± 0.2 ; mass of photocatalyst = 50 mg; solution volume $V = 50$ mL). Plots and error bars represent averages and standard deviations from triplicate experiments.

4.3.2 Effect of Photocatalyst Dose

The optimal dose of the catalyst was 1 g/L, showing high adsorption capacity (2.5 mg/g) and degradation rate (0.0135 min^{-1}) to remove 5 mg/l of CBZ with high removal (>95%) (**Fig. 4.2**). A higher catalyst dose led to greater CBZ adsorption as it provided more adsorption sites (Cao et al., 2018; Ramezanzadeh et al., 2018). At a dose of 2 g/L, most of the CBZ was adsorbed and only a small amount (<40%) remained in solution. However, the equilibrium adsorption at 2 g/L was smaller than those at lower dosages (0.5 and 1 g/L) due to low availability of CBZ in the reaction system, and aggregation of the catalyst, which reduced the effective number of active sites (Almasri et al., 2018) (**Fig. 4.2B**). The degradation rate (**Fig. 4.2B**) at 2 g/L was also lower than those with lower dosages (0.5 and 1 g/L) because of light-shielding (H. Chen et al., 2017). Although the highest equilibrium adsorption (3.42 mg/g) was seen at 0.5 g/L, the degradation rate was low (0.0091 min^{-1}); this dose was insufficient to remove 5 mg/l of CBZ, resulting in a low photodegradation efficiency (<85%).

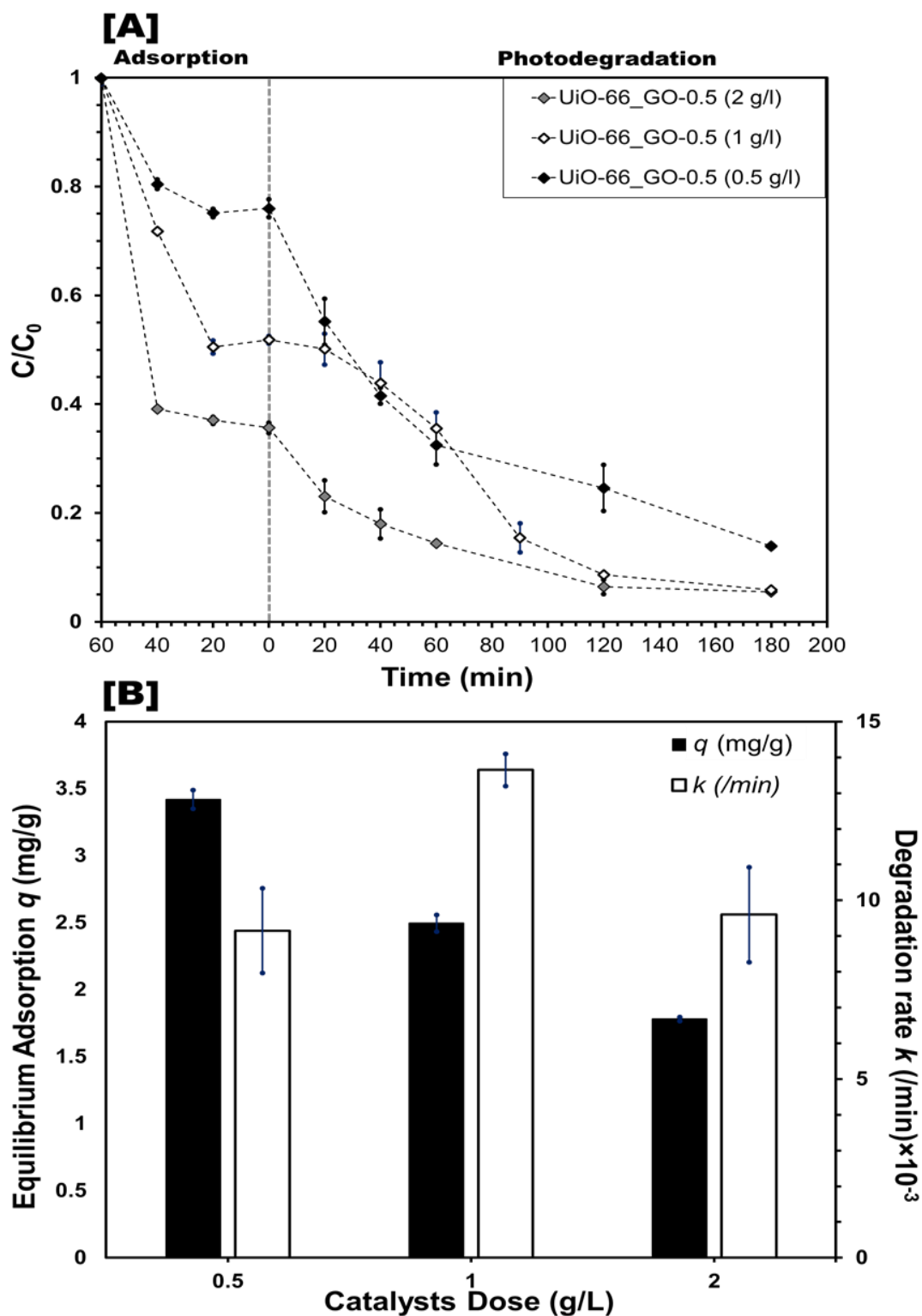


Fig. 4.2 [A] Adsorption and photodegradation and [B] equilibrium adsorption and photocatalytic rate k of CBZ at loadings of 0.5, 1, and 2 mg/L (experimental conditions: initial CBZ concentration = 5 mg/L; pH 7 ± 0.2 ; mass of UiO-66_G-0.5 $m = 25, 50$, or 100 mg; solution volume $V = 50$ mL). Plots and error bars represent averages and standard deviations from triplicate experiments.

4.3.3 Effect of Initial CBZ Concentration

The effect of initial CBZ concentration on its photodegradation was investigated by applying different initial CBZ concentrations of 3, 5, 10, and 20 mg/L. Equilibrium adsorption first increased with increasing CBZ concentration due to a higher driving force of the concentration gradient (Abdi et al., 2017; Cao et al., 2018) (Fig. 4.3). In contrast, when the initial concentration was increased from 3 to 20 mg/L, the degradation rate decreased. This was because excessive initial concentration could shield some UV light, reducing the amount of photons reaching the composite (A, 2014; Mamun et al., 2017). In addition, the higher initial CBZ concentration was expected to produce higher intermediates and those intermediates may compete with CBZ for $\text{OH}\cdot$, resulting in a lower degradation rate, as explained by Ali et al. and Khan et al. (Ali et al., 2018; J. A. Khan et al., 2013).

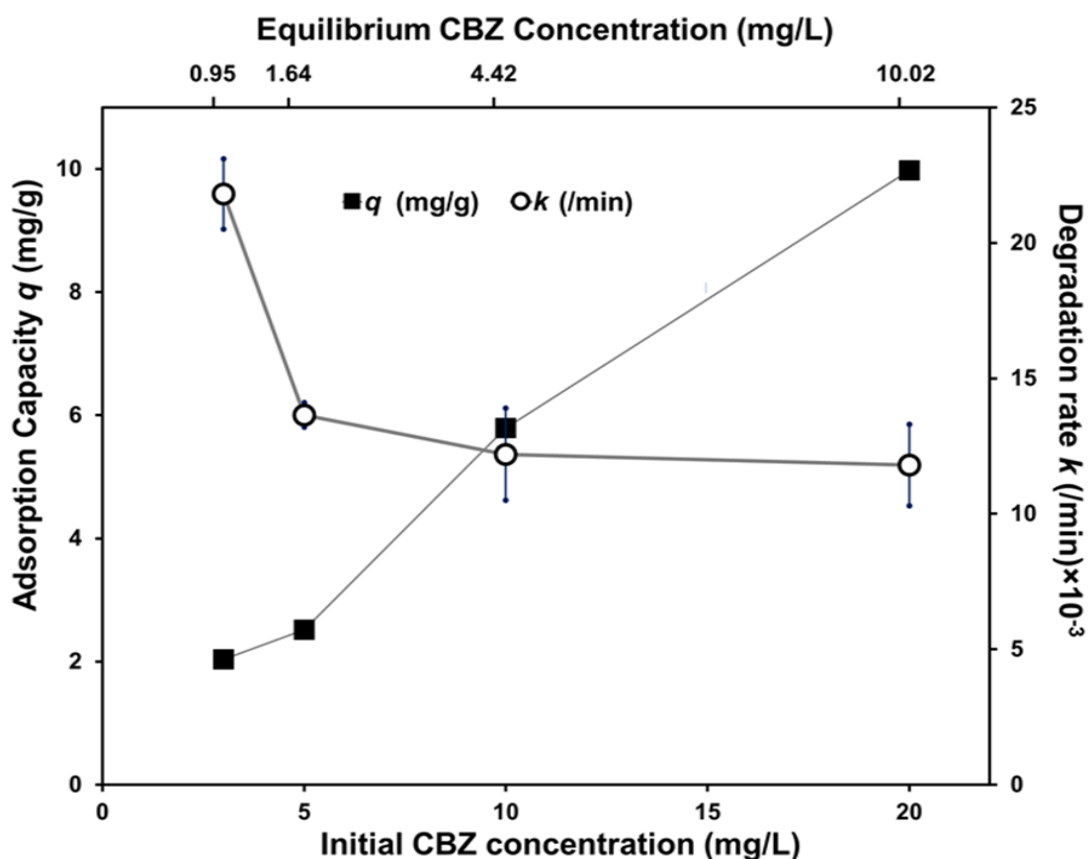


Fig. 4.3 Effect of initial CBZ concentration on equilibrium adsorption and degradation rate (experimental conditions: pH 7 ± 0.2 ; mass of UiO-66_GO-0.5 m = 50 mg; solution

volume $V = 50$ mL). Plots and error bars represent the averages and standard deviations from duplicate experiments.

4.3.4 Effect of pH

The photodegradation of CBZ proved to be pH-dependent, with higher degradation being observed in a low pH range of 2–6 (**Fig. 4.4**). Since the pK_a of CBZ is 13.9 (Moztahida et al., 2019; Oleszczuk et al., 2009), it would be neutral or bear a positive charge in acidic pH. Meanwhile, pH corresponding to the point of zero charge (pH_{pzc}) is at 6 for UiO-66 and at 4 for GO, and thus the surface of the composite adsorbent will be positively charged at $pH < 4$ and negatively charge at $pH > 6$ (Cai and Larese-casanova, 2014; Castarlenas et al., 2017; C. Chen et al., 2017). Therefore, the adsorption of CBZ at $pH < 4$ might be disfavored by repulsive interactions between the positive charges of CBZ and UiO-66_GO-0.5. The highest equilibrium adsorption was obtained at pH 4–6, at which the surface charge of UiO-66_GO-0.5 is almost neutral. Apparently, electrostatic interactions are not the main adsorption mechanism of CBZ. The adsorption of CBZ decreased when the pH was raised to 8–10. This might be related to the increased number of deprotonated Zr-O- groups on the metal clusters of UiO-66_GO-0.5, which might reduce the number of active sites for hydrogen bonding. Thus, due to higher equilibrium adsorption, the lower pH range ≤ 6 showed higher overall removal efficiency ($R\ 0.84$, $n\ 6$, $p\ 0.03$).

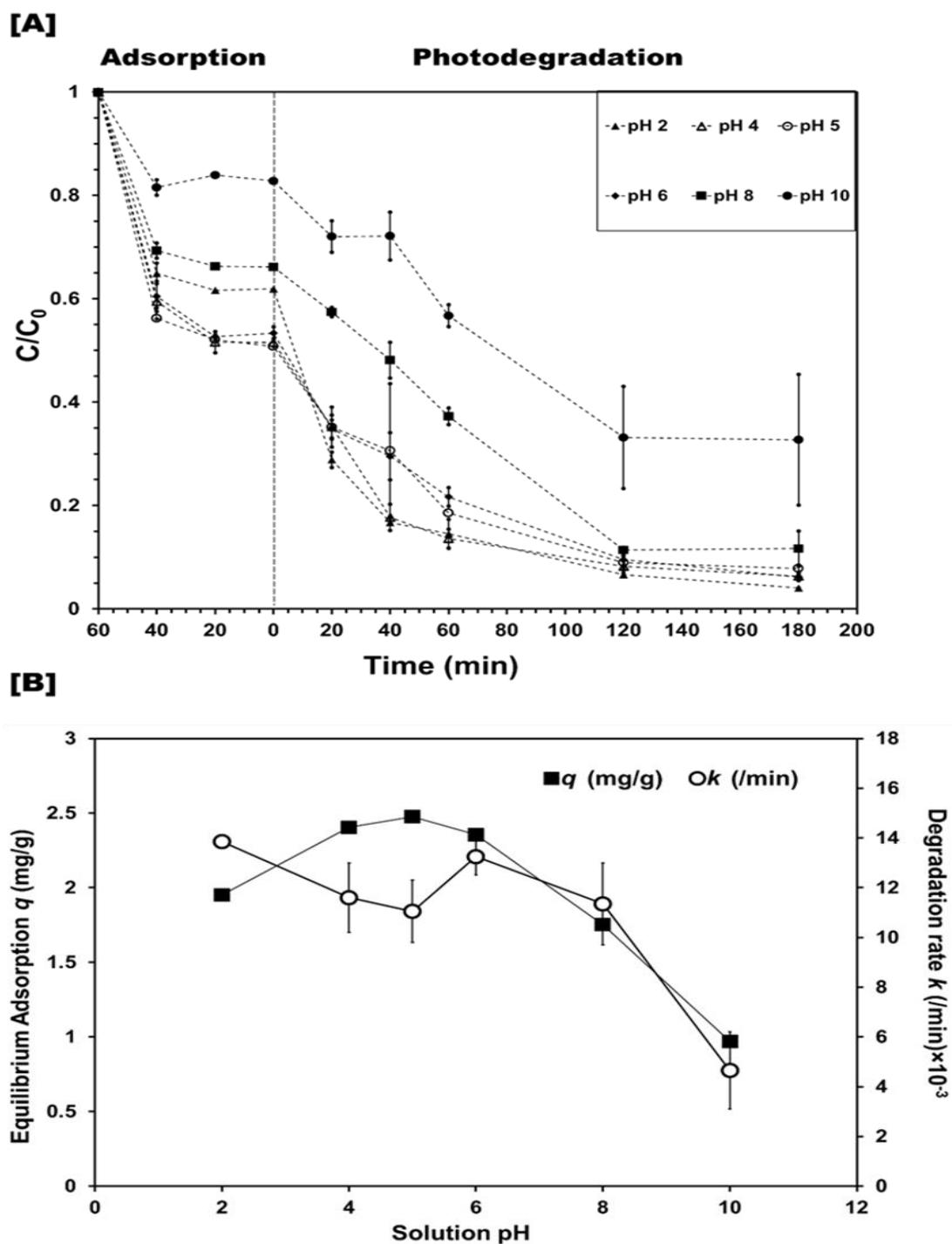


Fig. 4.4 [A] photodegradation of CBZ at different solution pH and [B] effect of solution pH on equilibrium adsorption q and degradation rate k (experimental conditions: initial CBZ concentration = 5 mg/L; concentration of UiO-66_GO-0.5 = 1 g/L; solution volume $V = 50$ mL). Plots and error bars represent averages and standard deviations from duplicate experiments.

4.3.5 Photodegradation Mechanism and Identification of Reactive Species

To gain further understanding of the role of photogenerated radicals in the CBZ degradation mechanism, *p*-benzoquinone (BQ), sodium oxalate (SO), isopropanol (IPA), and potassium persulfate ($K_2S_2O_8$) were used to quench superoxide radicals ($O_2^{\bullet-}$), holes (h^+), hydroxyl radicals (OH^{\bullet}), and electrons (e^-), respectively (Cao et al., 2018; Yang et al., 2013). The addition of BQ or IPA significantly inhibited the degradation of CBZ, whereas the addition of SO or $K_2S_2O_8$ had no significant effects (Fig. 4.5). These observations suggested that $O_2^{\bullet-}$ and OH^{\bullet} are the main active species for CBZ photodegradation over the UiO-66_GO system, which is in line with previously reported UiO-66 composites (Cao et al., 2018; Wang et al., 2016).

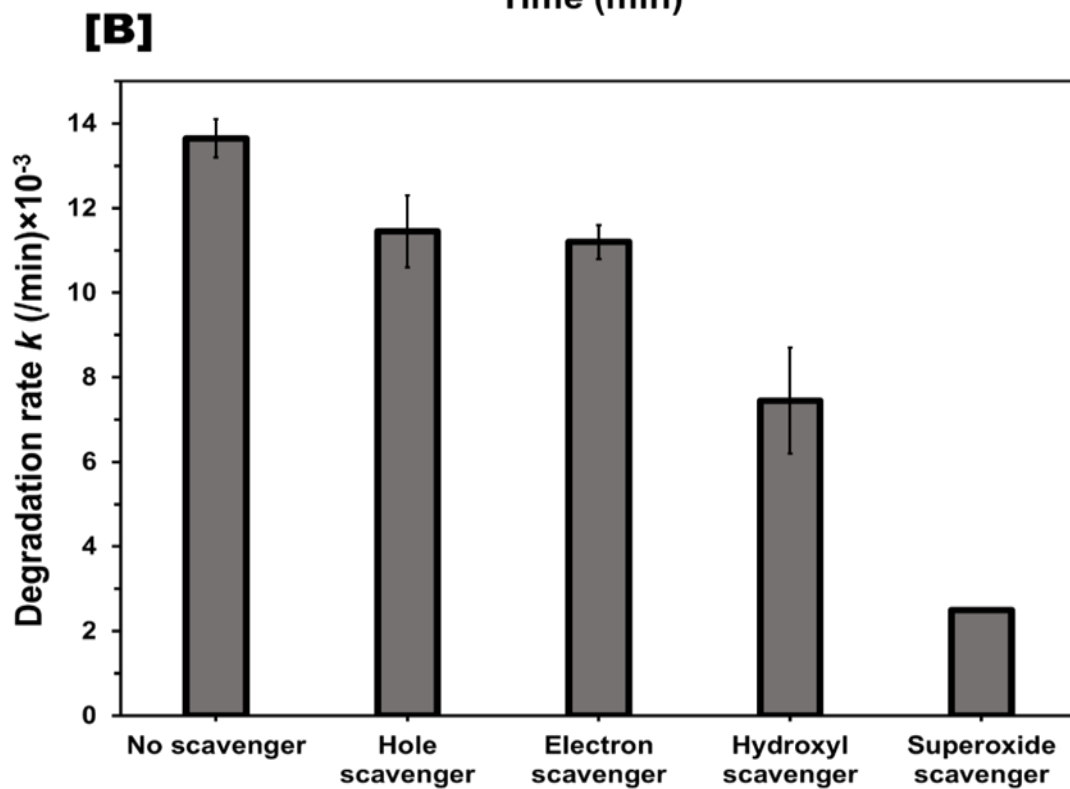
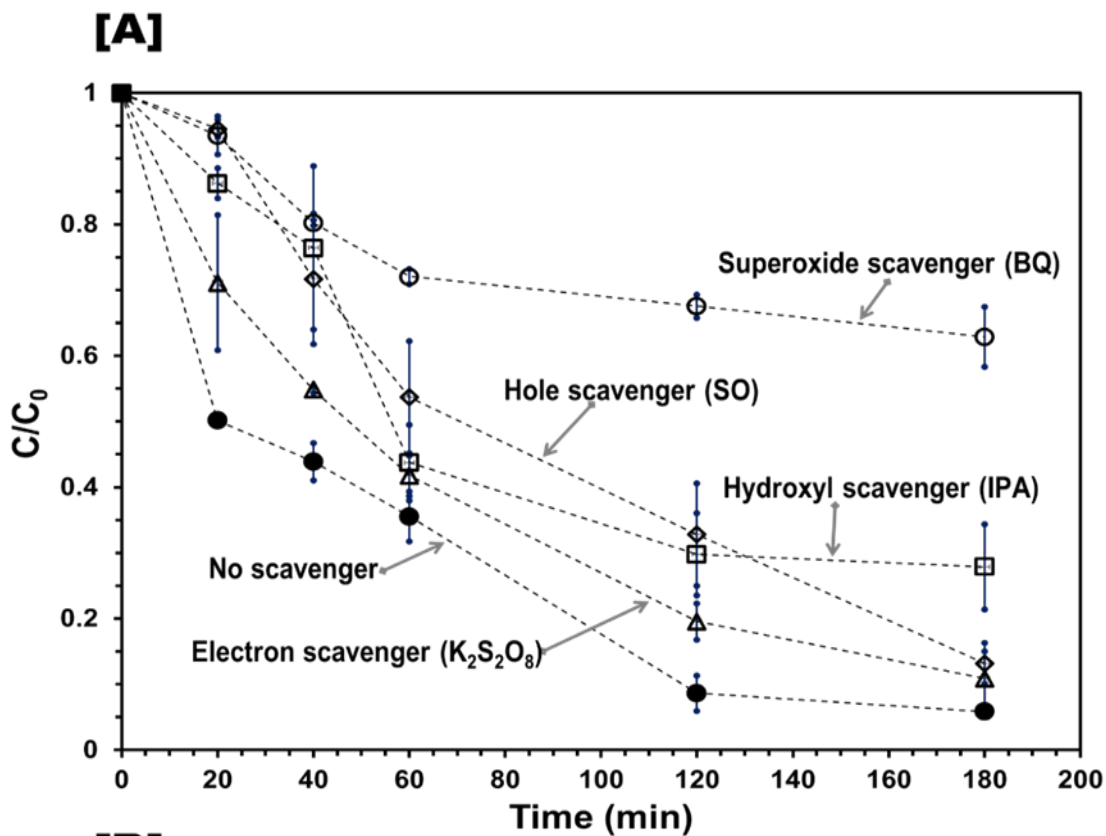


Fig. 4.5 Effects of the absence and presence of scavengers on [A] the photodegradation efficiency and [B] the degradation rate of CBZ over UiO-66_GO-0.5.

The mechanism of CBZ photodegradation over UiO-66 enhanced by GO (UiO-66_GO) is hypothesized to involve the following equations **Eq. (4.3)**, **(4.4)**, and **(4.5)** and is outlined in **Fig. 4.6**.



CBZ was most likely adsorbed on the benzene structure in UiO-66_GO nanoparticles. Under UV irradiation, the organic ligands (H₂BDC) of the composite catalyst were excited and could then transfer a photoelectron to the inorganic Zr-O clusters. The photogenerated electron (e⁻) in the conduction band of UiO-66 then quickly migrated to the GO support, greatly enhancing the carrier separation, resulting in improved photocatalytic activity. Subsequently, the photogenerated electron (e⁻) reacted with dissolved oxygen in the reaction system to form first O₂^{•-} and then OH[•]. The O₂^{•-} and OH[•] radicals then degraded the CBZ molecule to CO₂, H₂O, and other intermediates during the photolysis. This hypothesized mechanism is in good agreement with previous literature (Cao et al., 2018; Xu et al., 2015; Z. Yang et al., 2017).

The result of TOC analysis showed that the mineralization rate of CBZ after photodegradation was 25%. This mineralization rate indicated that CBZ was degraded into CO₂ and H₂O and other organic intermediate compounds about 75%. Thus, the chemical structure and toxicity of those intermediate products after CBZ photodegradation need to be further studied.

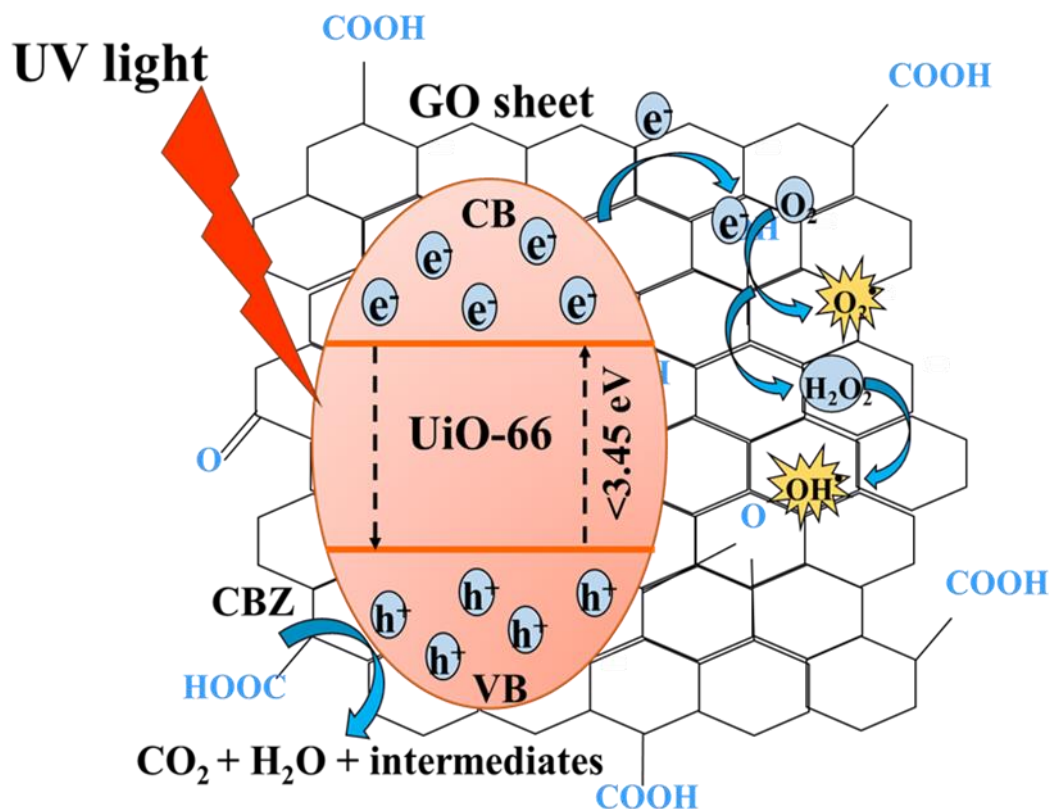


Fig. 4.6 Schematic diagram of the proposed mechanism for the enhanced photocatalytic oxidation over the UiO-66_GO composite catalyst

4.3.6 Recyclability of the Composites

After five consecutive runs, the photocatalytic activity of the UiO-66_GO-0.5 composite was still considerably high (>60%). It decreased by only 30% between the 1st and 3rd runs and maintained a similar level until the 5th run (**Fig. 4.7**). The decline in CBZ degradation could be due to its accumulation and deposition of its photodegradation by-products on the UiO-66_GO-0.5 nanoparticles, as confirmed by FTIR (**Fig. 4.8**). After five runs, no significant change in the structure of UiO-66_GO-0.5 was observed by XRD or SEM (**Figs. 4.9 and 4.10**), indicating good stability and recyclability of UiO-66_GO-0.5 for practical applications.

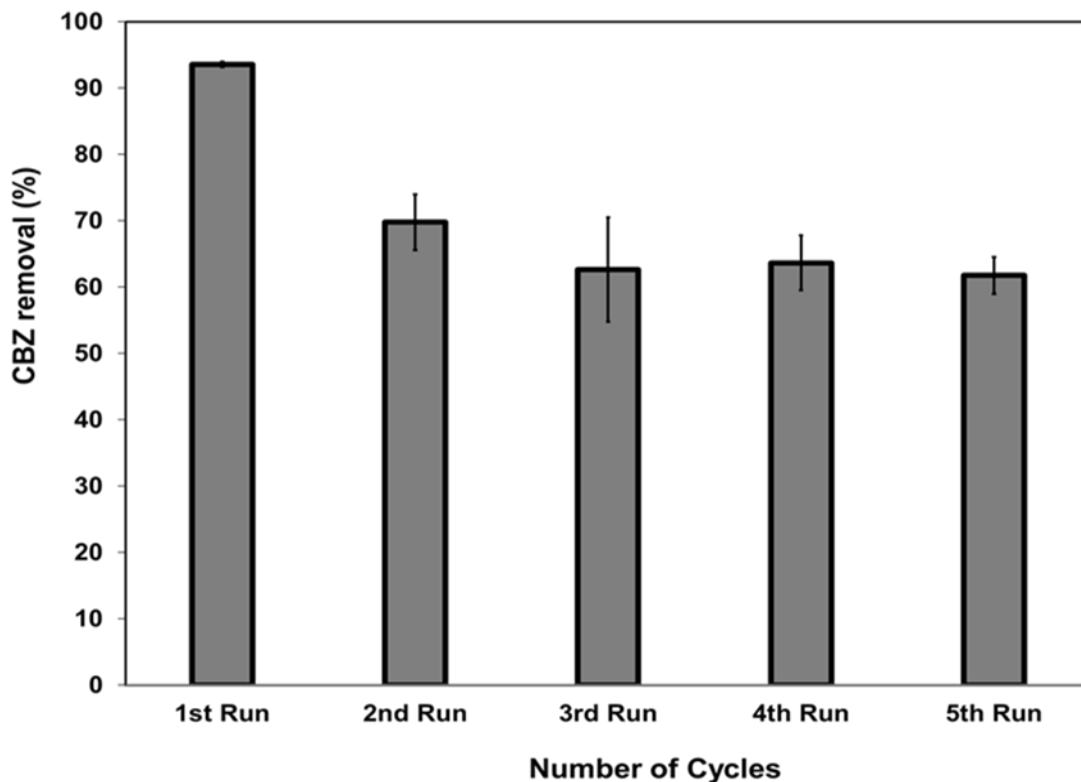


Fig. 4.7 Photocatalytic performance over five cycles (experimental conditions: initial CBZ concentration = 5 mg/L; pH 7; mass of UiO-66_GO-0.5 m = 50 mg; solution volume V = 50 mL). Plot and error bars represent averages and standard deviations from triplicate experiments.

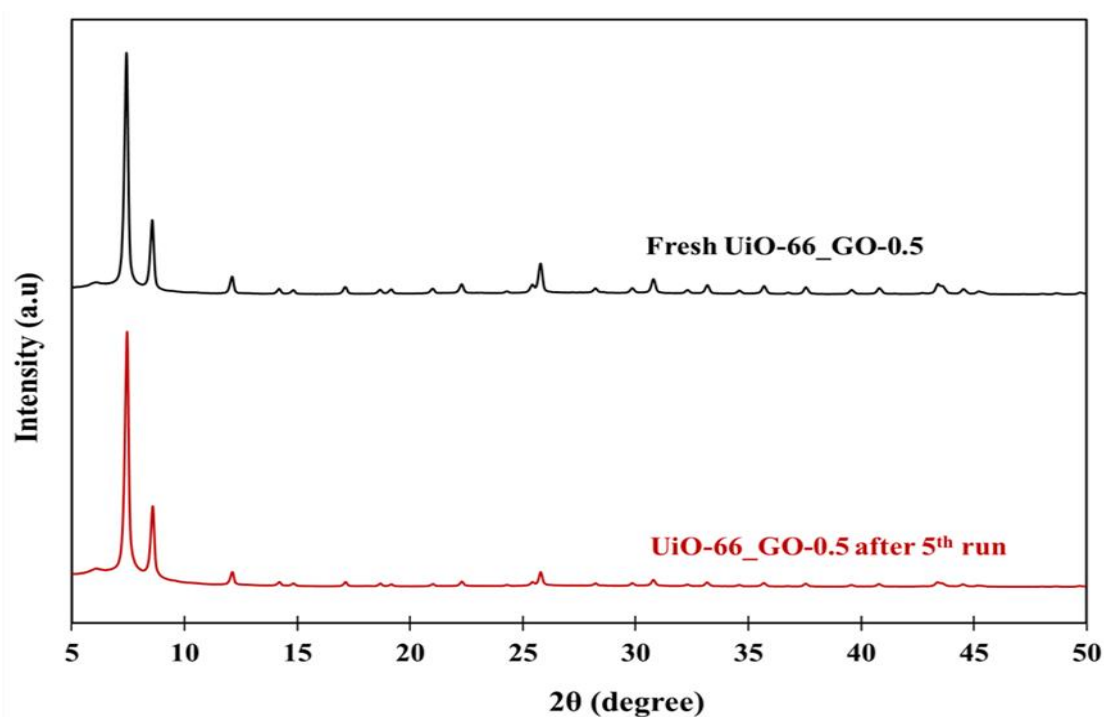


Fig.4.8 XRD spectra of fresh UiO-66_GO-0.5 and UiO-66_GO-0.5 after 5th run

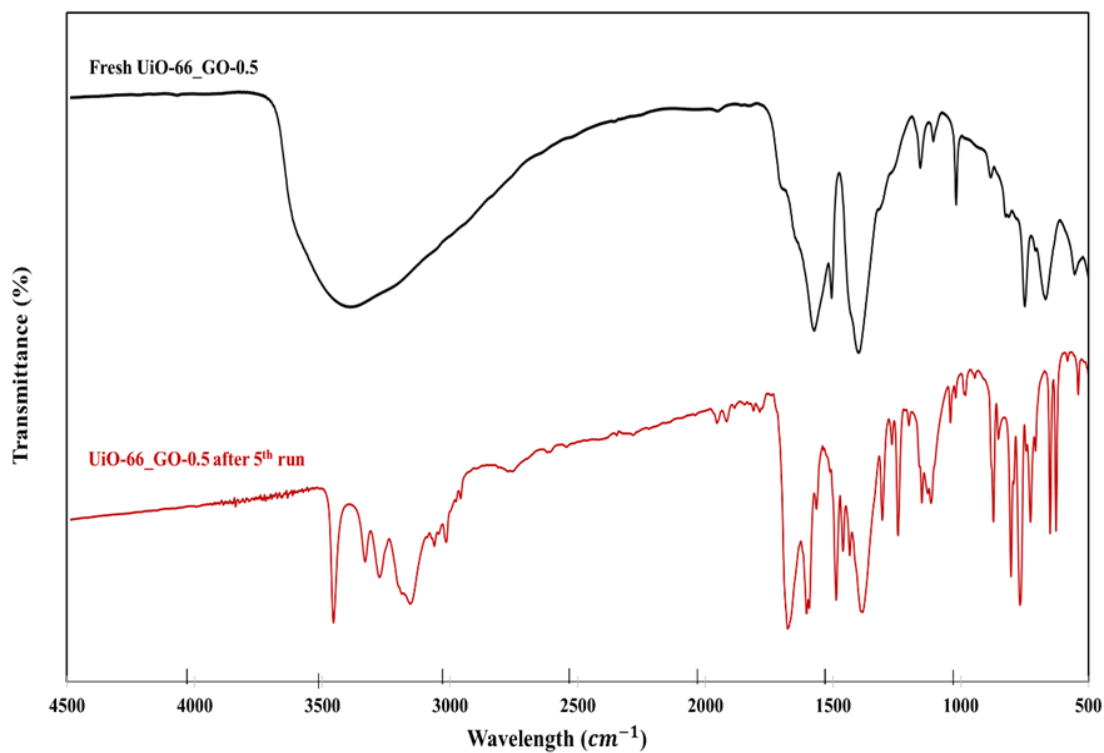


Fig. 4.9 XRD patterns of fresh UiO-66_GO-0.5 and UiO-66_GO-0.5 after 5th run

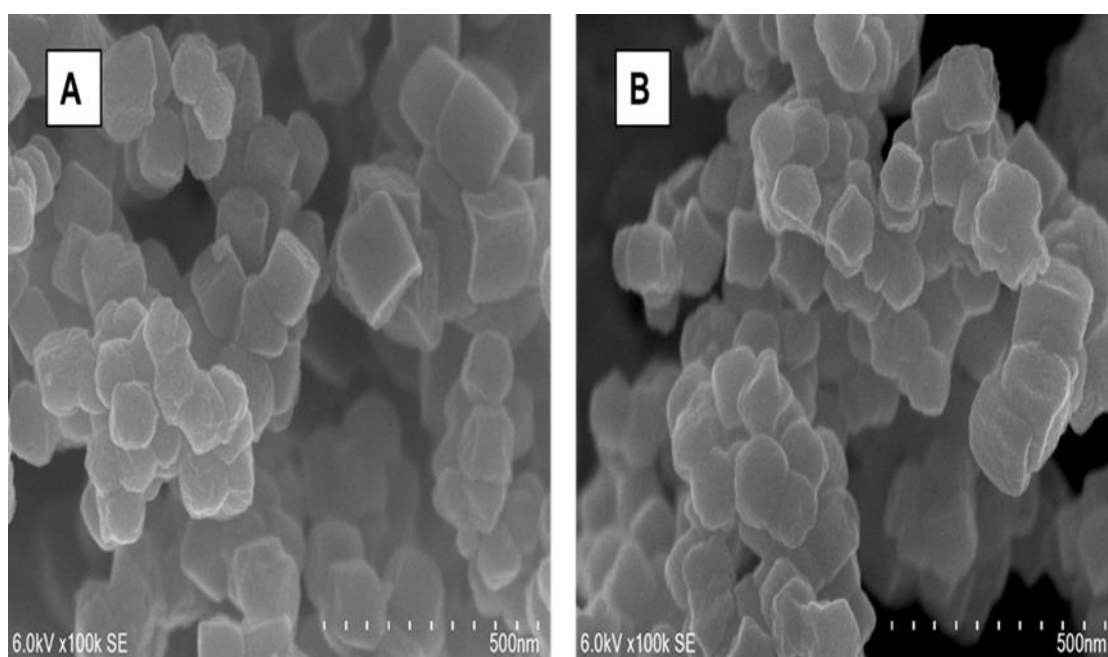


Fig. 4.10 SEM images of [A] fresh UiO-66_GO-0.5 and [B] UiO-66_GO-0.5 after 5th run

4.4. Conclusions

A UiO-66_GO composite catalyst prepared by a simple solvothermal method has been successfully applied in the photodegradation of the persistent pharmaceutical compound CBZ with an effective degradation efficiency ($\geq 95\%$) superior to those of its constituent materials: GO ($< 75\%$) and UiO-66 ($< 85\%$). The enhancement of the photocatalytic activity of UiO-66 by GO is most likely attributable to the increased SSA and porosity and the narrower band gap. The photocatalytic activity of UiO-66_GO composites has been shown to be significantly influenced by the GO loading, catalyst dose, initial pollutant concentration, and solution pH. The main reactive species responsible for the photodegradation of CBZ have been identified as $O_2^{\bullet-}$ and OH^{\bullet} radicals. Furthermore, the composite showed good recyclability, retaining a high CBZ degradation efficiency of more than 60% after five cycles. 0.5 wt% of GO loading and acidic pH (pH=5) were optimum condition and were selected for study in the chapter 5 due to their high photodegradation.

Overall, this work confirmed that the modification of semiconductors with GO as an electron acceptor is an effective technique for improving photocatalytic activity. It also gives a great inspiration for the development of other GO-based composite photocatalysts and expansion of the application of UiO-66 in water or wastewater treatment technologies. To the best of our knowledge, this is the first reported application of UiO-66_GO for photocatalysis, and the optimum experimental conditions have been investigated. Practical conditions, such as actual concentrations of target OMPs, the water matrix, and solar light usage, might also affect UiO-66_GO catalysts, and need to be investigated in further research.

CHAPTER V

UiO66_GO NF Membrane and Its Filtration Performance

5.1 Introduction

Organic micropollutants (OMPs) are the organic compounds whose persistent, toxic and bioaccumulative properties give negative effects on environment such as pesticides, pharmaceuticals, personal care products, plasticizer, solvents and endocrine disruptors. Currently, the occurrence and persistence of those OMPs in source water are becoming the concern in drinking water supply due to a poor removal efficiency and potential adverse health effects associated with those substances for consumer (Kostich et al., 2014; Herklotz et al., 2010; Ormad et al., 2008). The processes of conventional treatment including coagulation, flocculation, and sand filtration are ineffective to remove OMP residues (Klavarioti et al., 2009; H. Jiang & Adams, 2006). The additional methods including H₂O₂ or O₃ oxidation and activated carbon (AC) adsorption for final treatment steps show effective results but generation of toxic chemical by-products and saturation of AC are still their main challenges (Ali & Gupta, 2006; Reynolds et al., 1989).

Among those various treatment methods, nanofiltration (NF) membrane which give a high removal efficiency of hardness, multivalent ions, heavy metal and some of small organic molecules (micropollutants and colors) by sieving and charge effect mechanism (Lee et al., 2016) can be employed as a final process in treatment train to produce a high quality of drinking water production. Inorganic and polymeric membranes are mostly applied in NF membrane technology (Fane et al., 2011). Despite their advantages including stable pore structure, chemical inertness and temperature resistance, inorganic membranes have been suffering with several problems such as complicated fabrication process, nonselective cracks and prohibitive cost (Safarpour et al., 2014). Polymeric membranes, on the other hand, overcome the membrane market because of their easy and cheap fabrication (Alpatova et al., 2013). However, the hydrophobic surface and malleable characteristic of polymeric membranes which

causes low water flux and high fouling formation are the major drawbacks of using them in membrane applications (Wu et al., 2008). Integrate the composite material with polymeric substrates could be potential options. The recent studies of Ma et al and Ying et al reported that UiO66_GO membrane gave higher flux and anti-fouling compared to pristine PES membrane because of its hydrophilicity and membrane smoothness (Ma et al., 2017; Ying et al., 2017). However, they only applied UiO66_GO composite on ultrafiltration membrane to reject macromolecule compounds and up to date, there has no report on application of UiO66_GO composites on NF membrane.

Therefore, this chapter aims to modify hydrophobic surface of commercial NF membrane by hydrophilic UiO66_GO nanocomposite material to improve its water flux and anti-fouling properties. The synthesis method of composite nanofiltration, its stability, performance of OMP rejection and recovery of HA fouled membrane under photocatalysis were also demonstrated in this.

5.2 Experimental Method

The permeate flux of four membranes (pristine NF, UiO-66_GO/NF-5%, UiO-66_GO/NF-10%, and UiO-66_GO/NF-15%) were measured in a dead-end cell filtration system filled (Millipore stirred cell) with nitrogen gas as a pressure source (**Fig. 3.4**). The membrane sheet was cut into a circle 76 mm in diameter with an effective area of approximately 41.2 cm². Prior to the filtration experiment, each membrane was compacted under a pressure of 5 bar with Milli-Q water for 30 min to obtain a steady-state flux. To determine the pure water flux, Milli-Q water was filtered under a pressure of 4 bar and the permeate flux was recorded every 10 min for 1 h. Then, the pure water flux (J_{w1} , kg/m² h bar) was calculated by (Safarpour et al., 2014b).

$$J_{w1} = \frac{M}{AtP} \quad (5.1)$$

where M is the weight of the permeate (kg), A is the membrane active surface (m²), t is the permeation time (h), and P is the operational pressure (bar).

In addition, to examine the stability of the composite membranes (UiO-66_GO/NF-5%, UiO-66_GO/NF-10%, and UiO-66_GO/NF-15%), each composite

membrane was washed with Milli-Q five times and dried. The masses of the composite membranes before and after washing were determined to calculate the mass loss of the UiO-66_GO composite to indicate their stability.

To determine their flux recovery performance, immediately after pure water filtration (J_{w1}), MilliQ water was replaced with 50 mg/L SRHA as a model foulant, and it was filtered in an identical system for 3 h (J_{SRHA}). The fouled membrane was washed and kept in MilliQ water for 15 min and its pure water flux was determined again (J_{w2}). The anti-fouling properties of the pristine and composite membranes were quantified by the *FRR* (Kumar et al., 2016).

$$FRR(\%) = 100 \frac{J_{w2}}{J_{w1}} \quad (5.2)$$

Here, J_{w1} and J_{w2} are the pure water fluxes ($\text{kg/m}^2 \text{ h}$) before and after fouling, respectively. A higher *FRR* indicates better fouling resistance.

To understand the fouling behavior better, the additional indicators R_r , R_{ir} , and R_t were determined by **Eqs. 5.3, 4, and 5**, respectively (Safarpour et al., 2016).

$$R_r(\%) = 100 \frac{J_{w2} - J_{SRHA}}{J_{w1}} \quad (5.3)$$

$$R_{ir}(\%) = 100 \frac{J_{w1} - J_{w2}}{J_{w1}} \quad (5.4)$$

$$R_t(\%) = 100 \frac{J_{w1} - J_{SRHA}}{J_{w1}} \quad (5.5)$$

R_r indicates the proportion of fouling caused by concentration polarization. R_{ir} indicates the proportion of fouling caused by adsorption or/and deposition of SRHA molecules on the membrane surface. R_t is the sum of R_r and R_{ir} , indicating the degree of total flux decline. In general, a lower ratio shows better fouling resistance.

To confirm how photocatalysis regenerated the composite membrane, after the filtration with SRHA solution for 3 h, the fouled membrane was irradiated under UV light (wavelength, 254 nm; Power = 8 W, intensity, 0.16 W/cm^2) for 1 h. The membrane was then subjected to pure water filtration and *FRR* and R_{ir} were calculated by **Eqs. 5.2 and 4**, respectively.

The separation performance of fresh UiO-66_GO/NF membranes was evaluated by rejection of diclofenac (DCF), carbamazepine (CBZ), sulfamethoxazole (SMX) and atrazine (ATZ) with the same filtration apparatus. Solutions of 1.0 mg/L of OMPs at pH 5 were filtered by each of the UiO-66_GO/NF membranes for 2 h under a pressure of 4 bar. The residual concentrations were determined by high-performance liquid chromatography (Prominence UFLC, Shimadzu) equipped with a UV/Vis

absorbance detector (SPD-20 UFLC, Shimadzu) and a C18 column of dimensions 4.6 mm × 250 mm × 5 μm (Kinetex, Phenomenex, Torrance, CA, USA). Based on these measurements, the removal efficiencies of the OMPs were calculated by

$$Removal (\%) = 100 \frac{C_0 - C_p}{C_0} \quad (5.6)$$

where C_0 and C_p are the initial and permeate concentrations (mg/L), respectively.

The concentration of the nanocomposite and pollutants in the permeate water was analyzed by UV-Vis spectroscopy in scan mode with the wavelength ranging in 200-600 nm. The Milli-Q water and 5 g/l of UiO-66_GO-0.5 solution was analyzed the same way as permeate water for reference.

5.3 Results and Discussion

5.3.1 Water Flux

The pristine NF membrane had a water flux of 34 kg/m² h bar (**Fig. 5.1**), which was comparable to the reported range (1.5–30 kg/m² h bar) (Bruggen et al., 2003). The water fluxes of the UiO-66_GO/NF-5%, UiO-66_GO/NF-10%, and UiO-66_GO/NF-15% membranes were 44, 57, and 63 kg/m² h bar, respectively (**Fig. 5.1**). This result demonstrated that modifying the NF surface with the UiO-66_GO-0.5 nanocomposite increased the water flux of the pristine NF membrane substantially owing to the increase of the surface hydrophilicity (water contact angle), porosity, and membrane pore size (**Table 5.2**). The increased membrane hydrophilicity was attributed to the oxygen-containing functional groups, such as hydroxyl and carboxyl, on the UiO-66_GO nanocomposite, which increased the water permeability and wettability of membrane by attracting water molecules and the high water-holding capacity of these groups (Kumar et al., 2016; Safarpour et al., 2014b). In addition, the higher porosity and larger pore size of the membranes improved the water transport paths and decreased the resistance to water molecules (Safarpour et al., 2016; Ying et al., 2017), increasing the water flux.

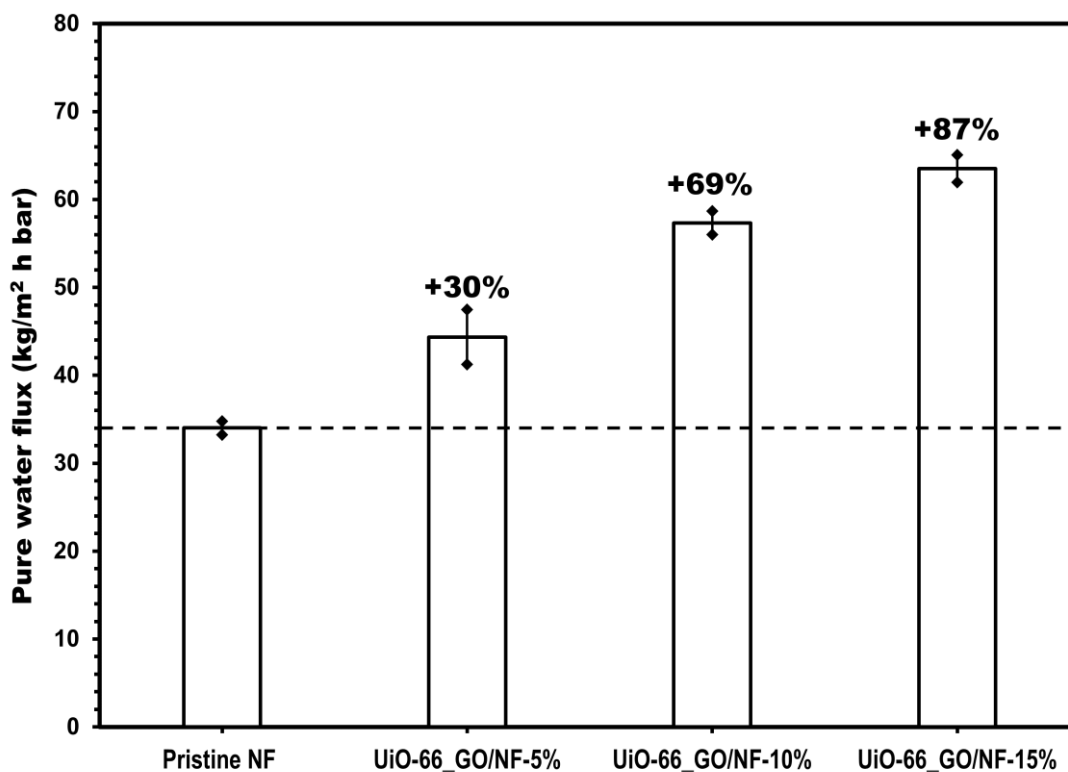


Fig. 5.1 Pure water flux of pristine and composite membranes (operation pressure = 4 bar; solution pH = 5). Plots and error bars represent averages and standard deviations from triplicate experiments.

5.3.2 Membrane Stability

The mass losses for UiO-66_GO loadings of 5 and 10 wt % after five washes were 4.49% and 8.64%, respectively (**Fig. 5.2 and Fig. 5.3**). Both loading rates allowed the strong adhesion of the UiO-66_GO nanocomposite to the membrane surface. The terephthalic ligand and various functional groups on the UiO-66_GO nanocomposite provide a supporting platform for the surface chemical modifications, which allows substantial adhesion to the polyamide membrane (Denny and Cohen, 2015; J. R. Li et al., 2012). However, when the UiO-66_GO loading was increased to 15 wt %, the mass loss increased to 23.1%, and voids were visible on the washed membranes (**Fig. 5.2 and Fig. 5.3**). SEM images showed many cracks on the as-prepared membrane surface, suggesting that the stability reduction was due to the poorly structured nanocomposite layer (Fig.3.12). Because of the high water flux and good adhesion, the range of 5 wt% < UiO-66_GO < 15 wt% was considered as the optimal loading range and 10 wt% was used in subsequent experiments.

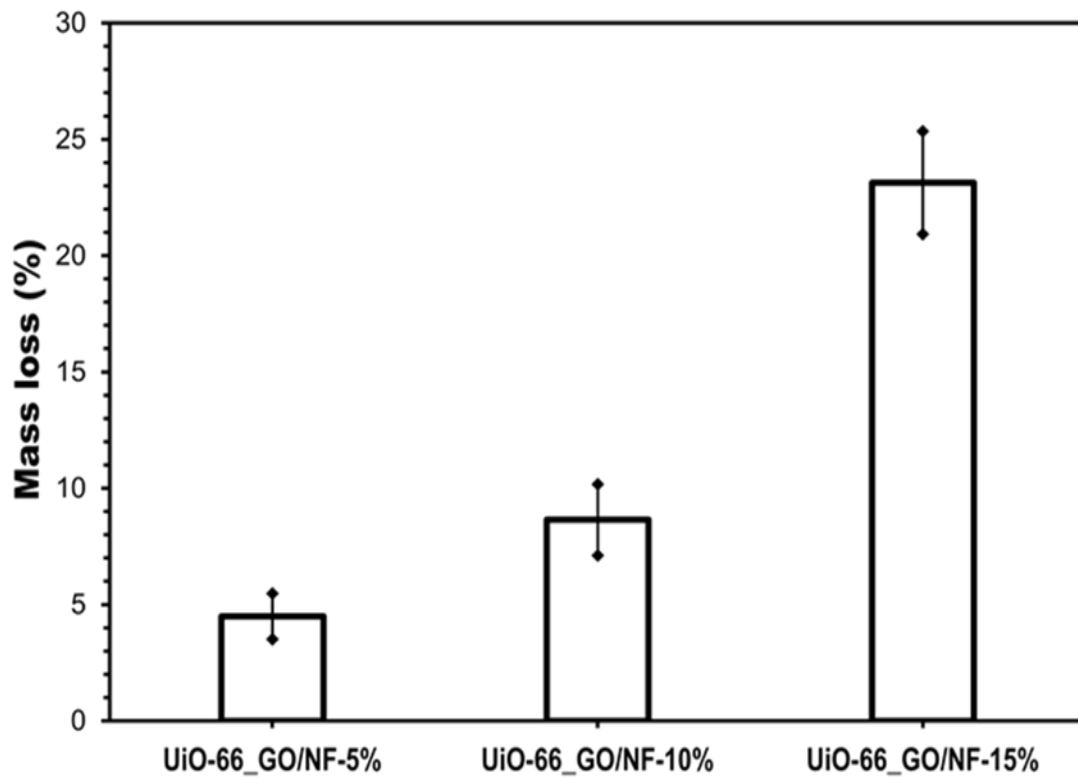
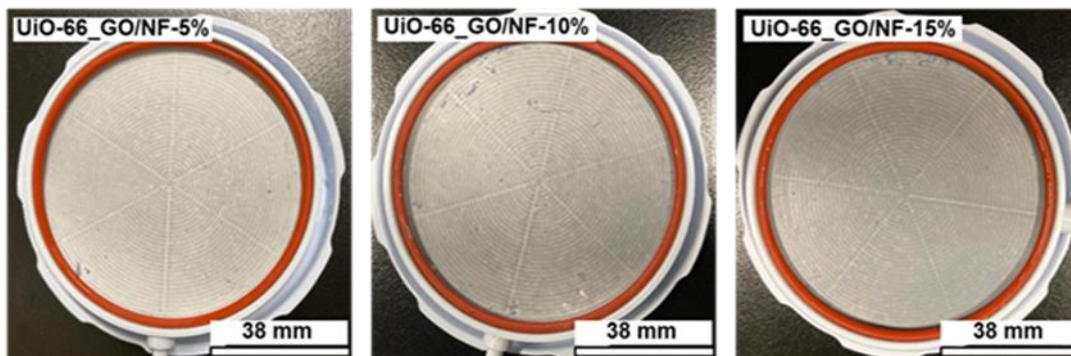


Fig. 5.2 Mass loss (%) of UiO-66_GO nanocomposites after five washes

[A]



[B]

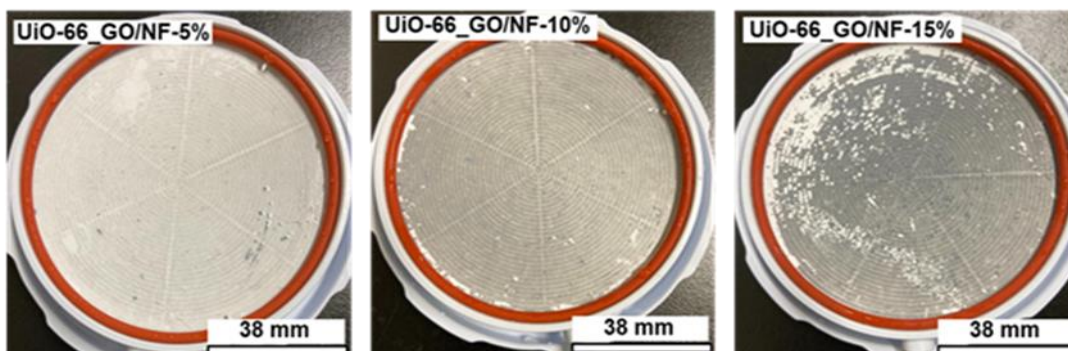


Fig. 5.3 Images of the composite membrane [A] before and [B] after washing five times

5.3.3 Anti-Fouling Properties

Milli-Q water was replaced with Suwannee River humic acid (SRHA) solution, and the permeate flux of pristine and composite membranes decreased constantly (**Fig. 5.4A**) due to SRHA molecules accumulating on the membrane surface (Kumar et al., 2016; Safarpour et al., 2015). After filtering SRHA solution for 180 min and washing with MilliQ water, the membranes were used to filter MilliQ water again, and the permeate flux was higher than for SRHA and stable over 1 h. The pristine membrane showed a reduction in pure water flux from 34 to 15 kg/m² h bar, whereas the UiO-66_GO/NF membrane showed a reduction from 57 to 29 kg/m² h bar. The flux recovery ratio (*FRR*), irreversible fouling ratio (*R_{ir}*), and total fouling ratio (*R_t*) of the pristine membrane were 49.9%, 49.8%, and 57.3%, respectively (**Fig. 5.4B**). This result demonstrated that the adsorption of SRHA caused substantial irreversible fouling, accounting for almost 90% of the total fouling of the pristine membrane. In contrast, for the UiO-66_GO/NF membrane, *FRR* was increased to 79.6% and *R_t* was decreased to 33.3%. Furthermore, *R_{ir}* was reduced to 20.7%, which accounted for only 60% of *R_t*, demonstrating that the nanocomposites prevented the adsorption of SRHA to the pristine membrane. For both pristine and composite membranes, the *R_{ir}* values were higher than the *R_r* values, implying that cake formation mainly contributed to fouling rather than concentration polarization. The higher *FRR* and lower fouling ratios of the UiO-66_GO/NF membrane than those of the pristine membrane further confirmed that the anti-fouling properties of the composite membrane arose from its hydrophilicity, surface roughness, and charge repulsion.

The hydrophilic character of the membrane made it less prone to fouling due to the abundance of hydrophilic functional groups, which decreases the adsorption of hydrophobic SRHA molecules on the membrane surface (Goosen et al., 2005; Zhang et al., 2013). Furthermore, surface roughness promotes membrane fouling due to the accumulation of SRHA molecules in the deep valleys of the rough surface (Safarpour et al., 2014b; Zinadini et al., 2014). Thus, the lower surface roughness of the UiO-66_GO/NF membrane observed by atomic force microscopy (AFM) (**Table 3.2, Fig. 5.4**) decreased membrane fouling compared with the pristine NF membrane. In addition, the membrane charge also affects its anti-fouling properties (Bernstein et al., 2011). The pK_a of SRHA is about 4.5 (Hebbar et al., 2015; Huang and Shiu, 1996), meaning

that SRHA had a negative charge under our experimental conditions of pH 5. The pH of the point of zero charge of UiO-66 and GO is about 4 (Cai and Larese-casanova, 2014; Castarlenas et al., 2017; C. Chen et al., 2017), and thus the UiO-66_GO/NF membrane also had a negative charge at pH 5. Therefore, the electrostatic repulsion between the negative charges on the SRHA molecules and the membrane may be important in reducing the adhesion of SRHA to the membrane.

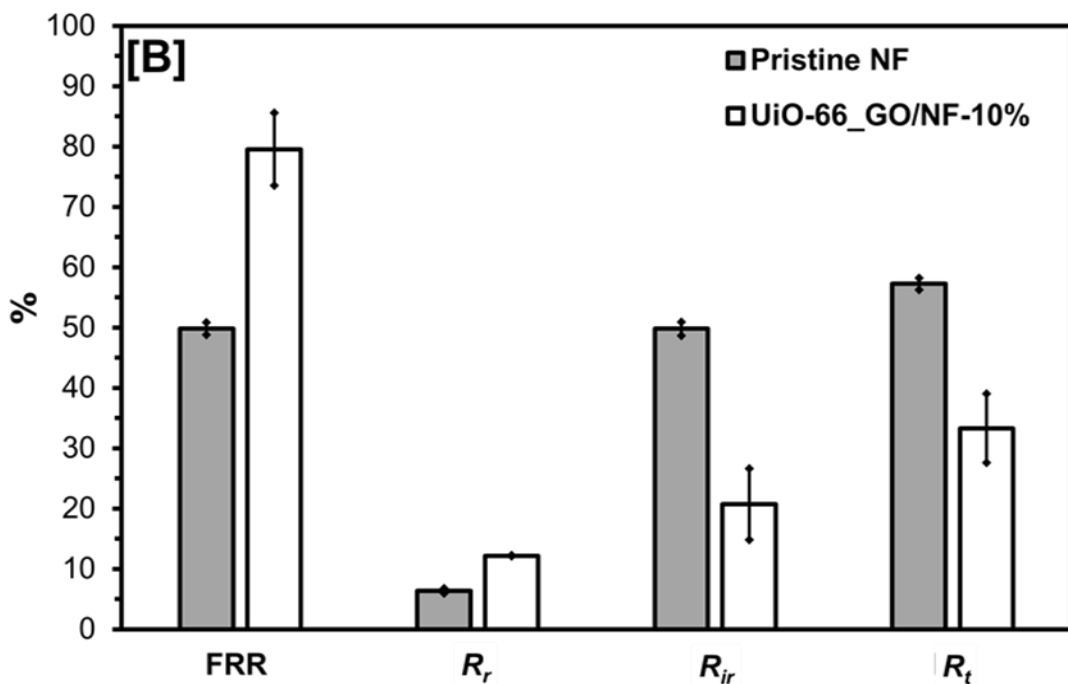
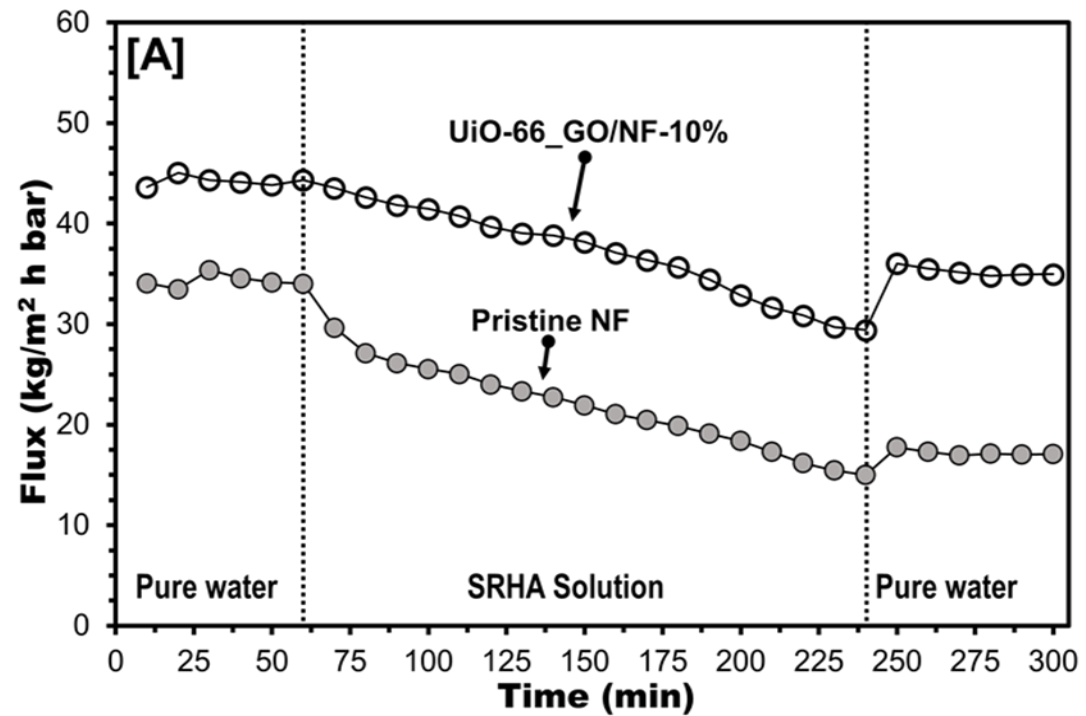


Fig. 5.4 [A] Flux versus time and [B] flux recovery ratio and fouling ratios of the pristine NF and UiO-66_GO/NF-10% membranes for SRHA filtration (experimental conditions: SRHA concentration = 50 mg/L; operation pressure = 4 bar; pH = 5). Plots and error bars represent averages and standard deviations from triplicate experiments.

5.3.4 Photocatalytic Activity of UiO-66_GO/NF for Flux Recovery

After the filtration of SRHA for 1 h, R_{ir} of the pristine and composite membranes were 49.8% and 20.7%, respectively (**Fig. 5.5A**). R_{ir} was probably due to complete or partial blockage caused by the adsorption of SRHA to the membrane surface and pores (Guan et al., 2018; Lin, 2017). After the fouled membrane was exposed to UV irradiation for 1 h, R_{ir} of the pristine membrane decreased slightly from 49.8% to 45.1%, whereas R_{ir} of the UiO-66_GO/NF membrane decreased substantially from 20.7% to only 2.4% (**Fig. 5.5A**). The photocatalytic degradation of SRHA by the UiO-66_GO nanocomposite caused this large decrease in R_{ir} . To evaluate the effect of photocatalysis further, we measured FRR for the fouled membranes with and without irradiation (**Fig. 5.5B**). FRR of the composite membrane after photodegradation increased by more than 18%, which was higher than that of the pristine membrane (4%). This result also suggested that under UV radiation, the composite membrane had substantial photocatalytic activity that degraded SRHA on the membrane surface and recovered water flux, resulting in the higher FRR (>97%), compared with no UV irradiation (**Fig. 5.5B**).

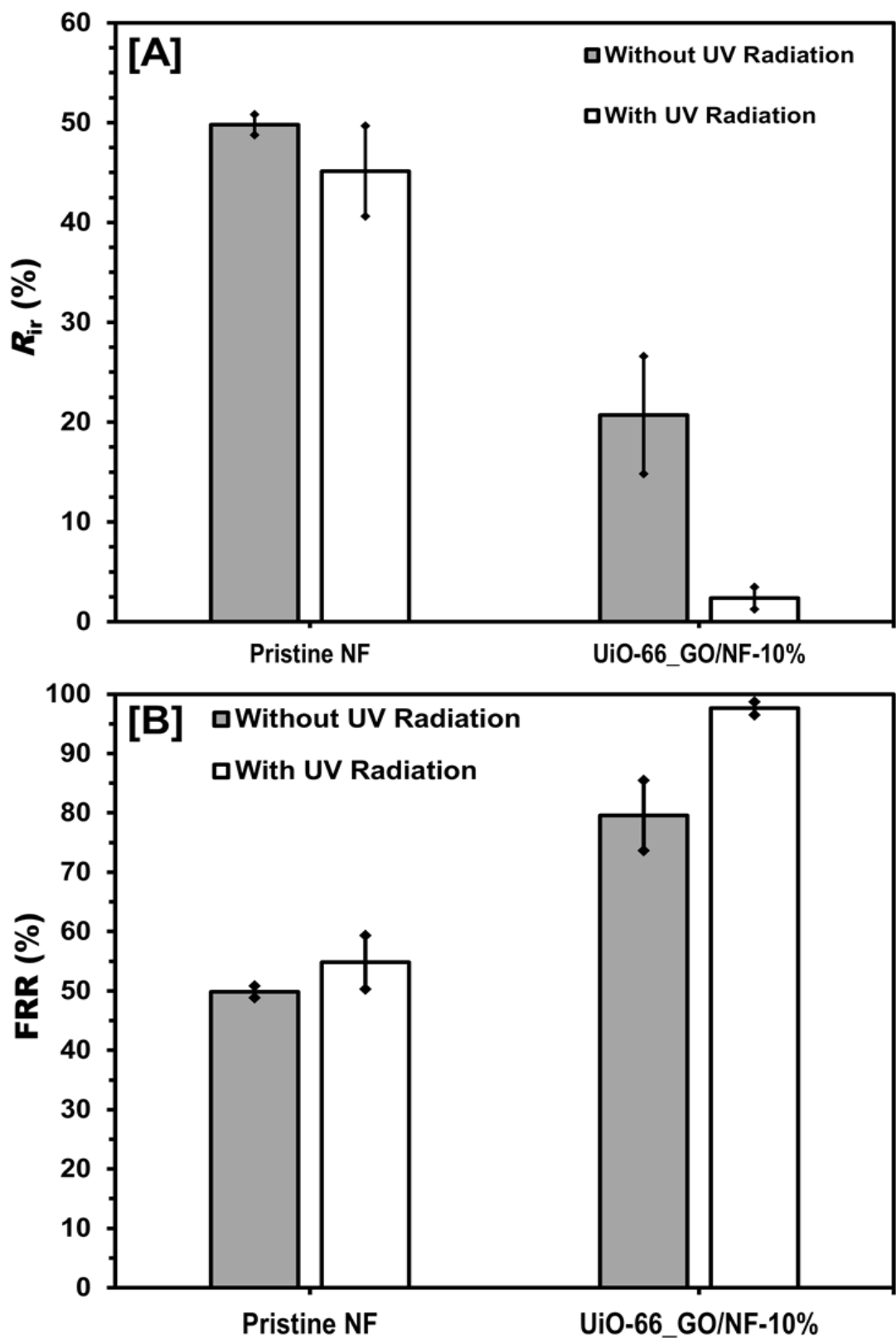


Fig. 5.5 [A] R_{ir} and [B] FRR with and without UV radiation for the pristine NF and UiO-66_GO/NF-10% membranes after SRHA filtration. Plots and error bars represent the averages and standard deviations from triplicate experiments.

5.3.5 Separation Performance

The separation of CBZ, ATZ, SMX and DCF by the UiO-66_GO/NF-10% membrane was examined. The initial removal rates were higher than 90% for the first 20 min of filtration (**Fig. 5.6**), which may arise from the effect of adsorption on the membrane surface in addition to physical separation. Over a longer filtration time, the rejection decreased while the adsorption equilibrium was reached, and then became stable after 2 h. The highest steady-state rejection got from DCF (93%), following by ATZ (73%) and CBZ (69%) and the lowest got from SMX (31%) (**Fig. 5.6**).

The OMP rejections are summarized: $DCF > ATZ > CBZ > SMX$ which corresponding their superior hydrophobicity (LogKow): $DCF > ATZ > CBZ > SMX$ ($R=0.96$). The molecular weight of OMP compounds didn't correspond to their rejections ($R=0.41$). In addition, DCF, ATZ and the UiO-66_GO nanocomposite had a negative charge at pH 5 (Cai and Larese-casanova, 2014; C. Chen et al., 2017; Kincl et al., 2004), which caused electrostatic repulsion between DCF and ATZ molecules and the membrane surface, increasing the rejection of DCF and ATZ, as described by Lin et al. (2017). In contrast, CBZ and SMX is charged positively at pH 5 (Moztahida et al., 2019; Oleszczuk et al., 2009), which allowed CBZ and SMX molecules to diffuse into the pores and the membrane surface, decreasing the rejection values (Liu et al., 2018). Overall, UiO-66_GO/NF-10% rejected ATZ and DCF with high removal efficiency rates (73-93%), which resulted from the combined effects of low hydrophobic interaction and charge repulsion (Donnan effects).

The result of UV-Vis analysis of nanocomposite concentration in the permeate showed that UiO-66_GO-0.5 solution showed the peak of absorbance at wavelength of 230 nm (**Fig. 5.7**). Meanwhile, the absorbance of Milli-Q and permeate water wasn't significant indicated that there aren't any nanocomposites in permeate water and composite membrane can separate nanocomposite from permeate water.

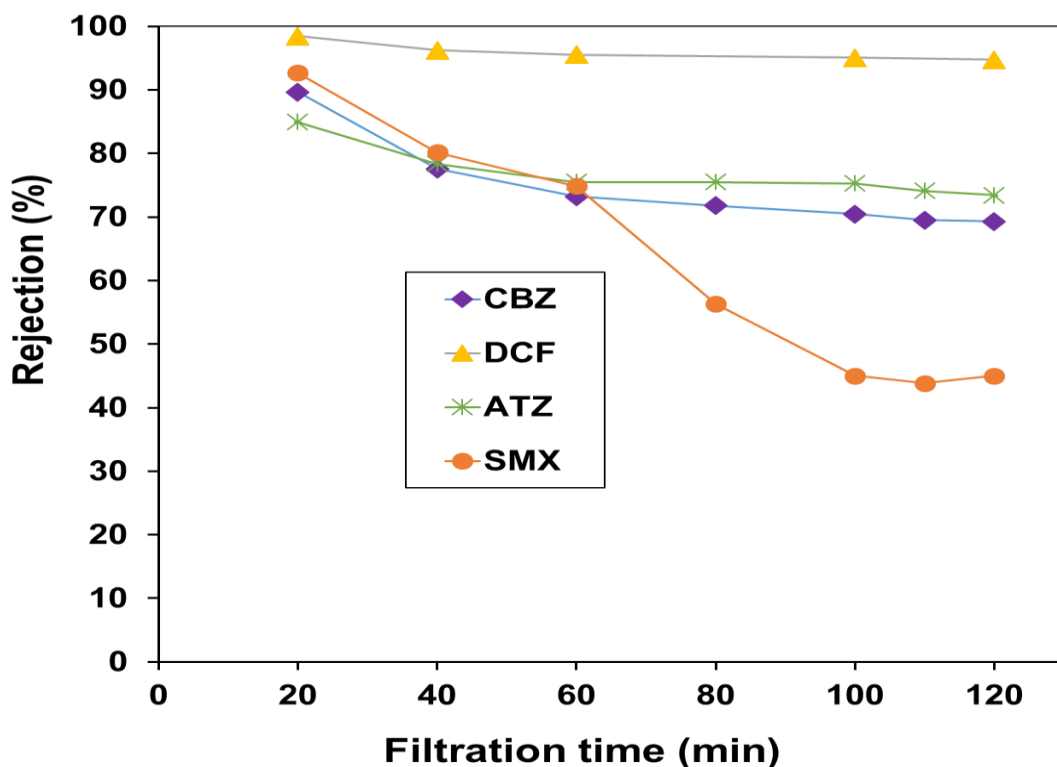


Fig. 5.6 DCF and CBZ removal over time by the UiO-66_GO/NF-10% membrane (experimental conditions: initial DCF and CBZ concentration = 1 mg/L; operation pressure = 4 bar; solution pH = 5). Plots and error bars represent averages and standard deviations from duplicate experiments.

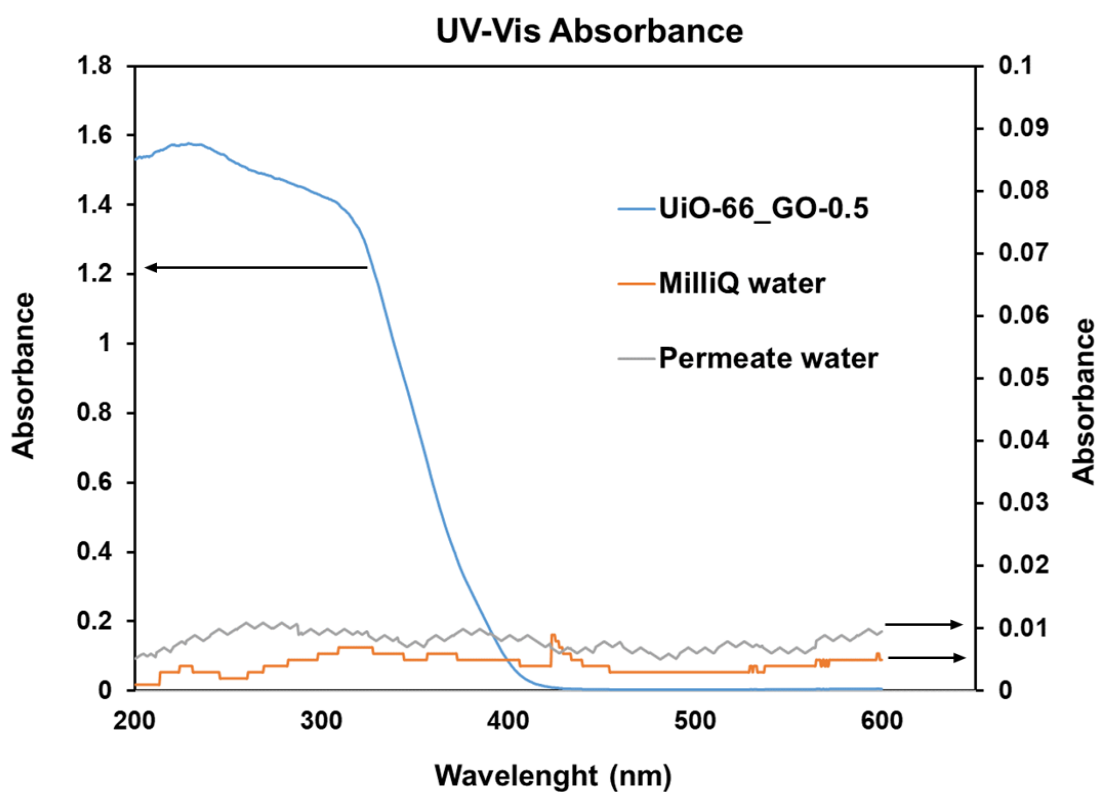


Fig. 5.7 UV-Vis absorbance of permeate water, UiO-66_GO-0.5 and Milli-Q water

5.4 Conclusion

Photocatalytic NF membranes were fabricated by depositing a 0.5% GO loading in the composite material (UiO-66_GO) synthesized by a hydrothermal method on NF membranes by PASA to improve the water flux and anti-fouling properties. The UiO-66_GO nanocomposite at a loading of 15 wt % increased pure water flux by 187% compared with the pristine NF membrane flux by increasing the surface smoothness and hydrophilicity of the membrane surface. However, the 10 wt % loading of the UiO-66_GO composite was optimal because of its high flux improvement (169%) and the good stability of the UiO-66_GO nanocomposite on the membrane surface. The UiO-66_GO/NF-10% membrane also showed higher *FRR* (80%) and lower *R_{ir}* (20%) than did the pristine NF membrane, which were attributed to the increased hydrophilicity, surface smoothness, and charge repulsion. In addition, the composite membrane showed photocatalytic activity that degraded accumulated SRHA and increased *FRR* to 98%. The composite membrane also high solute rejection of OMP (DCF), although it may necessary to measure the effects of photocatalytic activity of UiO-66_GO on solute rejection by the membrane and membrane lifetime for long term usage.

CHAPTER VI

Conclusion and Recommendations

6.1 Conclusion

This study aimed to develop a novel photocatalytic NF membrane using Zr-based organic framework enhanced by graphene oxide for water and wastewater treatment and consist of several specific objectives.

First, the specific objective is to present a facile hydrothermal method for preparing UiO-66_GO nanocomposites with different GO loading and characterize their physio-chemical properties. As the result, nanocomposite of UiO-66_GO with different GO loadings (0.1, 0.5, 1, and 5 wt%) was successfully synthesized by one-step hydrothermal method and their physio-chemical properties were confirmed by the analyses of their crystalline structure, surface functional groups, morphology, element compositions, specific surface area, porosity and light absorption.

Second, the specific objective is to investigate the enhancing effect of GO on the photocatalytic activity of UiO-66. Consequently, UiO-66_GO composite has been successfully applied in the photodegradation of the persistent pharmaceutical compound CBZ with an effective degradation efficiency ($\geq 95\%$) superior to those of its constituent materials: GO ($< 75\%$) and UiO-66 ($< 85\%$). Also, the photocatalytic rate constant over the UiO-66_GO nanocomposite was about 2.8 and 1.7 times higher than those over pristine GO and UiO-66, respectively. The improvement of the photocatalytic activity of UiO-66 by GO is most likely attributable to the increased SSA and porosity and the narrower band gap.

The third specific objective is to test the photodegradation of CBZ with different GO contents in the composites, catalyst doses and solution pH. The experimental result have indicated that the amount of GO loading, catalyst dose, initial pollutant concentration, and solution pH significantly affect the photodegradation of CBZ by UiO-66_GO nanocomposites and 0.5 wt% of GO loading and acidic pH

(pH=5) were optimum condition and were selected for study in the further chapter due to their high photodegradation.

Moreover, another objective in this study is to introduce the pressure-assisted self-assembly (PASA) method to fabricate UiO-66_GO/NF membranes and confirm the membrane stability with different loadings of UiO-66_GO nanocomposite. The result showed that the nanocomposite of UiO-66_GO-5 wt% with different loading (5, 10, 15 wt%) was successfully layered on commercial nanofiltration (Synder NFX) membrane by pressure-assisted self-assembly (PASA) method with a good adhesion of UiO-66_GO composite on NF membrane to fabricate a novel composite membrane.

To evaluate the effect of UiO66_GO nanocomposite on water flux improvement of commercial NF membranes, check stability of the composite membranes after five-time washes and point out the optimum loading of UiO66_GO composite on NF membrane are also other sub-objective in this study. The results confirmed that the presence of UiO-66_GO composite with different loadings (5, 10, 15%) significantly increase the water flux of NF membrane flux to 130, 168, 187 %, respectively due to the enhancement of hydrophilic surface of the membrane. UiO-66_GO composite loading 10 wt% is pointed out as the optimum loading because of its high-water flux improvement (168 %) and good adhesion on NF membrane surface after five-time washes.

In addition, the investigation of the effect of UiO66_GO nanocomposite on *FRR* and anti-fouling properties indicated that the UiO-66_GO/NF-10% membrane also showed higher *FRR* (80%) and lower R_{ir} (20%) than did the pristine NF membrane. Hence, UiO66_GO nanocomposite can improve *FRR* and anti-fouling properties of NF membrane, which were attributed to the increased hydrophilicity, surface smoothness, and charge repulsion.

Furthermore, the determination of the rejection of various OMP groups with different physio-chemical properties by UiO66_GO/ NF membranes demonstrated that adsorption of OMPs on membrane can remove all selected OMPs including ATZ, CBZ, DCF and SMX more than 85%. But when the composite membrane reaches equilibrium state, the steady-state rejections are summarized as: DCF > ATZ > CBZ > SMX which

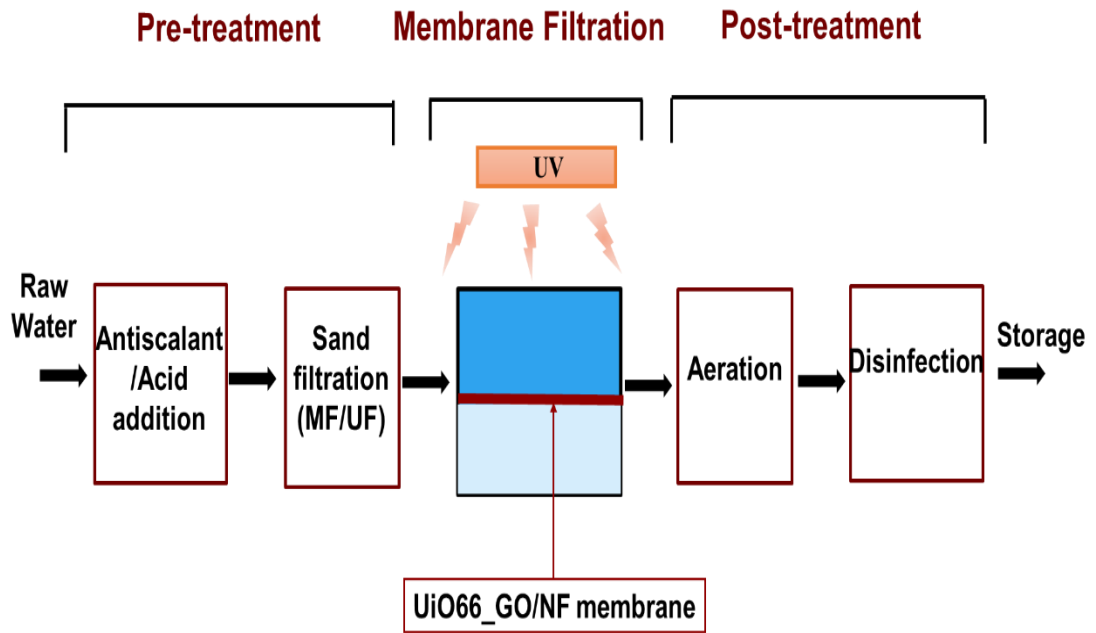
corresponding their superior hydrophobicity (Log_{kow}): $\text{DCF} > \text{ATZ} > \text{CBZ} > \text{SMX}$ ($R=0.96$), indicating that the hydrophobicity of solute plays important role in rejection by UiO-66_GO-0.5/NF (10%) membrane.

Finally, the examination of the effects of photocatalysis on regeneration of UiO66_GO/NF membranes in order to degrade irreversible foulant and improve flux recovery was concluded that the composite membrane has photocatalytic activity to degrade HA which adsorption on membrane surface and pore by decreasing irreversible fouling from 21 to 7 % and increasing flux recovery ratio from 79 to 93 %.

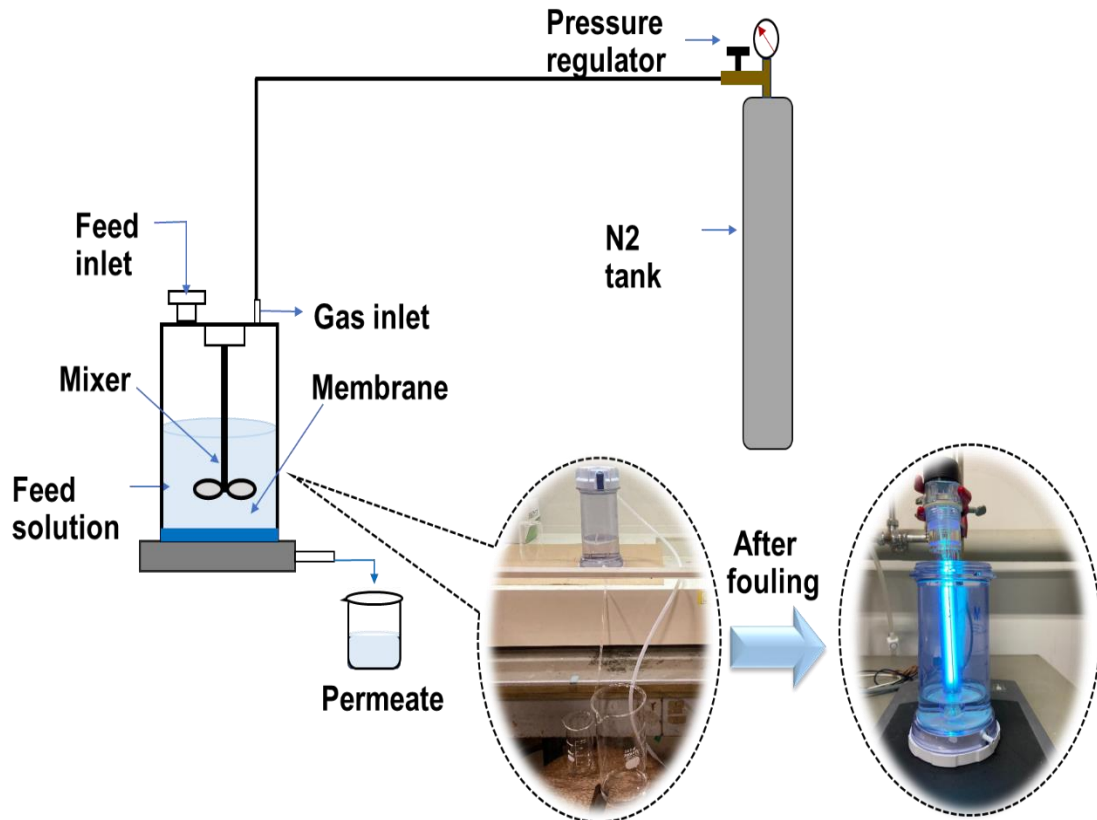
6.2 Recommendations and Further Research

After the safety of permeate water has been confirmed, this novel UiO-66_GO-0.5/NF membrane can be applied in water and wastewater treatment plant which use the NF membrane technology and for the point of use (POU) filter unit in household to product a high water capacity, good water quality and low energy consumption(**Fig. 6.1**). Also, when the filtration system suffers the flux decline approximately 20%, the composite membrane should be irradiated under UV irradiation to improve the water flux recovery (**Fig. 6.2**).

[A]



[B]



[C]

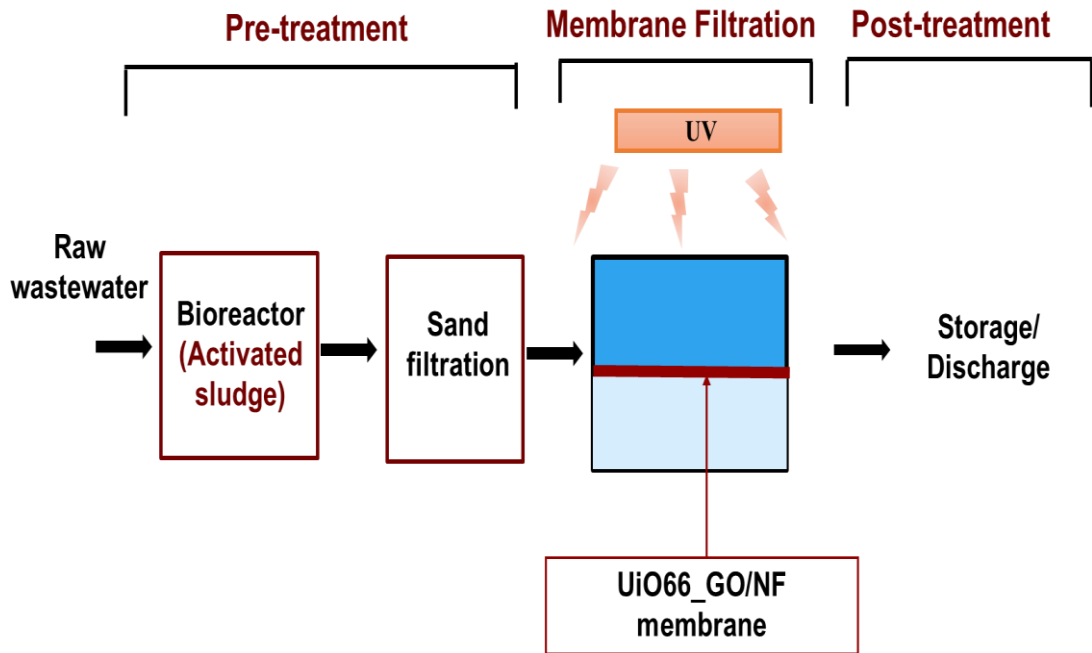


Fig. 6.1 Proposed schematic diagram of [A] water treatment plant using NF membrane technology, [B] POU filter unit in household, and [C] municipal wastewater treatment using NF membrane bioreactor

Overall, this novel composite NF (UiO-66_GO-0.5/NF) membrane product are expected to produce a high-water capacity, good water quality and low energy consumption but still there are some future works that need to be investigated and improved:

- Although, this composite NF membrane show a good rejection of hydrophobic OMPs but the rejection of hydrophilic OMP compounds is still low and need to be improved in the future work.
- In addition, installation UV lamp inside the practical filtration system for membrane recovery is complicated and need to be well designed.
- Moreover, the optimum experimental conditions have been applied in this study. Thus, practical conditions, such as actual concentrations of target OMPs, the water

matrix, and solar light usage, might also affect filtration performance, and need to be investigated in further study.

- Furthermore, the pristine membrane can be damaged by UV radiation; thus, the effect of photolysis on long-term use of composite membrane should be further investigation.
- The actual ratio of GO in composite catalysts should be measured in the future work.

REFERENCES

- A, A.Sq.Se.O.Ma.Aa., 2014. Factors influencing the photocatalytic degradation of reactive yellow 145 by TiO₂-coated non-woven fibers. *Am. J. Anal. Chem.* 05, 445–454.
- Abdi, J., Vossoughi, M., Mohammad, N., 2017. Synthesis of metal-organic framework hybrid nanocomposites based on GO and CNT with high adsorption capacity for dye removal. *Chem. Eng. J.* 326, 1145–1158. <https://doi.org/10.1016/j.cej.2017.06.054>
- Abdolhosseinzadeh, S., Asgharzadeh, H., Kim, H.S., 2015. Fast and fully-scalable synthesis of reduced graphene oxide. *Nat. Publ. Gr.* 1–7. <https://doi.org/10.1038/srep10160>
- Ahmed, I., Jhung, S.H., 2014. Composites of metal – organic frameworks : Preparation and application in adsorption. *Biochem. Pharmacol.* 17, 136–146. <https://doi.org/10.1016/j.mattod.2014.03.002>
- Akpinar, I., Yazaydin, A.O., 2018. Adsorption of atrazine from water in metal – organic framework materials. *J. Chem. Eng. Data* 63. <https://doi.org/10.1021/acs.jced.7b00930>
- Ali, F., Ali, J., Shah, N.S., Sayed, M., Khan, H.M., 2018. Carbamazepine degradation by UV and UV-assisted AOPs : Kinetics , mechanism and toxicity investigations. *Process Saf. Environ. Prot.* 117, 307–314. <https://doi.org/10.1016/j.psep.2018.05.004>
- Ali, I., Gupta, V.K., 2006. Advances in water treatment by adsorption technology. *Nat. Protoc.* 1, 2661.
- Almasri, D.A., Rhad, T., Atieh, M.A., Mckay, G., Ahzi, S., 2018. High performance hydroxyiron modified montmorillonite nanoclay adsorbent for arsenite removal. *Chem. Eng. J.* 335, 1–12. <https://doi.org/10.1016/j.cej.2017.10.031>
- Alpatova, A., Kim, E., Sun, X., Hwang, G., 2013. Fabrication of porous polymeric nanocomposite membranes with enhanced anti-fouling properties : Effect of casting composition. *J. Memb. Sci.* 444, 449–460.

<https://doi.org/10.1016/j.memsci.2013.05.034>

- Anbia, M., Sheykhi, S., 2013. Preparation of multi-walled carbon nanotube incorporated MIL-53-Cu composite metal-organic framework with enhanced methane sorption. *J. Ind. Eng. Chem.* 19, 1583–1586.
<https://doi.org/10.1016/j.jiec.2013.01.026>
- Atkinson, D.E., Brice-Bennett, S., D'Souza, S.W., 2007. Antiepileptic medication during pregnancy: does fetal genotype affect outcome? *Pediatr. Res.* 62, 120.
- Bernstein, R., Belfer, S., Freger, V., 2011. Bacterial attachment to RO membranes surface-modified by concentration-polarization-enhanced graft polymerization. *Environ. Sci. Technol.* 45, 5973–5980.
- Bolton, J.R., Cotton, C.A., 2011. *The ultraviolet disinfection handbook*. American Water Works Association.
- Bradder, P., Ling, S.K., Wang, S., Liu, S., 2011. Dye adsorption on layered graphite oxide. *J. Chem. Eng. Data* 56, 138–141.
- Bruggen, B. Van Der, Vandecasteele, C., Gestel, T. Van, Doyenb, W., Leysenb, R., 2003. Review of Pressure-Driven Membrane Processes. *Environ. Prog.* 22, 46–56.
<https://doi.org/10.1002/ep.670220116>
- Cai, D., Song, M., 2007. Preparation of fully exfoliated graphite oxide nanoplatelets in organic solvents. *J. Mater. Chem.* 17, 3678–3680.
<https://doi.org/10.1039/b705906j>
- Cai, N., Larese-casanova, P., 2014. Sorption of carbamazepine by commercial graphene oxides: A comparative study with granular activated carbon and multiwalled carbon nanotubes. *J. Colloid Interface Sci.* 426, 152–161.
<https://doi.org/10.1016/j.jcis.2014.03.038>
- Cantor, K., Lynch, C.F., Hildesheim, M., Dosemeci, M., Lubin, J., Alavanja, M., Craun, G., 1999. Drinking water sources and chlorination by-products in Iowa, III. Risk of brain cancer. *Am. J. Epidemiol.* 150, 552–560.
- Cao, J., Yang, Z., Xiong, W., Zhou, Y., Peng, Y., Li, X., 2018. One-step synthesis of Co-doped UiO-66 nanoparticle with enhanced removal efficiency of tetracycline: Simultaneous adsorption and photocatalysis. *Chem. Eng. J.* 353, 126–137.

- <https://doi.org/10.1016/j.cej.2018.07.060>
- Cao, Y., Zhao, Y., Lv, Z., Song, F., Zhong, Q., 2015. Preparation and enhanced CO₂ adsorption capacity of UiO-66/graphene oxide composites. *J. Ind. Eng. Chem.* 27, 102–107. <https://doi.org/10.1016/j.jiec.2014.12.021>
- Castarlenas, S., Téllez, C., Coronas, J., 2017. Gas separation with mixed matrix membranes obtained from MOF UiO-66- graphite oxide hybrids. *J. Memb. Sci.* 526, 205–211. <https://doi.org/10.1016/j.memsci.2016.12.041>
- Cavka, J.H., Olsbye, U., Guillou, N., Bordiga, S., Lillerud, K.P., 2008. A New Zirconium Inorganic Building Brick Forming Metal Organic Frameworks with Exceptional Stability - Supp. Info. *J. Am. Chem. Soc.* 6, 1–19. <https://doi.org/10.1021/ja8057953>
- Chavan, S.M., Shearer, G.C., Svelle, S., Olsbye, U., Bonino, F., Ethiraj, J., Lillerud, K.P., Bordiga, S., 2014. Synthesis and Characterization of Amine-Functionalized Mixed- Ligand Metal – Organic Frameworks of UiO-66 Topology. <https://doi.org/10.1021/ic500607a>
- Chen, C., Chen, D., Xie, S., Quan, H., Luo, X., Guo, L., 2017. Adsorption behaviors of organic micropollutants on zirconium metal – organic framework UiO-66 : Analysis of surface interactions. *ACS Appl. Mater. Interfaces* 9, 41043–41054. <https://doi.org/10.1021/acsami.7b13443>
- Chen, H., Wang, X., Bi, W., Wu, Y., Dong, W., 2017. Journal of Colloid and Interface Science Photodegradation of carbamazepine with BiOCl / Fe₃O₄ catalyst under simulated solar light irradiation. *J. Colloid Interface Sci.* 502, 89–99. <https://doi.org/10.1016/j.jcis.2017.04.031>
- Chen, S.S., Taylor, J.S., Mulford, L.A., Norris, C.D., 2004. Influences of molecular weight, molecular size, flux, and recovery for aromatic pesticide removal by nanofiltration membranes. *Desalination* 160, 103–111. [https://doi.org/10.1016/S0011-9164\(04\)90000-8](https://doi.org/10.1016/S0011-9164(04)90000-8)
- Chew, M.Y.C., Watanabe, C., Tou, Y., 2011. Technology in Society The challenges in Singapore NEWater development : Co-evolutionary development for innovation and industry evolution. *Technol. Soc.* 33, 200–211.

- <https://doi.org/10.1016/j.techsoc.2011.06.001>
- Compton, O.C., Nguyen, S.T., 2010. Graphene oxide, highly reduced graphene oxide, and graphene: Versatile building blocks for carbon-based materials. *Small* 6, 711–723. <https://doi.org/10.1002/sml.200901934>
- Dawoud, B., Amer, E., Gross, D., 2007. Experimental investigation of an adsorptive thermal energy storage. *Int. J. energy Res.* 31, 135–147. <https://doi.org/10.1002/er>
- Denny, M.S., Cohen, S.M., 2015. In situ modification of metal–organic frameworks in mixed-matrix membranes. *Angew. Chemie Int. Ed.* 54, 9029–9032.
- Deria, P., Mondloch, J.E., Karagiari, O., Bury, W., Hupp, J.T., Farha, O.K., 2014. Beyond post-synthesis modification: evolution of metal-organic frameworks via building block replacement. *Chem. Soc. Rev.* 43, 5896–5912.
- Ding, J., Yang, Z., He, C., Tong, X., Li, Y., Niu, X., Zhang, H., 2017. Journal of Colloid and Interface Science UiO-66 (Zr) coupled with Bi₂MoO₆ as photocatalyst for visible-light promoted dye degradation. *J. Colloid Interface Sci.* 497, 126–133. <https://doi.org/10.1016/j.jcis.2017.02.060>
- Dong, S., Feng, J., Fan, M., Pi, Y., Hu, L., Han, X., Liu, M., Sun, Jingyu, Sun, Jianhui, 2015. Recent developments in heterogeneous photocatalytic water treatment using visible light-responsive photocatalysts: a review. *RSC Adv.* 5, 14610–14630. <https://doi.org/10.1039/C4RA13734E>
- Eddaoudi, M., 2015. Quest for Anionic MOF Membranes: Continuous sod-ZMOF Membrane with CO₂ Adsorption-Driven Selectivity 2, 8–11. <https://doi.org/10.1021/ja511495j>
- Eriksson, P., 1988. Nanofiltration extends the range of membrane filtration. *Environ. Prog. Sustain. Energy* 7, 58–62.
- Fan, W., Lai, Q., Zhang, Q., Wang, Y., 2011. Nanocomposites of TiO₂ and reduced graphene oxide as efficient photocatalysts for hydrogen evolution. *J. Phys. Chem. C* 115, 10694–10701. <https://doi.org/10.1021/jp2008804>
- Fane, A.G., Tang, C., Wang, R., 2011. Membrane technology for water: microfiltration, ultrafiltration, nanofiltration, and reverse osmosis. *Treatise Water Sci.*
- Fathizadeh, M., Aroujalian, A., Raisi, A., 2011. Effect of added NaX nano-zeolite into

- polyamide as a top thin layer of membrane on water flux and salt rejection in a reverse osmosis process. *J. Memb. Sci.* 375, 88–95.
- Ferrari, B., Paxéus, N., Giudice, R. Lo, Pollio, A., Garric, J., 2003. Ecotoxicological impact of pharmaceuticals found in treated wastewaters: Study of carbamazepine, clofibrac acid, and diclofenac. *Ecotoxicol. Environ. Saf.* 55, 359–370. [https://doi.org/10.1016/S0147-6513\(02\)00082-9](https://doi.org/10.1016/S0147-6513(02)00082-9)
- Galus, M., Kirischian, N., Higgins, S., Purdy, J., Chow, J., Rangaranjan, S., Li, H., Metcalfe, C., Wilson, J.Y., 2013. Chronic, low concentration exposure to pharmaceuticals impacts multiple organ systems in zebrafish. *Aquat. Toxicol.* 132, 200–211.
- Geissen, V., Mol, H., Klumpp, E., Umlauf, G., Nadal, M., van der Ploeg, M., van de Zee, S.E.A.T.M., Ritsema, C.J., 2015. Emerging pollutants in the environment: A challenge for water resource management. *Int. Soil Water Conserv. Res.* 3, 57–65. <https://doi.org/10.1016/j.iswcr.2015.03.002>
- Geneva, S., 2011. Guidelines for drinking-water quality. World Heal. Organ. Geneva, Switz.
- Glassmeyer, S.T., Furlong, E.T., Kolpin, D.W., Batt, A.L., Benson, R., Boone, J.S., Conerly, O., Donohue, M.J., King, D.N., Kostich, M.S., Mash, H.E., Pfaller, S.L., Schenck, K.M., Simmons, J.E., Varughese, E.A., Vesper, S.J., Villegas, E.N., Wilson, V.S., 2017. Nationwide reconnaissance of contaminants of emerging concern in source and treated drinking waters of the United States. *Sci. Total Environ.* 581–582, 909–922. <https://doi.org/10.1016/j.scitotenv.2016.12.004>
- Goosen, M.F.A., Sablani, S.S., Al-Hinai, H., Al-Obeidani, S., Al-Belushi, R., Jackson, aD, 2005. Fouling of reverse osmosis and ultrafiltration membranes: a critical review. *Sep. Sci. Technol.* 39, 2261–2297.
- Guan, Y.-F., Qian, C., Chen, W., Huang, B.-C., Wang, Y.-J., Yu, H.-Q., 2018. Interaction between humic acid and protein in membrane fouling process: a spectroscopic insight. *Water Res.* 145, 146–152.
- Guo, H., Wang, X., Qian, Q., Wang, F., Xia, X., 2009. A green approach to the synthesis of graphene nanosheets. *ACS Nano* 3, 2653–2659.

- Hai, F.I., Yang, S., Id, M.B.A., Id, V.S., Shawkat, S., Sanderson-smith, M., Gorman, J., Xu, Z., Yamamoto, K., 2018. Carbamazepine as a possible anthropogenic marker in water : occurrences , toxicological effects , treatment technologies. *Water* 1–32. <https://doi.org/10.3390/w10020107>
- Hebbar, R.S., Isloor, A.M., Ismail, A.F., Shilton, S.J., Obaid, A., Fun, H.-K., 2015. Probing the morphology and anti-organic fouling behaviour of a polyetherimide membrane modified with hydrophilic organic acids as additives. *New J. Chem.* 39, 6141–6150.
- Herklotz, P.A., Gurung, P., Vanden, B., Kinney, C.A., 2010. Chemosphere Uptake of human pharmaceuticals by plants grown under hydroponic conditions. *Chemosphere* 78, 1416–1421. <https://doi.org/10.1016/j.chemosphere.2009.12.048>
- Heu, R., Ateia, M., Awfa, D., Punyapalakul, P., Yoshimura, C., 2020. Photocatalytic Degradation of Organic Micropollutants in Water by Zr-MOF / GO Composites. *J. Compos. Sci.* 4, 54. <https://doi.org/10.3390/jcs4020054>
- Hoskins, B.F., Robson, R., 1990. Design and Construction of a New Class of Scaffolding-like Materials Comprising Infinite Polymeric Frameworks of 3D-Linked Molecular Rods. A Reappraisal of the $Zn(CN)_2$ and $Cd(CN)_2$ Structures and the Synthesis and Structure of the Diamond-Related Frameworks . *J. Am. Chem. Soc.* 112, 1546–1554. <https://doi.org/10.1021/ja00160a038>
- Huang, C., Shiu, H., 1996. Interactions between alum and organics in coagulation. *Colloids Surfaces A Physicochemical Eng. Asp.* 113, 155–163.
- Jacangelo, J.G., Trussell, R.R., Watson, M., 1997. Role of membrane technology in drinking water treatment in the United States 9164.
- Jiang, H., Adams, C., 2006. Treatability of chloro-s-triazines by conventional drinking water treatment technologies. *Water Res.* 40, 1657–1667. <https://doi.org/10.1016/j.watres.2006.02.013>
- Jin, Z., Yang, H., 2017. Exploration of Zr–metal–organic framework as efficient photocatalyst for hydrogen production. *Nanoscale Res. Lett.* 12. <https://doi.org/10.1186/s11671-017-2311-6>
- Jönsson, J., Camm, R., Hall, T., 2013. Removal and degradation of Glyphosate in water

- treatment: A review. *J. Water Supply Res. Technol. - AQUA* 62, 395–408.
<https://doi.org/10.2166/aqua.2013.080>
- Kalidindi, S.B., Nayak, S., Briggs, M.E., Jansat, S., Katsoulidis, A.P., Miller, G.J., Warren, J.E., Antypov, D., Corà, F., Slater, B., Prestly, M.R., Martí-gastaldo, C., Rosseinsky, M.J., 2015. Chemical and structural stability of zirconium-based metal – organic frameworks with large three-dimensional pores by linker engineering 221–226. <https://doi.org/10.1002/anie.201406501>
- Khan, J.A., He, X., Khan, H.M., Shah, N.S., Dionysiou, D.D., 2013. Oxidative degradation of atrazine in aqueous solution by UV/H₂O₂/Fe²⁺, UV/S₂O₈²⁻/Fe²⁺ and UV/H₂SO₅/Fe²⁺ processes: a comparative study. *Chem. Eng. J.* 218, 376–383.
- Khan, N.A., Hasan, Z., Jhung, S.H., 2013. Adsorptive removal of hazardous materials using metal-organic frameworks (MOFs): A review. *J. Hazard. Mater.* 244–245, 444–456. <https://doi.org/10.1016/j.jhazmat.2012.11.011>
- Kim, M., Cahill, J.F., Su, Y., Prather, K.A., Cohen, S.M., 2012. Postsynthetic ligand exchange as a route to functionalization of “inert” metal-organic frameworks. *Chem. Sci.* 3, 126–130. <https://doi.org/10.1039/c1sc00394a>
- Kim, S.D., Cho, J., Kim, I.S., Vanderford, B.J., Snyder, S.A., 2007. Occurrence and removal of pharmaceuticals and endocrine disruptors in South Korean surface, drinking, and waste waters. *Water Res.* 41, 1013–1021. <https://doi.org/10.1016/j.watres.2006.06.034>
- Kincl, M., Meleh, M., Veber, M., Vrecer, F., 2004. Study of physicochemical parameters affecting the release of diclofenac sodium from lipophilic matrix tablets. *Acta Chim. Slov.* 51, 409–425.
- Kisch, H., 2013. Semiconductor photocatalysis-mechanistic and synthetic aspects. *Angew. Chemie Int. Ed.* 52, 812–847.
- Kiso, Y., Nishimura, Y., Kitao, T., Nishimura, K., 2000. Rejection properties of non phenylic pesticides with nanofiltration membranes. *J. Membr. Sci.* 171, 229–237.
- Kiso, Yoshiaki, Nishimura, Y., Kitao, T., Nishimura, K., 2000. Rejection properties of non-phenylic pesticides with nanofiltration membranes. *J. Memb. Sci.* 171, 229–237. [https://doi.org/10.1016/S0376-7388\(00\)00305-7](https://doi.org/10.1016/S0376-7388(00)00305-7)

- Kiso, Y., Sugiura, Y., Kitao, T., Nishimura, K., 2001. Effects of hydrophobicity and molecular size on rejection of aromatic pesticides with nanofiltration membranes. *J. Memb. Sci.* 192, 1–10. [https://doi.org/10.1016/S0376-7388\(01\)00411-2](https://doi.org/10.1016/S0376-7388(01)00411-2)
- Kitagawa, S., Kitaura, R., Noro, S., 2004. Functional porous coordination polymers. *Angew. Chemie Int. Ed.* 43, 2334–2375.
- Klavarioti, M., Mantzavinos, D., Kassinos, D., 2009. Removal of residual pharmaceuticals from aqueous systems by advanced oxidation processes. *Environ. Int.* 35, 402–417. <https://doi.org/10.1016/j.envint.2008.07.009>
- Knepper, T.P., Sacher, F., Lange, F.T., Brauch, H.J., Karrenbrock, F., Roerden, O., Lindner, K., 1999. Detection of polar organic substances relevant for drinking water. *Waste Manag.* 19, 77–99. [https://doi.org/10.1016/S0956-053X\(99\)00003-3](https://doi.org/10.1016/S0956-053X(99)00003-3)
- Kostich, M.S., Batt, A.L., Lazorchak, J.M., 2014. Concentrations of prioritized pharmaceuticals in effluents from 50 large wastewater treatment plants in the US and implications for risk estimation. *Environ. Pollut.* 184, 354–359. <https://doi.org/10.1016/j.envpol.2013.09.013>
- Košutić, K., Kunst, B., 2002. Removal of organics from aqueous solutions by commercial RO and NF membranes of characterized porosities. *Desalination* 142, 47–56. [https://doi.org/10.1016/S0011-9164\(01\)00424-6](https://doi.org/10.1016/S0011-9164(01)00424-6)
- Kreno, L.E., Leong, K., Farha, O.K., Allendorf, M., Duyne, R.P. Van, Hupp, J.T., 2011. Metal À Organic Framework Materials as Chemical Sensors. <https://doi.org/10.1021/cr200324t>
- Kuila, A., Surib, N.A., Mishra, N.S., Nawaz, A., Leong, K.H., Sim, L.C., Saravanan, P., Ibrahim, S., 2017. Metal organic frameworks: A new generation coordination polymers for visible light photocatalysis. *Chem. Sel.* 2, 6163–6177. <https://doi.org/10.1002/slct.201700998>
- Kumar, M., Gholamvand, Z., Morrissey, A., Nolan, K., Ulbricht, M., Lawler, J., 2016. Preparation and characterization of low fouling novel hybrid ultrafiltration membranes based on the blends of GO-TiO₂nanocomposite and polysulfone for humic acid removal. *J. Memb. Sci.* 506, 38–49. <https://doi.org/10.1016/j.memsci.2016.02.005>

- Lee, A., Elam, J.W., Darling, S.B., 2016. Membrane materials for water purification: design, development, and application. *Environ. Sci. Water Res. Technol.* 2, 17–42. <https://doi.org/10.1039/C5EW00159E>
- Lee, S.-A., Choo, K.-H., Lee, C.-H., Lee, H.-I., Hyeon, T., Choi, W., Kwon, H.-H., 2001. Use of Ultrafiltration Membranes for the Separation of TiO₂ Photocatalysts in Drinking Water Treatment. *Ind. Eng. Chem. Res.* 40, 1712–1719. <https://doi.org/10.1021/ie000738p>
- Li, J., Sculley, J., Zhou, H., 2012. Metal-Organic Frameworks for Separations 869–932. <https://doi.org/10.1021/cr200190s>
- Li, J.R., Sculley, J., Zhou, H.C., 2012. Metal-organic frameworks for separations. *Chem. Rev.* 112, 869–932. <https://doi.org/10.1021/cr200190s>
- Lin, R., Shen, L., Ren, Z., Wu, W., Tan, Y., Fu, H., Zhang, J., Wu, L., 2014. Enhanced photocatalytic hydrogen production activity via dual modification of MOF and reduced graphene oxide on CdS. *Chem. Commun.* 50, 8533–8535. <https://doi.org/10.1039/c4cc01776e>
- Lin, Y.-L., 2017. Effects of organic, biological and colloidal fouling on the removal of pharmaceuticals and personal care products by nanofiltration and reverse osmosis membranes. *J. Memb. Sci.* 542, 342–351.
- Liu, W.M., Wang, X.Q., Wang, C.M., Chen, G.G., Sun, W.L., Zheng, C.T., 2016. Green and large-scale preparation of reduced graphene oxide for electroreduction of nitrobenzene to p-aminophenol. *Micro Nano Lett.* 11, 661–665. <https://doi.org/10.1049/mnl.2016.0334>
- Liu, Y., Wang, X., Yang, H., Xie, Y.F., 2018. Quantifying the influence of solute-membrane interactions on adsorption and rejection of pharmaceuticals by NF/RO membranes. *J. Memb. Sci.* 551, 37–46.
- Long, J., Wang, Sibao, Ding, Z., Wang, Shuchao, Zhou, Y., 2012. ChemComm Amine-functionalized zirconium metal – organic framework as efficient visible-light photocatalyst for aerobic organic transformations w 11656–11658. <https://doi.org/10.1039/c2cc34620f>
- Lonkar, S.P., Dubois, J.R.P., 2015. One-pot microwave-assisted synthesis of graphene

- / layered double hydroxide (LDH) nanohybrids. *Nano-Micro Lett.*
<https://doi.org/10.1007/s40820-015-0047-3>
- Luo, Y., Guo, W., Ngo, H.H., Nghiem, L.D., Hai, F.I., Zhang, J., Liang, S., Wang, X.C.,
 2014. A review on the occurrence of micropollutants in the aquatic environment
 and their fate and removal during wastewater treatment. *Sci. Total Environ.* 473–
 474, 619–641. <https://doi.org/10.1016/j.scitotenv.2013.12.065>
- Ma, J., Guo, X., Ying, Y., Liu, D., Zhong, C., 2017. Composite ultrafiltration membrane
 tailored by MOF @ GO with highly improved water purification performance.
Chem. Eng. J. 313, 890–898. <https://doi.org/10.1016/j.cej.2016.10.127>
- Madsen, H.T., Søgaaard, E.G., 2014. Applicability and modelling of nanofiltration and
 reverse osmosis for remediation of groundwater polluted with pesticides and
 pesticide transformation products. *Sep. Purif. Technol.* 125, 111–119.
<https://doi.org/10.1016/j.seppur.2014.01.038>
- Mahata, P., Madras, G., Natarajan, S., 2006. Novel Photocatalysts for the
 Decomposition of Organic Dyes Based on Metal-Organic Framework Compounds
 13759–13768. <https://doi.org/10.1021/jp0622381>
- Mamun, K., Asw, R., Fahmida, K., 2017. Parameters affecting the photocatalytic
 degradation of dyes using TiO₂: a review. *Appl. Water Sci.* 7, 1569–1578.
<https://doi.org/10.1007/s13201-015-0367-y>
- Matsuura, T., Sourirajan, S., 1973. Reverse Osmosis Separation of Hydrocarbons. *J.*
Appl. Polym. Sci. 17, 3683–3708.
- Mimoso, J., Pronk, W., Morgenroth, E., Hammes, F., 2015. Bacterial growth in batch-
 operated membrane filtration systems for drinking water treatment. *Sep. Purif.*
Technol. 156, 165–174. <https://doi.org/10.1016/j.seppur.2015.09.070>
- Mo, H., Tay, K.G., Ng, H.Y., 2008. Fouling of reverse osmosis membrane by protein
 (BSA): Effects of pH , calcium , magnesium , ionic strength and temperature 315,
 28–35. <https://doi.org/10.1016/j.memsci.2008.02.002>
- Mohammad, A.W., Teow, Y.H., Ang, W.L., Chung, Y.T., Oatley-Radcliffe, D.L., Hilal,
 N., 2015. Nanofiltration membranes review: Recent advances and future prospects.
Desalination 356, 226–254. <https://doi.org/10.1016/j.desal.2014.10.043>

- Moztahida, M., Jang, J., Nawaz, M., Lim, S., Sung, D., 2019. Effect of rGO loading on Fe₃O₄: A visible light assisted catalyst material for carbamazepine degradation. *Sci. Total Environ.* 667, 741–750. <https://doi.org/10.1016/j.scitotenv.2019.02.376>
- Musho, T., Li, J., Wu, N., 2014a. Band gap modulation of functionalized metal–organic frameworks. *Phys. Chem. Chem. Phys.* 16, 23646–23653. <https://doi.org/10.1039/C4CP03110E>
- Musho, T., Li, J., Wu, N., 2014b. Band gap modulation of functionalized metal–organic frameworks. *Phys. Chem. Chem. Phys.* 16, 23646–23653. <https://doi.org/10.1039/C4CP03110E>
- Nan, M., Jin, B., Chow, C.W.K., Saint, C., 2010. Recent developments in photocatalytic water treatment technology: A review. *Water Res.* 44, 2997–3027. <https://doi.org/10.1016/j.watres.2010.02.039>
- Nghiem, L.D., Schäfer, A.I., 2006. Critical risk points of nanofiltration and reverse osmosis processes in water recycling applications. *Desalination* 187, 303–312. <https://doi.org/10.1016/j.desal.2005.04.089>
- Oleszczuk, P., Pan, B., Xing, B., 2009. Adsorption and desorption of oxytetracycline and carbamazepine by multiwalled carbon nanotubes. *Environ. Sci. Technol.* 43, 9167–9173.
- Ormad, M.P., Miguel, N., Claver, A., Matesanz, J.M., Ovelleiro, J.L., 2008. Pesticides removal in the process of drinking water production. *Chemosphere* 71, 97–106. <https://doi.org/10.1016/j.chemosphere.2007.10.006>
- Padhye, L.P., Yao, H., Kung'u, F.T., Huang, C.H., 2014. Year-long evaluation on the occurrence and fate of pharmaceuticals, personal care products, and endocrine disrupting chemicals in an urban drinking water treatment plant. *Water Res.* 51, 266–276. <https://doi.org/10.1016/j.watres.2013.10.070>
- Painter, M.M., Buerkley, M.A., Julius, M.L., Vajda, A.M., Norris, D.O., Barber, L.B., Furlong, E.T., Schultz, M.M., Schoenfuss, H.L., 2009. Antidepressants at environmentally relevant concentrations affect predator avoidance behavior of larval fathead minnows (*Pimephales promelas*). *Environ. Toxicol. Chem.* 28, 2677–2684.

- Peng, T., Li, K., Zeng, P., Zhang, Q., Zhang, X., 2012. Enhanced photocatalytic hydrogen production over graphene oxide – cadmium sulfide nanocomposite under visible light irradiation. *J. Phys. Chem. C* 116, 22720–22726. <https://doi.org/10.1021/jp306947d>
- Peter-varbanets, M., Zurbru, C., Swartz, C., Pronk, W., 2009. Decentralized systems for potable water and the potential of membrane technology 43, 245–265. <https://doi.org/10.1016/j.watres.2008.10.030>
- Petit, C., Bandosz, T.J., 2009. MOF-graphite oxide nanocomposites: Surface characterization and evaluation as adsorbents of ammonia. *J. Mater. Chem.* 19, 6521–6528. <https://doi.org/10.1039/b908862h>
- Petrović, M., Gonzalez, S., Barceló, D., 2003. Analysis and removal of emerging contaminants in wastewater and drinking water. *TrAC - Trends Anal. Chem.* 22, 685–696. [https://doi.org/10.1016/S0165-9936\(03\)01105-1](https://doi.org/10.1016/S0165-9936(03)01105-1)
- Pignatello, J.J., 2005. Characterization of aromatic compound sorptive interactions with black carbon (charcoal) assisted by graphite as a model 2033–2041. <https://doi.org/10.1021/es0491376>
- Plakas, K. V, Karabelas, A.J., 2012. Removal of pesticides from water by NF and RO membranes — A review. *DES* 287, 255–265. <https://doi.org/10.1016/j.desal.2011.08.003>
- Plakas, K. V, Karabelas, A.J., Wintgens, T., Melin, T., 2006. A study of selected herbicides retention by nanofiltration membranes—the role of organic fouling. *J. Memb. Sci.* 284, 291–300.
- Prasanth, K.P., Rallapalli, P., Raj, M.C., Bajaj, H.C., Jasra, R.V., 2011. Enhanced hydrogen sorption in single walled carbon nanotube incorporated MIL-101 composite metal-organic framework. *Int. J. Hydrogen Energy* 36, 7594–7601. <https://doi.org/10.1016/j.ijhydene.2011.03.109>
- Qiu, X., Wang, X., Li, Y., 2015. Controlled growth of dense and ordered metal – organic framework nanoparticles on graphene oxide. *Chem. Commun.* 51, 3874–3877. <https://doi.org/10.1039/c4cc09933h>
- Ramezanzadeh, M., Asghari, M., Ramezanzadeh, B., 2018. Fabrication of an efficient

- system for Zn ions removal from industrial wastewater based on graphene oxide nanosheets decorated with highly crystalline polyaniline nano fibers (GO-PANI): Experimental and ab initio quantum mechanics approaches. *Chem. Eng. J.* 337, 385–397. <https://doi.org/10.1016/j.cej.2017.12.102>
- Reynolds, G., Graham, N., Perry, R., Rice, R.G., 1989. Aqueous ozonation of pesticides: a review.
- Richardson, S.D., 2003. Disinfection by-products and other emerging contaminants in drinking water. *TrAC - Trends Anal. Chem.* 22, 666–684. [https://doi.org/10.1016/S0165-9936\(03\)01003-3](https://doi.org/10.1016/S0165-9936(03)01003-3)
- Safarpour, M., Khataee, A., Vatanpour, V., 2014a. Preparation of a Novel Polyvinylidene Fluoride (PVDF) Ultra filtration Membrane Modified with Reduced Graphene Oxide / Titanium Dioxide (TiO₂) Nanocomposite with Enhanced Hydrophilicity and Antifouling Properties.
- Safarpour, M., Khataee, A., Vatanpour, V., 2014b. Preparation of a novel polyvinylidene fluoride (PVDF) ultrafiltration membrane modified with reduced graphene oxide/titanium dioxide (TiO₂) nanocomposite with enhanced hydrophilicity and antifouling properties. *Ind. Eng. Chem. Res.* 53, 13370–13382.
- Safarpour, M., Vatanpour, V., Khataee, A., 2016. Preparation and characterization of graphene oxide/TiO₂blended PES nanofiltration membrane with improved antifouling and separation performance. *Desalination* 393, 65–78. <https://doi.org/10.1016/j.desal.2015.07.003>
- Safarpour, M., Vatanpour, V., Khataee, A., Esmaeili, M., 2015. Development of a novel high flux and fouling-resistant thin film composite nanofiltration membrane by embedding reduced graphene oxide/TiO₂. *Sep. Purif. Technol.* 154, 96–107. <https://doi.org/10.1016/j.seppur.2015.09.039>
- Schaep, J., Vandecasteele, C., Wahab Mohammad, A., Richard Bowen, W., 2001. Modelling the retention of ionic components for different nanofiltration membranes. *Sep. Purif. Technol.* 22–23, 169–179. [https://doi.org/10.1016/S1383-5866\(00\)00163-5](https://doi.org/10.1016/S1383-5866(00)00163-5)
- Semiati, R., 2000. Present and future. *Water Int.* 25, 54–65.

- Shafiei-alavijeh, M., Alivand, M.S., Rashidi, A., Samimi, A., 2018. Thermally stable UiO-66 nano-adsorbent with high gasoline vapor recovery. 7th Int. Congr. Nanosci. Nanotechnol. 2–5.
- Sharma, V.K., Feng, M., 2017. Water depollution using metal-organic frameworks-catalyzed advanced oxidation processes: A review. *J. Hazard. Mater.* <https://doi.org/10.1016/j.jhazmat.2017.09.043>
- Shen, J.N., Yu, C.C., Ruan, H.M., Gao, C.J., Van der Bruggen, B., 2013. Preparation and characterization of thin-film nanocomposite membranes embedded with poly(methyl methacrylate) hydrophobic modified multiwalled carbon nanotubes by interfacial polymerization. *J. Memb. Sci.* 442, 18–26. <https://doi.org/10.1016/j.memsci.2013.04.018>
- Singh, B., Kochkodan, V., Hashaikeh, R., Hilal, N., 2013. A review on membrane fabrication : Structure , properties and performance relationship. *DES* 326, 77–95. <https://doi.org/10.1016/j.desal.2013.06.016>
- Smith, S.J.D., Ladewig, B.P., Hill, A.J., Lau, C.H., Hill, M.R., 2015. Post-synthetic Ti exchanged UiO-66 metal-organic frameworks that deliver exceptional gas permeability in mixed matrix membranes. *Sci. Rep.* 5, 15–18. <https://doi.org/10.1038/srep07823>
- Snyder, S., Westerhoff, P., Yoon, Y., Sedlak, D., 2003. Disruptors in Water : Implications for the Water Industry. *Environ. Eng. Sci.* 20, 449–469. <https://doi.org/doi:10.1089/109287503768335931>
- Sun, D., Liu, W., Qiu, M., Zhang, Y., Li, Z., 2015. Introduction of a mediator for enhancing photocatalytic performance via post-synthetic metal exchange in metal-organic frameworks (MOFs). *Chem. Commun.* 66, 2056–2059. <https://doi.org/10.1039/c4cc09407g>
- Tian, J., Chen, Z., Nan, J., Liang, H., Li, G., 2010. Integrative membrane coagulation adsorption bioreactor (MCABR) for enhanced organic matter removal in drinking water treatment. *J. Memb. Sci.* 352, 205–212. <https://doi.org/10.1016/j.memsci.2010.02.018>
- Tobergte, D.R., Curtis, S., 2013. Encyclopedia of surface and colloid science, Journal

of Chemical Information and Modeling.
<https://doi.org/10.1017/CBO9781107415324.004>

- Upadhyayula, V.K.K., Deng, S., Mitchell, M.C., Smith, G.B., 2009. Application of carbon nanotube technology for removal of contaminants in drinking water: A review. *Sci. Total Environ.* 408, 1–13.
<https://doi.org/10.1016/j.scitotenv.2009.09.027>
- Uyguner-Demirel, C.S., Birben, N.C., Bekbolet, M., 2017. Elucidation of background organic matter matrix effect on photocatalytic treatment of contaminants using TiO₂: a review. *Catal. Today* 284, 202–214.
- Van der Bruggen, B., 2008. Drawbacks of applying nanofiltration and how to avoid them : A review 63, 251–263. <https://doi.org/10.1016/j.seppur.2008.05.010>
- Van Der Bruggen, B., Everaert, K., Wilms, D., Vandecasteele, C., 2001. Application of nanofiltration for removal of pesticides, nitrate and hardness from ground water: Rejection properties and economic evaluation. *J. Memb. Sci.* 193, 239–248.
[https://doi.org/10.1016/S0376-7388\(01\)00517-8](https://doi.org/10.1016/S0376-7388(01)00517-8)
- Van der Bruggen, B., M??ntt??ri, M., Nystr??m, M., 2008. Drawbacks of applying nanofiltration and how to avoid them: A review. *Sep. Purif. Technol.* 63, 251–263.
<https://doi.org/10.1016/j.seppur.2008.05.010>
- Van Der Bruggen, B., Schaep, J., Maes, W., Wilms, D., Vandecasteele, C., 1998. Nanofiltration as a treatment method for the removal of pesticides from ground waters. *Desalination* 117, 139–147. [https://doi.org/10.1016/S0011-9164\(98\)00081-2](https://doi.org/10.1016/S0011-9164(98)00081-2)
- Van Der Bruggen, B., Schaep, J., Wilms, D., Vandecasteele, C., 1999. Influence of molecular size, polarity and charge on the retention of organic molecules by nanofiltration. *J. Memb. Sci.* 156, 29–41. [https://doi.org/10.1016/S0376-7388\(98\)00326-3](https://doi.org/10.1016/S0376-7388(98)00326-3)
- Van der Bruggen, B., Vandecasteele, C., 2002. Modelling of the retention of uncharged molecules with nanofiltration. *Water Res.* 36, 1360–1368.
[https://doi.org/10.1016/S0043-1354\(01\)00318-9](https://doi.org/10.1016/S0043-1354(01)00318-9)
- Vatanpour, V., Esmacili, M., Hossein, M., Abadi, D., 2014. Fouling reduction and

- retention increment of polyethersulfone nano filtration membranes embedded by amine-functionalized multi-walled carbon nanotubes. *J. Memb. Sci.* 466, 70–81. <https://doi.org/10.1016/j.memsci.2014.04.031>
- Vatanpour, V., Madaeni, S.S., Rajabi, L., Zinadini, S., Derakhshan, A.A., 2012. Boehmite nanoparticles as a new nanofiller for preparation of antifouling mixed matrix membranes. *J. Memb. Sci.* 401–402, 132–143. <https://doi.org/10.1016/j.memsci.2012.01.040>
- Wang, A., Zhou, Y., Wang, Z., Chen, M., Sun, L., Liu, X., 2016. Titanium incorporated with UiO-66(Zr)-type Metal–Organic Framework (MOF) for photocatalytic application. *RSC Adv.* 6, 3671–3679. <https://doi.org/10.1039/C5RA24135A>
- Wang, C., Li, H., Liao, S., Zheng, H., Wang, Z., Pan, B., 2013. Coadsorption , desorption hysteresis and sorption thermodynamics of sulfamethoxazole and carbamazepine on graphene oxide and graphite. *Carbon N. Y.* 65, 243–251. <https://doi.org/10.1016/j.carbon.2013.08.020>
- Wang, C., Xie, Z., Kathryn, E., Lin, W., 2011. Doping Metal À Organic Frameworks for Water Oxidation , Carbon Dioxide Reduction , and Organic Photocatalysis 13445–13454. <https://doi.org/10.1021/ja203564w>
- Wang, S., Wang, X., 2015. Multifunctional metal – organic frameworks for photocatalysis. *Small* 3097–3112. <https://doi.org/10.1002/sml.201500084>
- Waypa, J.J., Elimelech, M., 1997. Arsenic removal by RO and NF membranes 89, 102–114.
- Waypa, J.J., Elimelech, M., Hering, J.G., 1997. Arsenic removal by RO and NF membranes. *Journal-American Water Work. Assoc.* 89, 102–114.
- Wen, M., Mori, K., Kuwahara, Y., An, T., Yamashita, H., 2017. Design and architecture of metal organic frameworks for visible light enhanced hydrogen production. *Appl. Catal. B Environ.* 218, 555–569. <https://doi.org/10.1016/j.apcatb.2017.06.082>
- Wu, G., Gan, S., Cui, L., Xu, Y., 2008. Applied Surface Science Preparation and characterization of PES / TiO₂ composite membranes 254, 7080–7086. <https://doi.org/10.1016/j.apsusc.2008.05.221>
- Wu, H., Mansouri, J., Chen, V., 2013. Silica nanoparticles as carriers of antifouling

- ligands for PVDF ultrafiltration membranes. *J. Memb. Sci.* 433, 135–151. <https://doi.org/10.1016/j.memsci.2013.01.029>
- Xu, J., He, S., Zhang, H., Huang, J., Lin, H., Wang, X., Long, J., 2015. Layered metal-organic framework/graphene nanoarchitectures for organic photosynthesis under visible light. *J. Mater. Chem. A* 3, 24261–24271. <https://doi.org/10.1039/c5ta06838j>
- Yang, C., You, X., Cheng, J., Zheng, H., Chen, Y., 2017. A novel visible-light-driven In-based MOF/graphene oxide composite photocatalyst with enhanced photocatalytic activity toward the degradation of amoxicillin. *Appl. Catal. B, Environ.* 200, 673–680. <https://doi.org/10.1016/j.apcatb.2016.07.057>
- Yang, M.-Q., Zhang, Y., Zhang, N., Tang, Z.-R., Xu, Y.-J., 2013. Visible-light-driven oxidation of primary C–H bonds over CdS with dual co-catalysts graphene and TiO₂. *Sci. Rep.* 3, 3314.
- Yang, Z., Xu, X., Liang, X., Lei, C., Gao, L., Hao, R., Lu, D., Lei, Z., 2017. Fabrication of Ce doped UiO-66/graphene nanocomposites with enhanced visible light driven photoactivity for reduction of nitroaromatic compounds. *Appl. Surf. Sci.* 420, 276–285. <https://doi.org/10.1016/j.apsusc.2017.05.158>
- Ying, Y., Liu, D., Zhang, W., Huang, H., Yang, Q., Zhong, C., 2017. High-Flux Graphene Oxide Membranes Intercalated by Metal – Organic Framework with Highly Selective Separation of Aqueous Organic Solution. *ACS Appl. Mater. Interfaces* 9, 1710–1718. <https://doi.org/10.1021/acsami.6b14371>
- Yoon, Y., Westerhoff, P., Snyder, S.A., Wert, E.C., 2007. Removal of endocrine disrupting compounds and pharmaceuticals by nanofiltration and ultrafiltration membranes 202, 16–23. <https://doi.org/10.1016/j.desal.2005.12.033>
- Yu, J., Jin, J., Jaroniec, M., 2014. A noble metal-free reduced graphene oxide-cds nanorod composite for the enhanced visible-light photocatalytic reduction of CO₂ to solar fuel. *J. Mater. Chem. A* 10, 3407–3416. <https://doi.org/10.1039/c3ta14493c>
- Zhang, J., Xu, Z., Mai, W., Min, C., Zhou, B., Shan, M., Li, Y., Yang, C., Wang, Z., Qian, X., 2013. Improved hydrophilicity, permeability, antifouling and mechanical

- performance of PVDF composite ultrafiltration membranes tailored by oxidized low-dimensional carbon nanomaterials. *J. Mater. Chem. A* 1, 3101–3111.
- Zhang, Yang, Causserand, C., Aimar, P., Cravedi, J.-P., 2006. Removal of bisphenol A by a nanofiltration membrane in view of drinking water production. *Water Res.* 40, 3793–3799.
- Zhang, Y, Causserand, C., Aimar, P., Cravedi, J.P., 2006. Removal of bisphenol A by a nanofiltration membrane in view of drinking water production 40, 3793–3799. <https://doi.org/10.1016/j.watres.2006.09.011>
- Zhao, Y., Seredych, M., Zhong, Q., Bandosz, T.J., 2013. Superior performance of copper based MOF and aminated graphite oxide composites as CO₂ adsorbents at room temperature. *ACS Appl. Mater. Interfaces* 5, 4951–4959. <https://doi.org/10.1021/am4006989>
- Zhou, Y., Apul, O.G., Karanfil, T., 2015. Adsorption of halogenated aliphatic contaminants by graphene nanomaterials. *Water Res.* 79, 57–67. <https://doi.org/10.1016/j.watres.2015.04.017>
- Zinadini, S., Zinatizadeh, A.A., Rahimi, M., Vatanpour, V., Zangeneh, H., 2014. Preparation of a novel antifouling mixed matrix PES membrane by embedding graphene oxide nanoplates. *J. Memb. Sci.* 453, 292–301.

APPENDICES

Table .S1 Analytical conditions of HPLC for DCF analysis

Parameters	Conditions
Column	C18 column of dimensions 4.6 mm × 250 mm × 5 μm
Detector mode	UV/Vis absorbance
Wavelength	276 nm
Mobile phase	Methanol (75%): water (25%)
Oven temperature	40°C

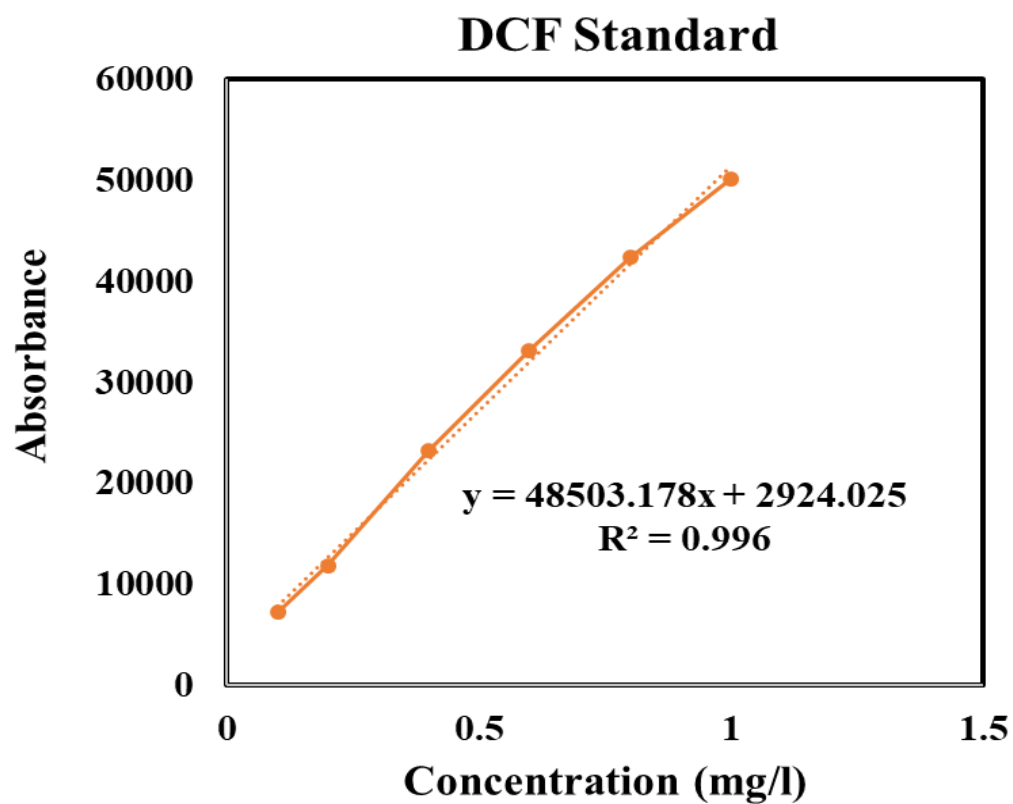


Fig. S1 Calibration curve of DCF standard from HPCL analysis

Table. S2 Analytical conditions of HPLC for CBZ analysis

Parameters	Conditions
Column	C18 column of dimensions 4.6 mm × 250 mm × 5 μm
Detector mode	UV/Vis absorbance
Wavelength	285 nm
Mobile phase	Methanol (60%): water (40%)
Oven temperature	40°C

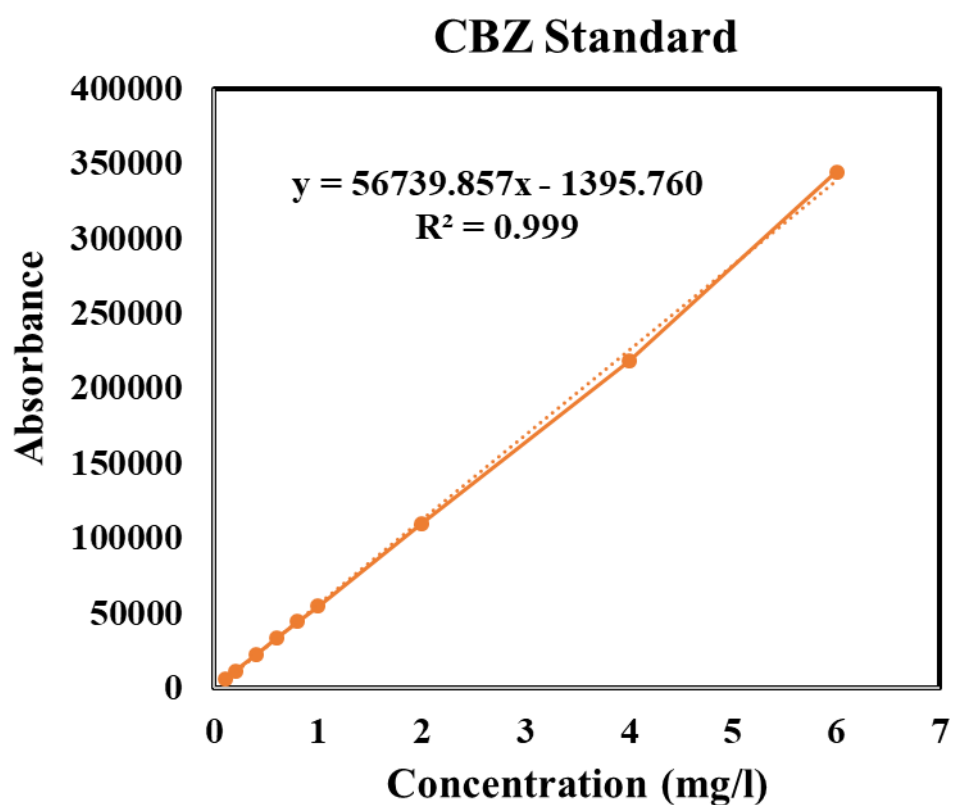


Fig. S2 Calibration curve of CBZ standard from HPCL analysis

Table. S3 Analytical conditions of HPLC for SMX analysis

Parameters	Conditions
Column	C18 column of dimensions 4.6 mm × 250 mm × 5 μm
Detector mode	UV/Vis absorbance
Wavelength	270 nm
Mobile phase	Acetone (40%): water (60%)
Oven temperature	40°C

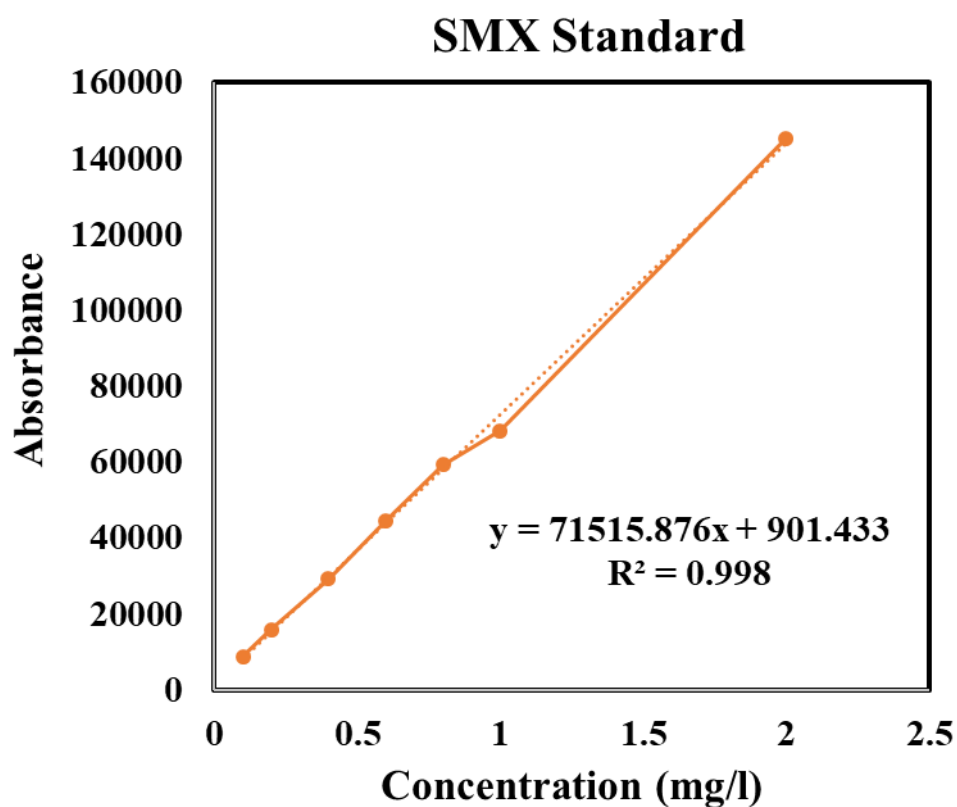


Fig. S3 Calibration curve of SMX standard from HPCL analysis

Table. S4 Analytical conditions of HPLC for ATZ analysis

Parameters	Conditions
Column	C18 column of dimensions 4.6 mm × 250 mm × 5 μm
Detector mode	UV/Vis absorbance
Wavelength	222 nm
Mobile phase	Methanol (60%): water (40%)
Oven temperature	40°C

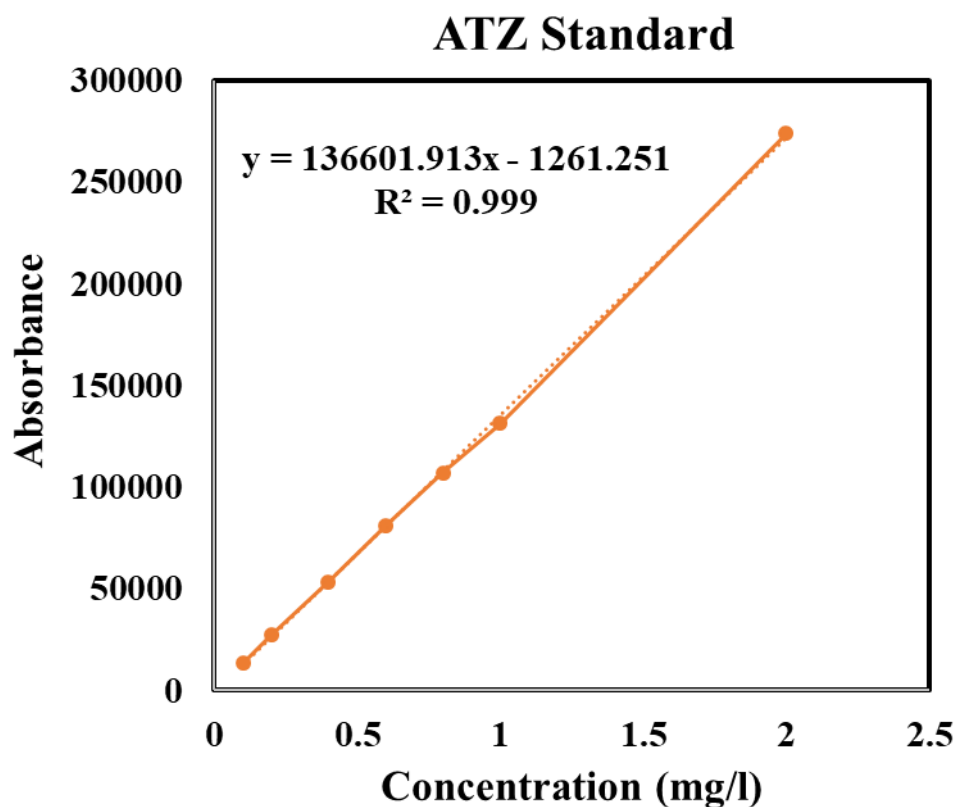


Fig. S4 Calibration curve of SMX standard from HPCL analysis

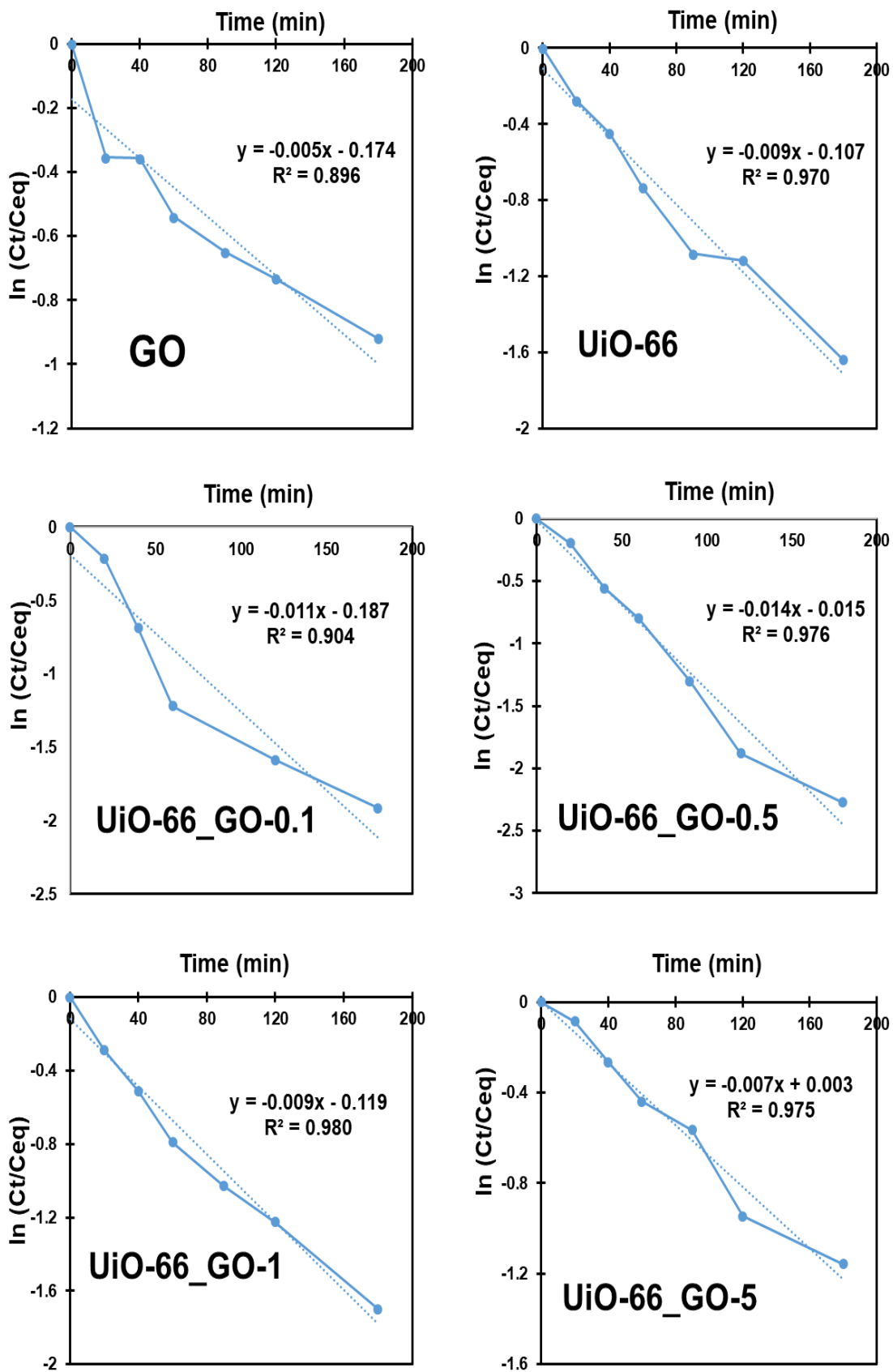


Fig. S5 Kinetic rate of CBZ photodegradation by GO, UiO-66 and composites